Cell

Progestogen-driven B7-H4 contributes to onco-fetal immune tolerance

Graphical abstract

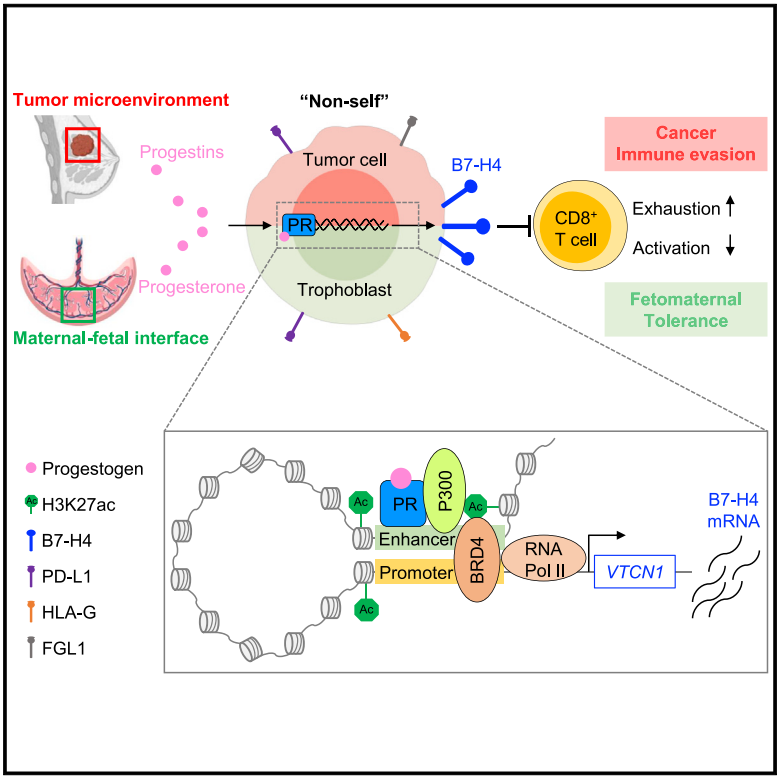

Highlights

- B7-H4 contributes to the onco-fetal immune tolerance
- Progesterone drives B7-H4 expression via the PR-P300-BRD4 axis
- B7-H4 expression is controlled by the −58 kb enhancer
- PR antagonist or selective BRD4 degrader sensitizes B7-H4^{+} tumors to immunotherapy

Authors

Jiali Yu, Yijian Yan, Shasha Li, ..., Shaomeng Wang, Lieping Chen, Weiping Zou

Correspondence

wzou@umich.edu

In brief

Immune tolerance mechanisms are shared in cancer and pregnancy. B7-H4 is identified as an immune checkpoint molecule contributing to onco-fetal immune tolerance, whose expression is regulated by a sex-hormone progesterone.

Yu et al., 2024, Cell *187*, 4713–4732
August 22, 2024
https://doi.org/10.1016/j.cell.2024.06.012

CellPress

Cell

CellPress
OPEN ACCESS

Article

Progestogen-driven B7-H4 contributes to onco-fetal immune tolerance

Jiali Yu,[1,2,17] Yijian Yan,[1,2,17] Shasha Li,[1,2] Ying Xu,[1,2] Abhijit Parolia,[3] Syed Rizvi,[4] Weichao Wang,[1,2] Yiwen Zhai,[5] Rongxin Xiao,[1,2] Xiong Li,[1,2] Peng Liao,[1,2] Jiajia Zhou,[1,2] Karolina Okla,[1,2,6] Heng Lin,[1,2] Xun Lin,[1,2] Sara Grove,[1,2] Shuang Wei,[1,2] Linda Vatan,[1,2] Jiantao Hu,[7] Justyna Szumilo,[8] Jan Kotarski,[6] Zachary T. Freeman,[9] Stephanie Skala,[3] Max Wicha,[7] Kathleen R. Cho,[3] Arul M. Chinnaiyan,[3,10,11] Samantha Schon,[12] Fei Wen,[4] Ilona Kryczek,[1,2] Shaomeng Wang,[7,13] Lieping Chen,[14] and Weiping Zou[1,2,3,15,16,18,*]

[1]Department of Surgery, University of Michigan Medical School, Ann Arbor, MI, USA
[2]Center of Excellence for Cancer Immunology and Immunotherapy, University of Michigan Rogel Cancer Center, Ann Arbor, MI, USA
[3]Department of Pathology, University of Michigan Medical School, Ann Arbor, MI, USA
[4]Department of Chemical Engineering, University of Michigan School of Engineering, Ann Arbor, MI, USA
[5]Department of Pediatrics, University of Michigan Medical School, Ann Arbor, MI, USA
[6]Department of Oncological Gynecology and Gynecology, Medical University of Lublin, Lublin, Poland
[7]Department of Internal Medicine, University of Michigan Medical School, Ann Arbor, MI, USA
[8]Department of Clinical Pathomorphology, Medical University of Lublin, Lublin, Poland
[9]Unit for Laboratory Animal Medicine, University of Michigan, Ann Arbor, MI, USA
[10]Michigan Center for Translational Pathology, University of Michigan Medical School, Ann Arbor, MI, USA
[11]Howard Hughes Medical Institute, University of Michigan Medical School, Ann Arbor, MI, USA
[12]Department of Obstetrics and Gynecology, University of Michigan Medical School, Ann Arbor, MI, USA
[13]Department of Pharmacology, University of Michigan Medical School, Ann Arbor, MI, USA
[14]Department of Immunobiology, Yale University School of Medicine, New Haven, CT, USA
[15]Graduate Program in Immunology, University of Michigan, Ann Arbor, MI, USA
[16]Graduate Program in Cancer Biology, University of Michigan, Ann Arbor, MI, USA
[17]These authors contributed equally
[18]Lead contact
*Correspondence: wzou@umich.edu
https://doi.org/10.1016/j.cell.2024.06.012

SUMMARY

Immune tolerance mechanisms are shared in cancer and pregnancy. Through cross-analyzing single-cell RNA-sequencing data from multiple human cancer types and the maternal-fetal interface, we found B7-H4 (*VTCN1*) is an onco-fetal immune tolerance checkpoint. We showed that genetic deficiency of B7-H4 resulted in immune activation and fetal resorption in allogeneic pregnancy models. Analogously, B7-H4 contributed to MPA/DMBA-induced breast cancer progression, accompanied by $CD8^+$ T cell exhaustion. Female hormone screening revealed that progesterone stimulated B7-H4 expression in placental and breast cancer cells. Mechanistically, progesterone receptor (PR) bound to a newly identified −58 kb enhancer, thereby mediating B7-H4 transcription via the PR-P300-BRD4 axis. PR antagonist or BRD4 degrader potentiated immunotherapy in a murine $B7\text{-}H4^+$ breast cancer model. Thus, our work unravels a mechanistic and biological connection of a female sex hormone (progesterone) to onco-fetal immune tolerance via B7-H4 and suggests that the PR-P300-BRD4 axis is targetable for treating $B7\text{-}H4^+$ cancer.

INTRODUCTION

Immune checkpoint blockade (ICB) induces durable responses across diverse cancers.[1–3] However, most cancer patients do not respond to current immunotherapy.[4] Key immune-regulatory mechanisms foster suppressive networks in the tumor microenvironment (TME), leading to cancer immune evasion and therapeutic resistance to ICB.[4–6] While immune tolerance toward genetically mutated cancer cells is detrimental to the host, immune tolerance toward normal cells from a semi-allogeneic fetus during pregnancy is beneficial—making pregnancy an ideal physiological model to explore immune-tolerance mechanisms. As immune tolerance is critical for both cancer progression during oncogenesis and fetal development during pregnancy,[5–10] it is not surprising that several shared immunosuppressive pathways, like PD-L1 (B7-H1, *CD274*),[2,5,11] HLA-G,[7,12,13] indoleamine 2,3-dioxygenase (IDO),[5,14–16] and regulatory T cells (Tregs),[17–19] are activated in the TME and placenta. In this work, we explored immune regulatory molecules and pathways shared by the TME and placenta and found that B7-H4

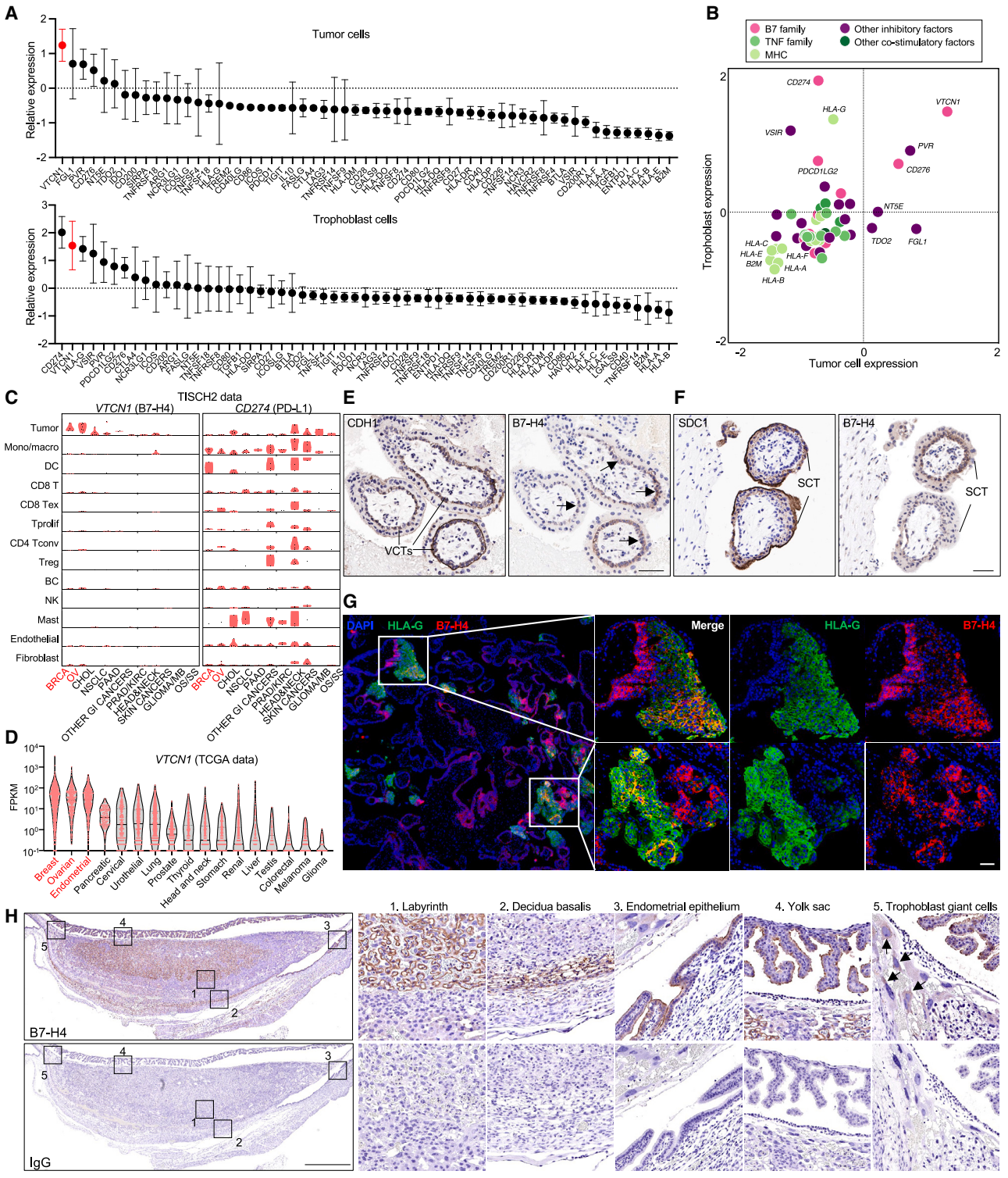

Figure 1. B7-H4 is an onco-fetal immune tolerance checkpoint

(A and B) Gene expression score (*Z* score) of B7 family members, TNF family members, major histocompatibility complex (MHC) molecules, and other typical inhibitory and co-stimulatory molecules in tumor and trophoblast cells (for datasets see STAR Methods). Average scores from multiple datasets were shown in (B).

(C) Gene expression of *VTCN1* and *CD274* in different immune cell subsets across different cancers (TISCH2).

(D) Gene expression of *VTCN1* across different cancers in The Cancer Genome Atlas (TCGA) data.

(legend continued on next page)

(*VTCN1*) (also known as B7x, B7S1) is a potential shared onco-fetal immune-tolerance checkpoint.

B7-H4 has been identified as an inhibitory B7 family member[20–22] and is thought to be an immune checkpoint molecule in the context of tumor immunity.[23–26] High B7-H4 expression often correlates with shorter cancer patient survival.[27–29] However, an immune inhibitory role of endogenous B7-H4 in tumor cells remains elusive in the immune competent system *in vivo*. In the context of pregnancy, it has been reported that B7-H4 is expressed in trophoblast cells and decidual macrophages,[30–34] and its expression is associated with pregnancy complications.[30,35] However, whether B7-H4 plays an active immunological role in maternal-fetal tolerance remains unclear. Furthermore, it is unknown whether and how environmental cues regulate B7-H4 expression in non-immune cells, including trophoblast cells in the placenta and tumor cells in the TME. In this work, we studied the role of endogenous B7-H4 in an induced breast cancer model and multiple pregnancy models.

Crosstalk between the immune system and other systems, like the nervous and endocrine systems, is crucial for generating appropriate immune responses.[36–40] Recent studies on the intersection of endocrine and immune systems have shed light on a role of androgen, a male sex hormone, in regulating T cell function in cancers, including prostate cancer.[41–43] However, it is poorly understood if and how female sex hormone(s) alter T cell-mediated anti-tumor immunity in women with cancer. To fill this knowledge gap, we discovered the effect of female hormones on B7-H4 expression in the placenta and breast cancer and dissected the underlying molecular mechanisms and potential translation.

RESULTS

B7-H4 is an onco-fetal immune tolerance checkpoint

To explore previously unappreciated onco-fetal immune tolerance mechanism(s), we cross-analyzed 14 single-cell RNA-sequencing (scRNA-seq) datasets from multiple human tumor microenvironment (TME)[44–51] and placenta,[52–57] focusing on the "non-self" cellular components of tumor cells and trophoblast cells. Given the importance of the major histocompatibility complex (MHC) and the co-accessary molecules in immune response, we assessed the expression patterns of MHC, key B7 family members, and TNF family members. Our analysis confidently recapitulated previously reported key genes expressed in tumor and trophoblast cells (Figures 1A, 1B, S1A, and S1B). For instance, we found high Fibrinogen-like protein 1 (FGL1) expression in tumor cells[58] and high HLA-G expression in trophoblast cells in the placenta.[7,12,13] Interestingly, B7-H4 (*VTCN1*) was ranked as the top 1 and 2 genes highly expressed in tumor cells in the TME and trophoblast cells in the placenta, respectively (Figures 1A and 1B). Thus, B7-H4 transcripts are expressed in the major cellular components of both TME and placenta.

We extended our analysis to the Tumor Immune Single-cell Hub 2 (TISCH2) database[59] and compared the expression pattern of B7-H4 to that of PD-L1 (B7-H1, *CD274*). Again, B7-H4 was mainly expressed by tumor cells, while PD-L1 was widely expressed by different types of cells, including myeloid cells (Figure 1C). Interestingly, among many cancer types, the highest levels of B7-H4 transcripts were in cancers originating from female reproductive organs, such as breast and ovarian cancers. This scRNA-seq data analysis was in line with the bulk RNA-seq data in TCGA (Figure 1D), showing the highest levels of B7-H4 transcripts in breast, ovarian, and endometrial cancers. We detected high levels of B7-H4 protein in breast and endometrial cancers (Figure S1C). Notably, intermediate levels of B7-H4 transcripts were detected in cervical cancer (Figure 1D). Hence, B7-H4 transcript and protein are highly expressed in pan-gynecological cancers.

At the maternal-fetal interface, B7-H4 was mainly expressed by trophoblast cells (Figure S1D). Human trophoblast cells consist of anatomically and functionally different subsets, including extravillous trophoblast cells (EVTs), villous cytotrophoblast cells (VCTs), and syncytiotrophoblast (SCT).[7] We analyzed the expression of B7-H4 transcripts in trophoblast subsets from human first-trimester pregnancies, which is a critical stage for establishing maternal-fetal immune tolerance. In the scRNA-seq datasets[52–57] we found that *HLA-G* expression was mainly detected in EVTs, *CD274* expression was in EVTs and SCT, and *VTCN1* was in all three subsets of trophoblast cells (Figure S1E). VTCN1 transcripts were detected in the *in vitro* differentiated EVTs (Figure S1F). We next evaluated the expression of B7-H4 protein in trophoblast subsets from human first-trimester gestations. To this end, we performed immunohistochemistry (IHC) staining in products of conception (POCs) from human first-trimester pregnancies. Using a series of consecutive tissue sections, we showed that EVTs expressed HLA-G (Figure S1G), VCTs were Cadherin-1 (CDH1)-expressing inner liner cells of villi (Figure 1E), and SCT was Syndecan-1 (SDC1)-expressing cells arrayed in a continuous layer overlying the VCTs and surrounding the villi (Figure 1F). It was evident that HLA-G$^+$ EVTs expressed B7-H4 protein in placental tissues from POCs (Figure S1G). Multiplex IHC staining revealed concurrent expression of B7-H4 and HLA-G in EVTs (Figure 1G). In line with this, the trophoblast cell line JEG-3 expressed both HLA-G and B7-H4 (Figure S1H). VCTs expressed different levels of B7-H4 protein across different villi and within the same villi (Figures 1E and S1G, arrows). SCT also expressed different levels of B7-H4 protein among different villi (Figure 1F). Consistent with previous reports,[60] amnion epithelial cells also expressed B7-H4 (Figures S1I and S1J), providing an additional B7-H4$^+$ cell type at the human maternal-fetal interface.

We next evaluated B7-H4 expression in the mouse placenta. In line with human data, the scRNA-seq analysis showed that high B7-H4 gene expression was detected in syncytiotrophoblast layer II (SynTII) cells (Figures S1K and S1L).[61] Then, we

(E–G) Representative immunohistochemistry (IHC) (E and F) and multiplex IHC (G) staining of CDH1, B7-H4, SDC1, and HLA-G in human first-trimester products of conception (POCs). Scale bar, 50 μm.

(H) Representative IHC staining of B7-H4 in mouse placenta. Scale bar, 1 mm. Data are presented as mean ± SD (A). Each dot represents a dataset (C) or a tumor sample (D) for violin plots. See also Figure S1.

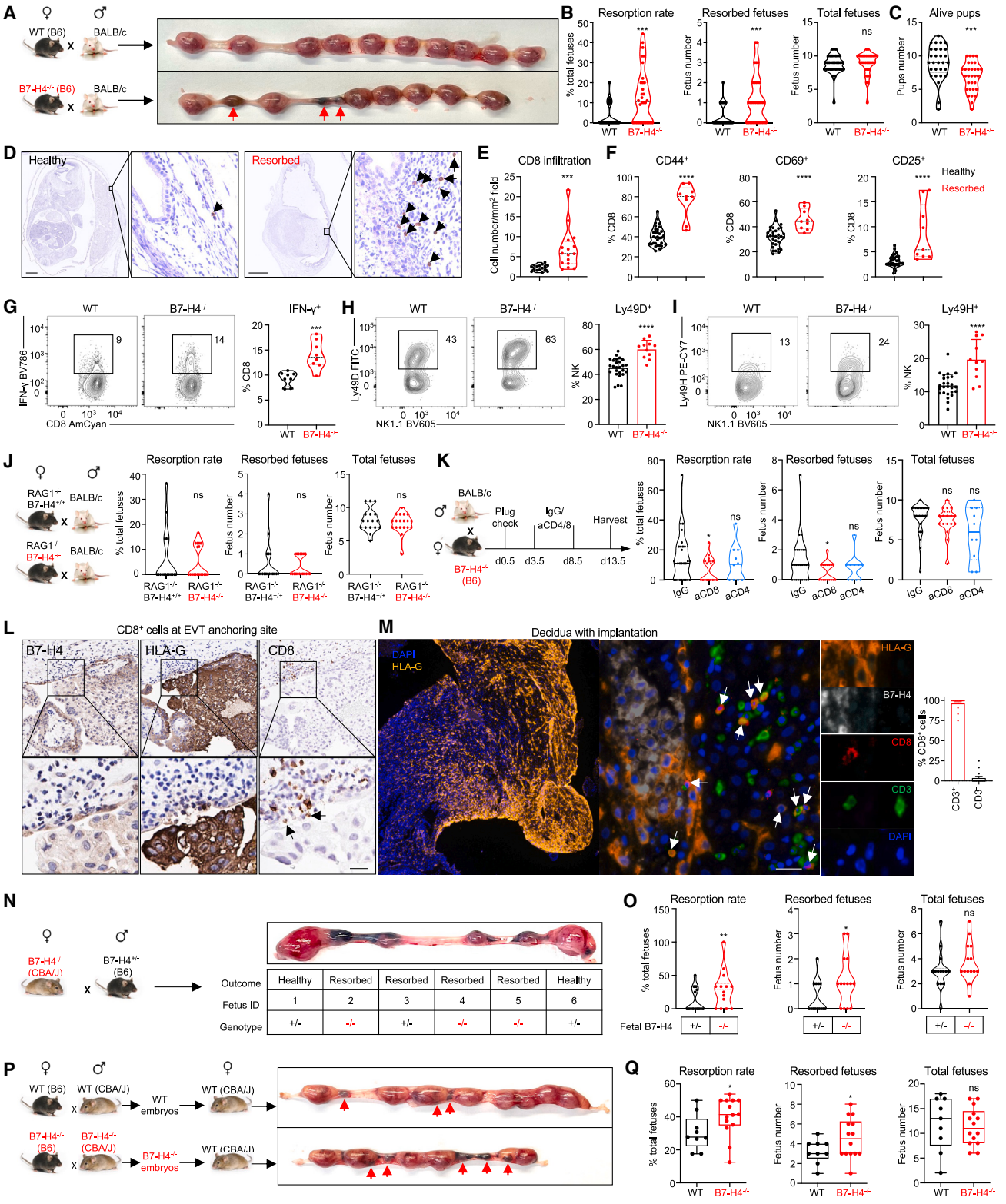

Figure 2. B7-H4 supports maternal-fetal immune tolerance

(A and B) Allogeneic mating strategy for WT (n = 34) and B7-H4$^{-/-}$ C57BL/6 (n = 32) female mice with male BALB/c mice. Representative images of healthy and absorbed fetuses (A, arrows) and statistical data (B).

(legend continued on next page)

performed IHC to assess B7-H4 protein at the mouse maternal-fetal interface. IHC detected B7-H4 protein in the labyrinth (the interface for fetal and maternal blood exchange in the mouse placenta), decidua basalis, endometrial epithelium, yolk sac cells, and trophoblast giant cells (TGCs) (Figure 1G). TGCs are the counterparts of human EVTs. Western blotting validated B7-H4 protein expression in these tissues (Figure S1M). Moreover, IHC demonstrated B7-H4 expression in murine (Figure S1N) and human[62] (Figure S1O) endometrial glandular cells. Thus, B7-H4 is expressed by cells and tissues of both maternal and fetal origin, and its expression pattern is conserved in human and mouse. B7-H4 may serve in junction with PD-L1 and HLA-G to safeguard the fetus via fostering an immunosuppressive network. Given that B7-H4 mediates immune suppression in the TME[5] and is highly expressed in cancer types of female reproductive organ origin, we suggest that B7-H4 is a potential onco-fetal immune tolerance checkpoint.

B7-H4 supports the maternal-fetal immune tolerance

To explore whether B7-H4 plays an active immunological role in maternal-fetal immune tolerance, we bred B7-H4 knockout (B7-H4$^{-/-}$)[63] and wild-type (WT) C57BL/6 (B6) female mice with BALB/c male mice for allogeneic mating. As expected, the expression levels of B7-H4 protein were largely decreased at the maternal-fetal interface in B7-H4$^{-/-}$ female mice, while B7-H4 expression remained detectable at the maternal-fetal interface due to fetal-originated trophoblast cells with B7-H4$^{+/-}$ genotype (Figure S2A). Surprisingly, despite similar fetus numbers, there were more resorbed fetuses in pregnant B7-H4$^{-/-}$ mice than in pregnant WT mice (Figures 2A–2C). This difference held true in pregnant mice from allogeneic mating, but not from syngeneic mating (Figures S2B and S2C). The data suggest that B7-H4 regulates allogeneic mating-associated immune activation. In support of this possibility, there were higher levels of T cells infiltrating the placental and decidual areas of the resorbed fetuses (Figures 2D and 2E). We detected higher levels of activation markers (such as CD25, CD44, and CD69) in T cells from the placental and decidual tissues of the resorbed fetuses as compared to healthy fetuses (Figure 2F). We also observed higher levels of chemokines, CXCL9 and CXCL10, and cytokines, such as IFN-γ and TNF-α, in placental and decidual tissues of the resorbed fetuses (Figure S2D). This is consistent with a previous report showing that IFN-γ and TNF-α can induce chemokine expression in the decidual stromal cells.[64] Moreover, there were more IFN-γ$^+$CD8$^+$ T cells in the uterus-draining lymph nodes (LNs) from pregnant B7-H4$^{-/-}$ mice than WT mice (Figure 2G). Interestingly, natural killer (NK) cells expressed higher levels of activating receptors, including Ly49D and Ly49H (Figures 2H and 2I), and comparable levels of inhibitory receptors, including Ly49A, Ly49C, and Ly49G2 (Figure S2E) in placental and decidual tissues from B7-H4$^{-/-}$ mice compared to WT mice.[65] Therefore, increased fetus resorption in B7-H4$^{-/-}$ mice is accompanied by immune activation. To determine whether T cells were involved in fetus resorption, we bred B7-H4$^{-/-}$ mice with RAG1$^{-/-}$ mice to generate T cell-deficient B7-H4$^{-/-}$ (RAG1$^{-/-}$B7-H4$^{-/-}$) mice. Then, female RAG1$^{-/-}$B7-H4$^{-/-}$ mice were mated with male BALB/c mice. We observed comparable levels of fetus resorption in female RAG1$^{-/-}$B7-H4$^{-/-}$ and RAG1$^{-/-}$ mice (Figure 2J). However, the levels of Ly49D and Ly49H expression on NK cells were comparable in placental and decidual tissues from RAG1$^{-/-}$B7-H4$^{-/-}$ and RAG1$^{-/-}$ mice (Figure S2F), suggesting that elevated expression levels of these activating receptors on NK cells in B7-H4$^{-/-}$ mice were dependent on adaptive immunity. In addition, we treated B7-H4$^{-/-}$ mice with anti-CD4 monoclonal antibody (mAb) or anti-CD8 mAb to deplete CD4$^+$ or CD8$^+$ T cells (Figures 2K, S2G, and S2H). Depletion of CD8$^+$ T cells, but not CD4$^+$ T cells, resulted in reduced fetus resorption (Figure 2K). Thus, the data suggest that activated CD8$^+$ T cells contribute to fetus resorption in B7-H4$^{-/-}$ mice.

In further support of this possibility, in the human first-trimester POC samples, we observed considerable amount of CD8$^+$ cells infiltrating the decidua with implantation, where HLA-G$^+$ EVTs were localized (Figure S2I). Moreover, CD8$^+$ cells were located at the anchoring sites and the invasive front of B7-H4$^+$ EVTs (Figures 2L, S2J, and S2K). Multiplex IHC staining demonstrated that most CD8$^+$ cells were CD3$^+$ T cells in the decidua with implantation (Figure 2M, arrows). Notably, some CD8$^+$ T cells were in close contact with B7-H4$^+$HLA-G$^+$ EVTs (Figure 2M). Altogether, the data suggest that CD8$^+$ T cells

(C) The number of surviving pups from setup in (A). WT, n = 29 litters; B7-H4$^{-/-}$, n = 31 litters.
(D–F) Representative IHC staining of CD8 (D and E) and immune phenotyping of CD8$^+$ T cells (F) at the maternal-fetal interface of healthy and resorbed fetuses from the B7-H4$^{-/-}$ mating group. (E) Healthy, n = 16; resorbed, n = 16. (F) Healthy, n = 32; resorbed, n = 9. Scale bar, 1 mm.
(G) IFN-γ$^+$CD8$^+$ T cells in uterus-draining lymph nodes from pregnant WT (n = 8) and B7-H4$^{-/-}$ (n = 8) mice.
(H and I) Frequency of Ly49D$^+$ and Ly49H$^+$ NK cells in placental and decidual tissues from pregnant WT (n = 26) and B7-H4$^{-/-}$ (n = 11) mice.
(J) Mating strategy and statistics for RAG1$^{-/-}$B7H4$^{+/+}$ (n = 17) and RAG1$^{-/-}$B7H4$^{-/-}$ (n = 19) mice mated with male BALB/c mice.
(K) Effect of CD4 and CD8 depletion on fetus resorption in female B7-H4$^{-/-}$ mice mated with male BALB/c mice. IgG (n = 27), anti-CD8 (n = 17), or anti-CD4 (n = 10).
(L and M) Representative IHC (L) and multiplex IHC (M) staining of B7-H4, HLA-G, CD8, and CD3 in human first-trimester POCs. Arrow: CD8$^+$CD3$^+$ T cells. Scale bars, 20 μm.
(N and O) Female CBA/J B7-H4$^{+/-}$ mice mated male C57BL/6 B7-H4$^{+/-}$ mice. Comparison of fetus resorption between B7-H4$^{+/-}$ and B7-H4$^{-/-}$ fetuses from the same uterus (O).
(P and Q) Strategy for embryo transfer and representative images of the resorbed fetus (arrows) (P). Statistical data were pooled from 4 independent experiments (Q). WT embryos were collected from n = 30 WT (B6) mice and transferred to n = 9 recipient CBA/J mice. B7H4$^{-/-}$ embryos were collected from n = 35 B7H4$^{-/-}$ (B6) mice and transferred to n = 14 recipient CBA/J mice.
Data are presented as violin plots (B–G, J, K, O), mean ± SD (H, I, M), min to max (Q). Each dot represents a litter (B, C, J, K, O, Q), a mouse (G), a fetus (E, F, H, I), or a high-magnification field (M). ****p < 0.0001; ***p < 0.001; **p < 0.01; *p < 0.05; ns, not significant; by unpaired t test (B–J, Q), one-way ANOVA (K, compared to IgG) and paired t test (O). See also Figure S2.

may interact with B7-H4^{+} EVTs during the first trimester of human pregnancy.

We further examined the MHC-I expression on mouse trophoblast cells. We detected a subset of trophoblast cells expressing H-2K (both maternal and paternal) but not H-2D molecules (Figures S2L and S2M). This is consistent with previous reports that TGCs express H-2K but not H-2D.[66] The percentage of H-2K^{+} trophoblast cells was comparable in placental and decidual tissues from WT and B7-H4$^{-/-}$ mice (Figures S2L and S2M). Moreover, H-2K^{+} trophoblast cells also expressed B7-H4 (Figure S2N), suggesting a potential immune regulatory role of B7-H4 in this subset during pregnancy.

To overcome the limitation of using whole-body knockout mice and further demonstrate the role of fetal B7-H4 in fetus resorption, we first bred B7-H4$^{-/-}$ mice with CBA/J mice to generate B7-H4$^{-/-}$ CBA/J mice. Then, we used B7-H4$^{-/-}$ CBA/J female mice and B7-H4$^{+/-}$ B6 males as mating pairs (Figure 2N). In the maternal-fetal interface from these mating pairs, maternal B7-H4 was deficient, while fetal B7-H4 comprised two genotypes: B7-H4$^{+/-}$ and B7-H4$^{-/-}$ (Figures 2N and S2O). This experimental setting allowed us to evaluate the role of fetal B7-H4 by comparing the fetus-resorption outcome of B7-H4$^{-/-}$ and B7-H4$^{+/-}$ fetuses within the same uterus (the same maternal immune environment). We observed more resorption of B7-H4$^{-/-}$ fetuses than B7-H4$^{+/-}$ fetuses (Figure 2O). Furthermore, we performed embryo transfer experiments. WT female B6 mice and WT male CBA/J mice were mated to generate WT embryos on a B6CBAF1 background (Figure 2P). B7-H4$^{-/-}$ female B6 mice and B7-H4$^{-/-}$ male CBA/J mice were mated to generate B7-H4$^{-/-}$ embryos on a B6CBAF1 background. Given that female CBA/J mice ovulate limited numbers of eggs and are not ideal for superovulation,[67] we used female B6 mice for this mating strategy. WT and B7-H4$^{-/-}$ embryos on B6CBAF1 background were collected and transferred to the same pool of female CBA/J mice (Figure 2P). B7-H4$^{-/-}$ embryos developed more fetus resorption than WT embryos, while the total numbers of implantation sites were comparable between these two groups (Figures 2P and 2Q). Consistent with previous data, T cells expressed higher levels of the activation marker CD44 in placental and decidual tissues from resorbed fetuses compared to healthy ones (Figure S2P). The well-established fetuses in WT and B7-H4$^{-/-}$ groups had comparable weights and showed similar histology (Figures S2Q and S2R). These data demonstrate a protective role of fetal B7-H4. Considered together, the data suggest that B7-H4 expression supports the maternal-fetal immune tolerance via potentially keeping CD8^{+} T cells in check.

Progesterone promotes B7-H4 expression in cancer and placenta

B7-H4 is highly expressed in the maternal-fetal interface and pan-gynecological cancers. This phenomenon prompted us to explore environmental cues capable of stimulating B7-H4 expression. We hypothesized that female hormones regulate B7-H4 expression in the placenta and cancer. To test this hypothesis, we tested the response of T-47D, a human breast cancer cell line, to three major types of female hormones: sex hormones (i.e., estrogen and progesterone), pregnancy-related hormones (i.e, human chorionic gonadotropin [hCG] and human placental lactogen [hPL]), and menstrual cycle-related hormones (i.e., luteinizing hormone [LH] and follicle-stimulating hormone [FSH]). Interestingly, treatment with progesterone, but not other hormones, dramatically increased B7-H4 protein expression (Figure 3A). Two progesterone receptor (PR) agonists, medroxyprogesterone acetate (MPA) and levonorgestrel (LNG), promoted B7-H4 expression (Figures 3B and 3C). RU486 (mifepristone), an antagonist of PR, abolished the effect of progesterone on B7-H4 expression (Figure 3D). Progesterone treatment upregulated B7-H4 expression in hormone-receptor-positive breast cancer cells, including ZR-75-1, UACC-812, and CAMA-1 (Figures S3A–S3C), but not in hormone-receptor-negative breast cancer cells, such as MDA-MB-231 and 4T1 (Figures S3D and S3E). These data indicate that progesterone promotes B7-H4 expression in a PR-dependent manner. Moreover, progesterone treatment upregulated B7-H4 expression in OVKATE, an ovarian cancer cell line (Figure S3F), but not in LNCaP, a prostate cancer cell line (Figure S3G). Progesterone-mediated B7-H4 expression occurred in the absence and presence of β-Estradiol in T-47D and UACC-812 cells (Figures S3H and S3I). We extended our study to additional relevant cell types. Treatment with progesterone resulted in an increase in B7-H4 expression in JEG-3 cells (a human trophoblast cell line) (Figure 3E), primary human endometrial epithelial cells (Figure 3F), and mouse endometrial epithelial cells (Figure 3G). As a control, progesterone and MPA failed to affect PD-L1 expression in T-47D and JEG-3 cells (Figures S3J and S3K). Moreover, we treated mice with RU486, which has been studied in patients with breast cancer,[68] and observed reduced B7-H4 expression in endometrial epithelial cells *in vivo* (Figures 3H and 3I). RNA-seq data from paired pre- and post-treatment breast cancer samples showed that RU486 treatment resulted in decreased B7-H4 transcripts in 6 out of 8 patients (Figure 3J).[68] Thus, progesterone promotes B7-H4 expression in human breast cancer cells and cells at the maternal-fetal interface.

B7-H4 promotes breast cancer progression by inhibiting CD8^{+} T cells

The immunological role of progesterone signaling in breast cancer progression and its potential mechanistic connection with B7-H4 are unknown. Despite its reported immune inhibitory role,[20–24,27] the immunological effect of tumor-intrinsic B7-H4 is not fully understood in the syngeneic immune-competent model *in vivo*. Breast cancer cells express the highest levels of B7-H4 (Figures 1C and 1D). Progesterone promotes B7-H4 expression in breast cancer cells (Figures 3A and S3A–S3C). We hypothesized that progesterone promotes cancer immune evasion by controlling B7-H4 expression. To test this hypothesis, we employed a mouse breast cancer model induced by MPA, a synthetic progestogen associated with a potential risk for breast cancer,[69,70] and DMBA (7,12-dimethyl-1,2-benz[*a*]anthracene), a mutagen and carcinogen (Figure 4A).[71,72] In line with this, we observed an increase in breast cancer rate and progression in WT mice receiving MPA plus DMBA compared to mice receiving DMBA alone (Figures 4B–4E). Although MPA plus DMBA induced breast cancer in both WT and B7-H4$^{-/-}$ mice, B7-H4$^{-/-}$ mice had fewer tumor nodules (Figure 4B), manifested

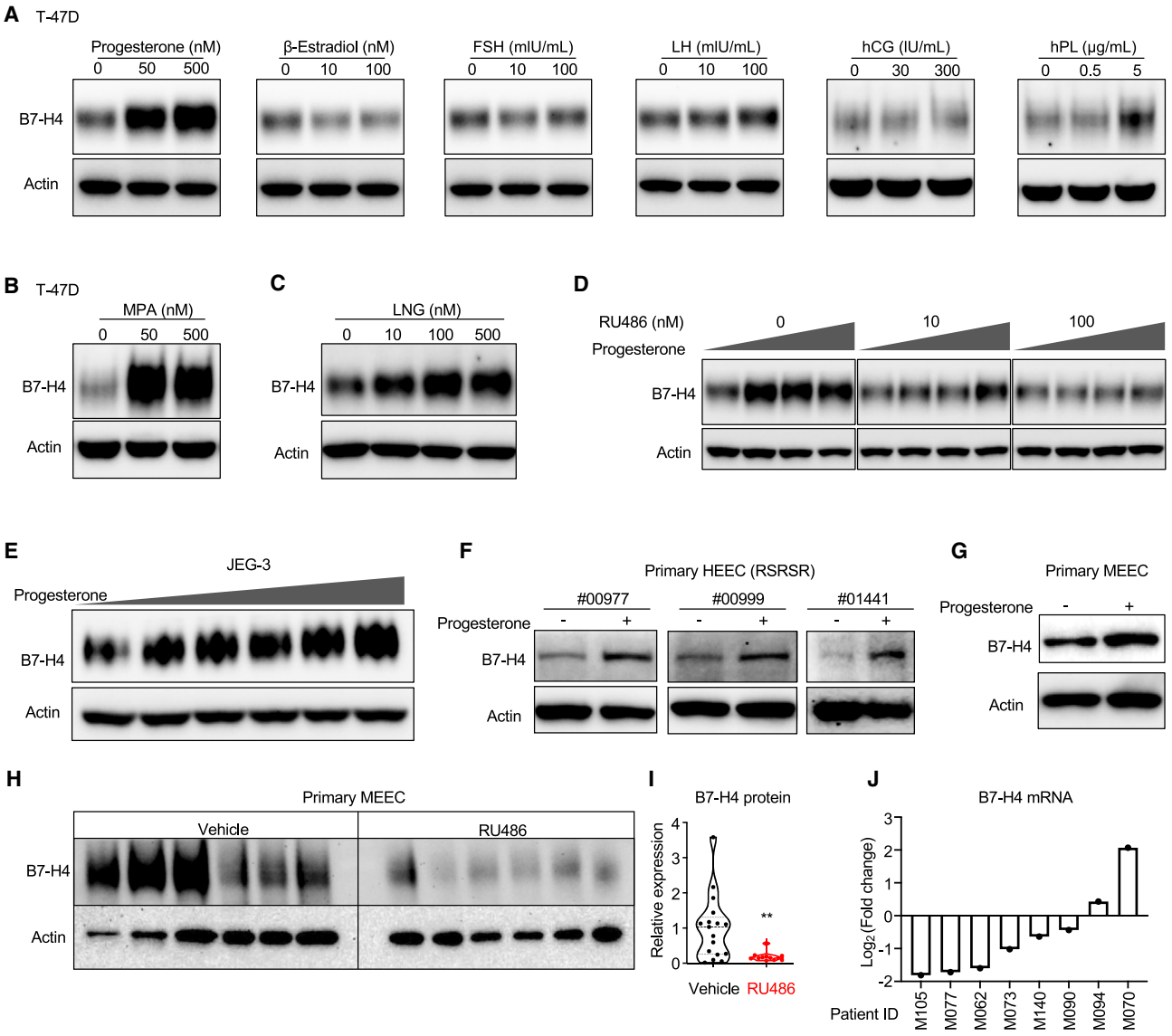

Figure 3. Progesterone promotes B7-H4 expression in cancer and placenta

(A) B7-H4 expression in T-47D treated with different hormones. FSH, follicle-stimulating hormone; LH, luteinizing hormone; hCG, human chorionic gonadotropin; hPL, human placental lactogen.

(B and C) B7-H4 expression in T-47D cells treated with medroxyprogesterone acetate (MPA) and levonorgestrel (LNG).

(D) Western blot of T-47D cells treated with progesterone (0, 1, 10, 100 nM) and the indicated concentrations of RU486.

(E) Western blot of JEG-3 cells treated with progesterone from 0, 1, 10, 100, 500, or 1,000 nM.

(F and G) B7-H4 expression in primary human endometrial epithelial cells (HEECs) and mouse endometrial epithelial cells (MEECs) treated with 100 nM progesterone.

(H and I) B7-H4 protein levels in MEEC isolated from mice treated either with vehicle (n = 17) or RU486 (n = 13).

(J) *VTCN1* gene expression in breast cancer tissues from patients treated with RU486 (GEO: GSE212690). Cells were treated for 48 h *in vitro*.

Representative data from three independent experiments are shown (A–I). Data are presented as violin plot (I). Each dot represents an individual mouse (I). $^{**}p < 0.01$; by unpaired t test (I). See also Figure S3.

slower tumor progression (Figures 4C and 4D), and experienced longer survival as compared to WT mice (Figures 4D and 4E). Notably, this difference was not observed in WT and B7-H4$^{-/-}$ mice that received DMBA alone (Figures 4B–4E). The results suggest that progesterone and B7-H4 act together to enhance breast tumor development and progression.

In line with this notion, high B7-H4 expression was detected in tumor tissues compared to normal mammary fat pad tissues (Figure 4F). IHC staining demonstrated that tumor cells expressed B7-H4 in the TME (Figure 4G). MPA treatment upregulated B7-H4 expression in tumor cell clones (4H11 and 3E10) isolated from primary tumors induced by MPA plus DMBA

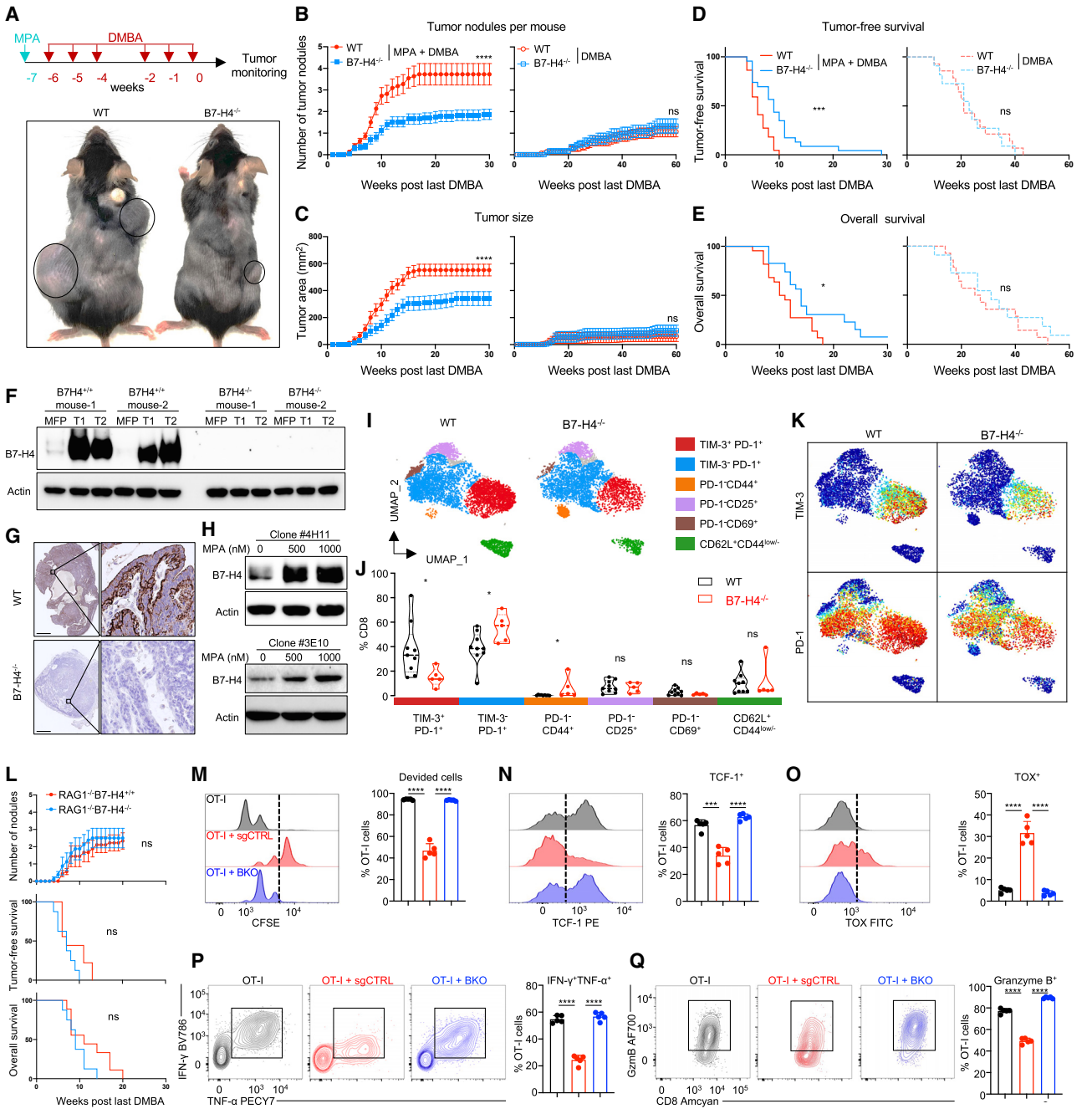

Figure 4. B7-H4 promotes breast cancer progression by inhibiting CD8$^+$ T cells

(A–G) The spontaneous breast cancer model induced by MPA plus DMBA (A). The number of evaluable tumor nodules per mouse (B), tumor growth curves (C), tumor-free survival (D), and overall survival (E) were presented. Western blot and IHC staining of B7-H4 from the indicated tumor samples (F and G). MFP, mammary fat pad; T, tumor. WT, MPA plus DMBA, $n = 22$; B7-H4$^{-/-}$, MPA plus DMBA, $n = 23$; WT, DMBA, $n = 14$; B7-H4$^{-/-}$, DMBA, $n = 12$. Scale bar, 1 mm (G).

(H) Western blot of MPA-treated 4H11 and 3E10, clones derived from primary tumor cells from (A).

(I–K) CyTOF analysis of cells isolated from tumors in WT or B7-H4$^{-/-}$ mice. Subsets of CD8$^+$ T cells (I) and statistics are shown (J). UMAP plots showing PD-1 and TIM-3 expression in concatenated WT and B7-H4$^{-/-}$ samples (K). WT, $n = 9$ tumors; B7-H4$^{-/-}$, $n = 5$ tumors.

(L) The spontaneous breast cancer model in RAG1$^{-/-}$B7-H4$^{+/+}$ ($n = 9$) and RAG$^{-/-}$B7-H4$^{-/-}$ ($n = 8$) mice.

(M–Q) Coculture of OT-I cells with B7-H4$^{+/+}$ (sgCTRL) or B7-H4$^{-/-}$ (BKO) 4H11 tumor cells. The proliferation (M), transcription factor expression (N, O), and cytokine expression (P, Q) of OT-I cells were examined by flow cytometry. Data are presented as mean ± SEM (B, C, L), violin plot (J), or mean ± SD (M–Q). ****$p < 0.0001$; ***$p < 0.001$; *$p < 0.05$; ns, not significant; by two-way ANOVA (B, C, L), log rank test (D, E, L), unpaired t test (J), or one-way ANOVA (M–Q). See also Figure S4.

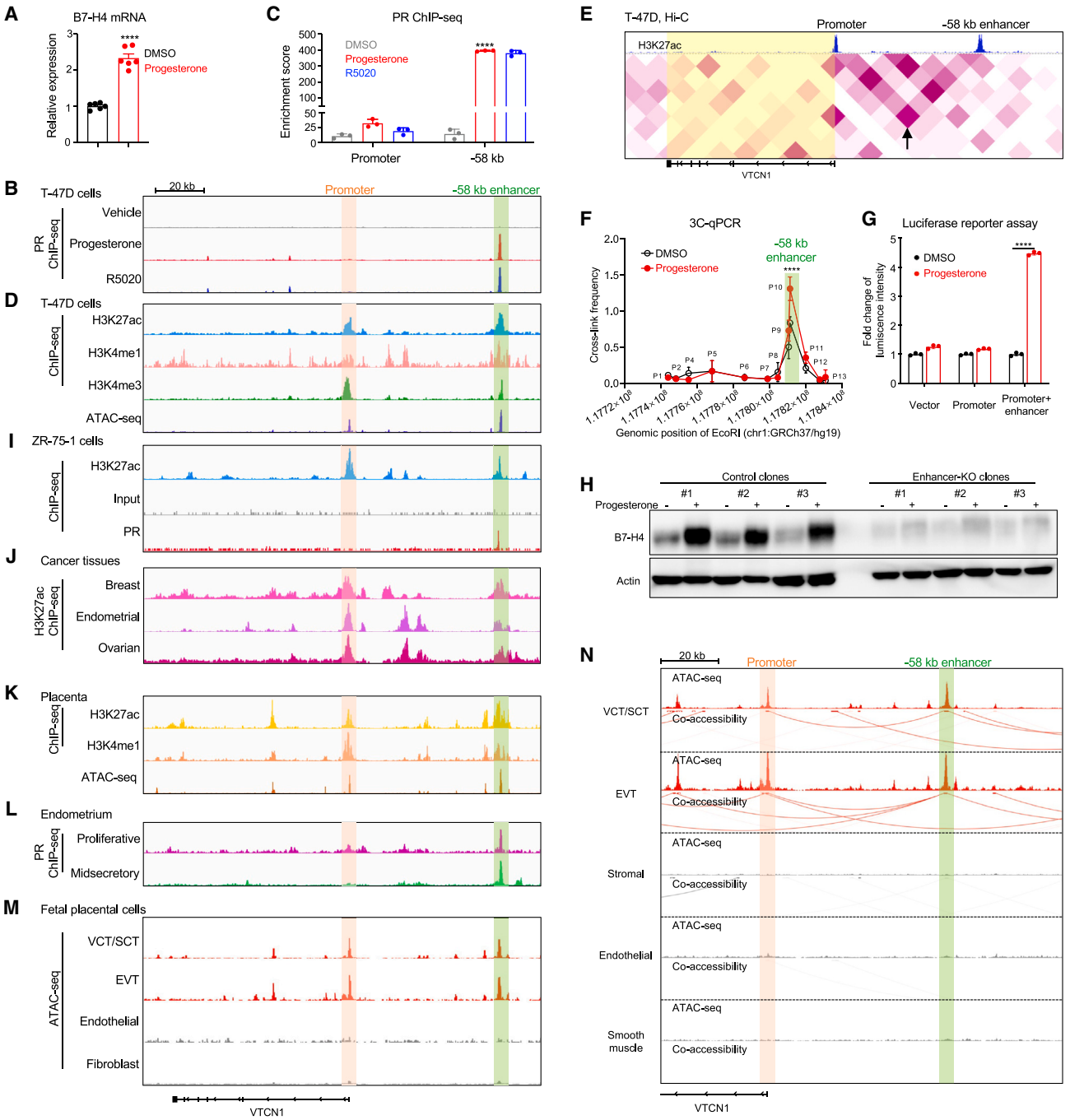

Figure 5. PR signaling promotes B7-H4 transcription via binding to the −58 kb enhancer

(A) mRNA level of B7-H4 in T-47D cells treated with 100 nM progesterone for 24 h.

(B and C) PR ChIP-seq signal tracks and enrichment scores at the indicated region in T-47D cells.

(D) H3K27ac, H3K4me1, and H3K4me3 ChIP-seq and ATAC-seq signal tracks in T-47D cells.

(E) Hi-C and H3K27ac ChIP-seq signal tracks in T-47D cells treated with R5020.

(F) 3C-qPCR for the promoter and putative enhancers in T-47D cells with or without progesterone treatment. P3 is the anchor primer.

(G) Luciferase-reporter assay in HEK293T showing increased transcription by adding the putative enhancer to the promoter region.

(H) B7-H4 expression after progesterone treatment (100 nM) in T-47D clones with or without −58 kb enhancer region.

(I) H3K27ac and PR ChIP-seq signal tracks in ZR-75-1 cells.

(J) H3K27ac ChIP-seq signal tracks in human cancer tissues.

(K) H3K27ac and H3K4me1 ChIP-seq and ATAC-seq signal tracks in human placental tissues.

(legend continued on next page)

(Figure 4H). These data suggest that MPA stimulates tumor B7-H4 expression, thereby contributing to breast cancer progression. To determine the role of B7-H4 in tumor immune response, we used mass cytometry (CyTOF) to analyze immune cell subsets in the TME. We detected similar percentages of tumor-infiltrating immune cell subsets in WT and B7-H4$^{-/-}$ mice, including T cells, B cells, NK cells, dendritic cells (DCs), macrophages, and neutrophils (Figures S4A–S4C). However, there were fewer Tim-3^{+}PD-1^{+}CD8^{+} (exhausted) T cells, but more activated CD8^{+} T cells in B7-H4$^{-/-}$ tumors compared to WT tumors (Figures 4I–4K and S4D). The levels of CD4^{+} T cells and Foxp3^{+} Treg cells were comparable in B7-H4$^{-/-}$ tumors and WT tumors (Figures S4E–S4G). To directly explore the role of tumor-intrinsic B7-H4 in controlling adaptive immune response, we evaluated breast tumors induced by MPA plus DMBA in RAG1$^{-/-}$ mice and RAG1$^{-/-}$B7H4$^{-/-}$ mice. Despite high levels of B7-H4 expression in tumors in RAG1$^{-/-}$ mice (Figure S4H), we observed comparable tumor loads and similar survival in RAG1$^{-/-}$ mice and RAG1$^{-/-}$B7H4$^{-/-}$ mice (Figure 4L). The data suggest that B7-H4 targets adaptive immunity to mediate a protumor role *in vivo*. To further validate this notion, we established B7-H4$^{+/+}$ (sgCTRL) and B7-H4$^{-/-}$ (BKO) tumor cells from clone 4H11 (Figure S4I), which was isolated from primary tumors induced by MPA plus DMBA. Then, we co-cultured OT-I cells with 4H11 tumor cells. OT-I cells showed reduced proliferation (Figure 4M), decreased TCF1 expression (Figure 4N), increased TOX expression (Figure 4O), and diminished expression of effector cytokines and granzyme B (Figures 4P and 4Q) when cultured with B7-H4$^{+/+}$ 4H11 tumor cells as compared to B7-H4$^{-/-}$ 4H11 tumor cells. When 4H11 tumor cells and T cells were cultured in transwell settings, B7-H4$^{+/+}$ 4H11 tumor cells failed to inhibit T cell proliferation (Figure S4J). There was no detectable soluble B7-H4 in this coculture system (Figure S4K). Thus, consistent with its immune tolerogenic role in pregnancy, B7-H4 enhances breast cancer progression via inhibiting T cell activation and promoting T cell exhaustion.

PR signaling promotes B7-H4 transcription via binding to the −58 kb enhancer

We next explored how progesterone-PR signaling regulates B7-H4 expression at the molecular level. Progesterone treatment increased B7-H4 mRNA expression (Figure 5A), suggesting a transcriptional regulation. As a nuclear receptor, PR can function as a transcription factor via binding to the regulatory elements, thereby altering gene expression. Unexpectedly, chromatin immunoprecipitation (ChIP)-seq showed only a modest binding of PR to the plausible promoter region of B7-H4 upon treatment with progesterone or R5020 (also known as promegestone, a PR agonist) in T-47D cells (Figures 5B and 5C). In sharp contrast, there was a strong PR-binding peak at the −58 kb region (Figures 5B and 5C). ChIP-qPCR validated the PR binding to the −58 kb region in T-47D cells in response to progesterone (Figure S5A). This region and the promoter region of B7-H4 had high chromatin accessibilities as shown by ATAC-Seq (assay for transposase-accessible chromatin using sequencing) and harbored histone modification marks for enhancers, including H3K27ac and H3K4me1 (Figure 5D). Published Hi-C (Figure 5E) and 3C-qPCR data generated in-house (Figures 5F and S5B) demonstrated that this −58 kb region directly interacted with the promoter region of B7-H4, while progesterone treatment enhanced their interaction (Figures 5F and S5B). Thus, this −58 kb region is a putative enhancer for B7-H4. To explore whether this putative enhancer can regulate the transcriptional activity of the B7-H4 promoter, we cloned the B7-H4 promoter region with or without the −58 kb putative enhancer region and established a reporter system to assess the B7-H4 promoter activity in PR-expressing HEK293T cells. We found that progesterone treatment enhanced the B7-H4 promoter activity in the presence of the −58 kb putative enhancer (Figure 5G). Moreover, we used CRSPR-Cas9 to genetically delete the −58 kb putative enhancer region in T-47D cells. This deletion abolished the effect of progesterone on B7-H4 expression (Figures 5H and S5C). PR also bound to the enhancer region in progesterone-treated ZR-75-1, UACC-812, and CAMA-1 cells (Figures 5I and S5D). As a control, ChIP-seq data showed that PR failed to bind to the promoter and enhancer regions of PD-L1 in T-47D cells (Figure S5E).[73–75] Thus, the −58 kb region is the specific enhancer for B7-H4 and contributes to progesterone-mediated B7-H4 transcriptional regulation.

We next asked whether this enhancer is active in tissues originating from the reproductive organs in women. Indeed, the −58 kb enhancer exhibited H3K27ac and H3K4me1 signals in human breast cancer, endometrial cancer, ovarian cancer, and placental tissues (Figures 5J and 5K). PR ChIP-seq data showed a strong binding peak at the −58 kb enhancer region in human endometrial tissues (Figure 5L). Single-cell ATAC-Seq[76] results demonstrated that the −58 kb enhancer region had higher chromatin accessibility in trophoblast cells, including VCTs/SCT and EVTs, compared to endothelial cells and fibroblasts in the placenta (Figure 5M). Moreover, based on Cicero analysis,[77,78] the −58 kb enhancer region had co-accessibility with the B7-H4 promoter region in trophoblast cells, but not in stromal, endothelial, or muscle cells (Figure 5N). We also found a series of putative enhancer regions demonstrating histone marks of enhancers and PR-binding peaks in mouse uterus (Figure S5F). Hi-C data indicated that these enhancers could directly interact with the B7-H4 promoter region (Figure S5G). Moreover, treatment with progesterone enhanced the interaction between these enhancers and the B7-H4 promoter region (Figure S5H). Taken together, these data support the conclusion that PR promotes B7-H4 transcription through the specific −58 kb enhancer.

Progesterone promotes B7-H4 expression via the PR-P300-BRD4 axis

PR regulates gene transcription by recruiting epigenetic modifiers.[79] Indeed, upon treatment with progesterone and R5020,

(L) PR ChIP-seq in human endometrium.
(M) ATAC-seq signal tracks in different human placental cells. Tracks are shown in the same data range.
(N) Cicero analysis of co-accessibility score between −58 kb enhancer and the B7-H4 promoter region in trophoblast cells.
All datasets used are listed in the STAR Methods. Data are presented as mean ± SD (A, C, F, G). ****$p < 0.0001$; by unpaired t test. See also Figure S5.

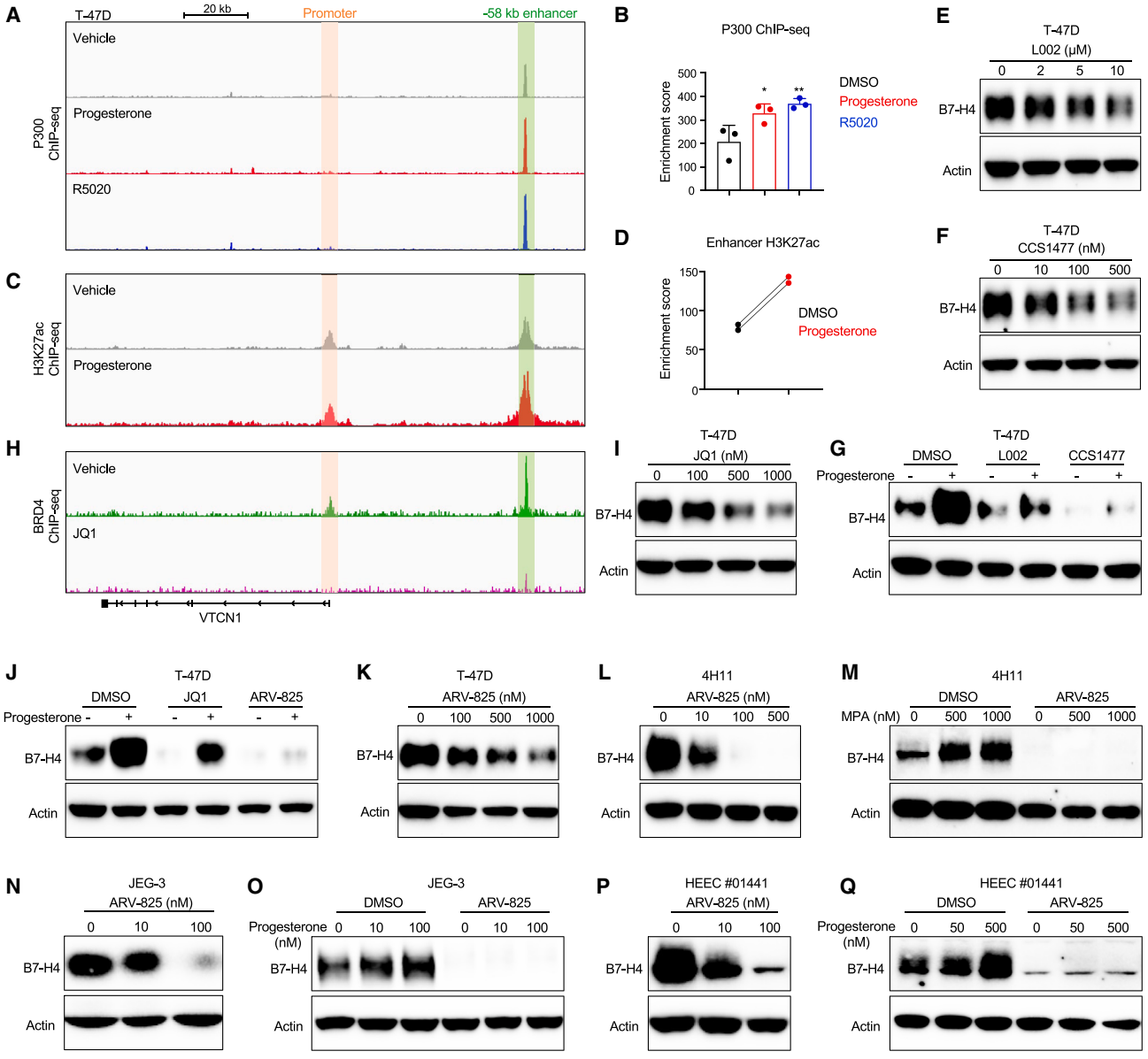

Figure 6. Progesterone promotes B7-H4 expression via the PR-P300-BRD4 axis

(A–D) P300 (A and B) and H3K27ac (C and D) ChIP-seq signal tracks and enrichment scores in T-47D cells.

(E–G) B7-H4 expression in T-47D cells with indicated treatments. 50 nM progesterone, 4 μM L002, and 500 nM CCS1477 were used in (G).

(H) BRD4 ChIP-seq signal tracks in T-47D cells.

(I–K) B7-H4 expression in T-47D cells. 50 nM progesterone, 1,000 nM JQ1, and 1,000 nM ARV-825 were used in (J).

(L and M) B7-H4 expression in 4H11 cells.

(N and O) B7-H4 expression in JEG-3 cells.

(P and Q) B7-H4 expression in HEECs (RSRSR#01441) cells. Cells were treated for 48 h. Representative data from three independent experiments are shown (E–G and I–Q). Data are presented as mean ± SD (B). $^{**}p < 0.01$; $^{*}p < 0.05$; by one-way ANOVA. See also Figure S6.

histone acetyltransferase P300 showed enhanced binding to the −58 kb enhancer region (Figures 6A and 6B). This was consistent with the enhanced H3K27ac signal at the enhancer region (Figures 6C and 6D). Treatment with P300 inhibitors L002 and CCS1477 inhibited B7-H4 protein expression in a dose-dependent manner in multiple breast cancer cell lines (Figures 6E, 6F, and S6A–S6C) and largely impaired the stimulatory effect of progesterone on B7-H4 in T-47D and UACC-812 (Figures 6G and S6D) cells. The data indicate that P300 regulates B7-H4 expression mediated by progesterone.

Epigenetic readers recognize histone modifications and recruit transcriptional activation or repression complexes to

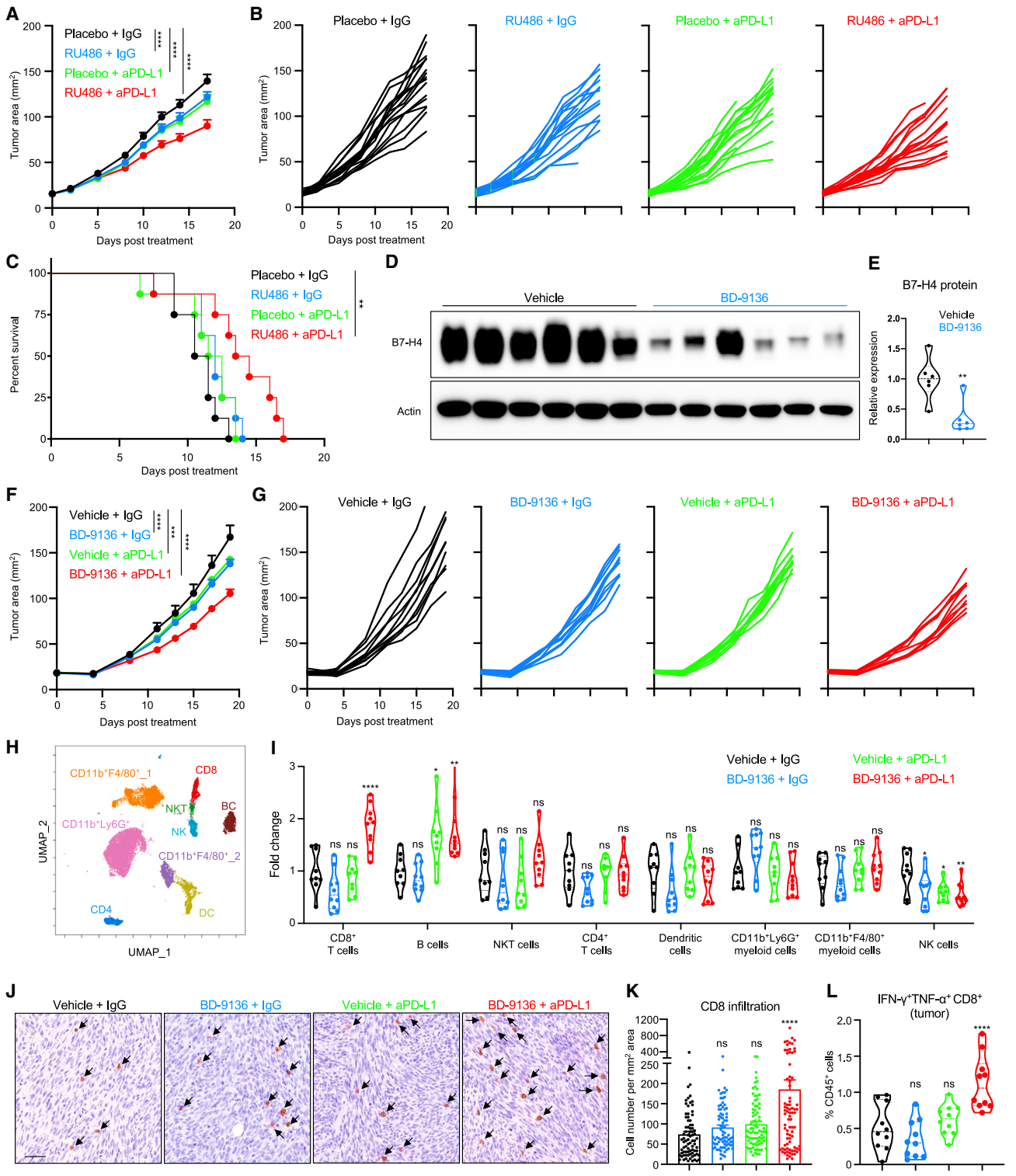

Figure 7. Targeting the regulatory axis of B7-H4 potentiates ICB efficacy

(A–C) Syngeneic tumors were established with primary tumor cells derived from MPA+DMBA breast cancer model. Mice were treated with RU486, anti-PD-L1, or their combination. Tumor growth curves (A and B) and mouse survival (C) were presented. *n* = 16 tumors per group.

(legend continued on next page)

regulate downstream genes.[80] Bromodomain-containing protein 4 (BRD4) is an epigenetic reader for H3K27ac and is important for enhancer functions.[80] BRD4 had a strong binding peak at −58 kb enhancer region in T-47D cells (Figure 6H). JQ1, a potent BET inhibitor, largely impaired the binding of BRD4 to this region in T-47D cells and downregulated B7-H4 expression in multiple breast cancer cell lines (Figures 6H, 6I, and S6E–S6G). Treatment with JQ1 largely impaired the stimulatory effect of progesterone of B7-H4 in T-47D and UACC-812 cells (Figures 6J and S6D). ARV-825, a PROTAC degrader for BRD4,[81] also downregulated B7-H4 expression and impaired progesterone or MPA-induced B7-H4 expression in human breast cancer cell line T-47D cells (Figures 6J, 6K, and S6H), mouse breast cancer cell clone 4H11 (Figures 6L and 6M), human trophoblast JEG-3 (Figures 6N and 6O), and human endometrial epithelial cells (HEECs) (Figures 6P and 6Q). Inhibition of BRD4 also downregulated B7-H4 expression in ovarian cancer cell line OVCAR-3 (Figures S6I and S6J). Taken together, B7-H4 expression is regulated by the PR-P300-BRD4 axis.

Targeting the regulatory axis of B7-H4 potentiates ICB efficacy

Patients with breast cancer and ovarian cancer are often poorly responsive to ICB. Given high levels of B7-H4 expression in these patients, we sought to target B7-H4 to improve ICB efficacy. For this purpose, we established a primary PR^+ER^+ breast cancer model in syngeneic WT mice using cells isolated from B7-$H4^+$ primary tumors induced by MPA plus DMBA (Figures 4F and S7A). We first treated tumor-bearing mice with RU486 (a PR antagonist), anti-PD-L1, and their combination. RU486 or anti-PD-L1 alone resulted in moderate suppressive effects on tumor progression; their combination enhanced this tumor inhibition and prolonged mouse survival (Figures 7A–7C). We next used BD-9136, a highly selective BRD4 degrader we previously synthesized,[82] to target B7-H4. We treated T-47D breast cancer cells with BD-9136. As expected, treatment with BD-9136 effectively reduced B7-H4 expression in a dose-dependent manner (Figure S7B). We then treated mice bearing syngeneic B7-$H4^+$ tumors with BD-9136, anti-PD-L1, and their combination. Treatment with BD-9136 reduced B7-H4 protein expression in tumor tissues (Figures 7D and 7E). BD-9136 alone moderately inhibited tumor growth, and the combination with anti-PD-L1 further enhanced this inhibition (Figures 7F and 7G). In line with this, we detected higher levels of $CD8^+$ T cells in tumor tissues in the combination group as shown by CyTOF analysis (Figures 7H, 7I, S7C, and S7D) and IHC (Figures 7J and 7K). Furthermore, there were more polyfunctional $CD8^+$ T cells expressing IFN-γ and TNF-α in the TME (Figure 7L) and tumor-draining lymph nodes (Figure S7E) from mice treated with combination therapy. Taken together, the data suggest that targeting the regulatory axis of B7-H4 with PR antagonist or BRD4 degrader can potentiate the therapeutic efficacy of ICB in B7-$H4^+$ breast cancer model.

DISCUSSION

Immune tolerance acts as a key mechanism for cancer progression and resistance to ICB[1–6] and is critical for successful fetal development during pregnancy.[7–10] Several immunosuppressive pathways (such as PD-L1, HLA-G, IDO, and Tregs) are shared in the TME and placenta, two anatomically different locations.[2,5,7–19] Here, we demonstrate that B7-H4 is a previously unappreciated onco-fetal immune tolerance checkpoint, contributing to both cancer immune evasion and maternal-fetal immune tolerance. Interestingly, the progesterone signal drives B7-H4 expression to support local immune suppression in the TME and at the maternal-fetal interface. This microenvironmental B7-H4 regulation results in immune compartmentalization, ensuring that the TME and placenta are immune-privileged sites during cancer progression and pregnancy. Moreover, this molecular regulation is part of a cellular immunosuppressive network, consisting of key cellular components in the TME[1–6] and at the maternal-fetus interface.[7–10] Like the TME, T cells,[8,14–19,83] NK cells,[7,10,84–86] DCs,[15,87] and macrophages[88] participate in the establishment of maternal-fetal tolerance. Trophoblast cells, including VCTs, EVTs, and SCT, are the major cell types of fetal origin located at the maternal-fetal interface. Trophoblast cells critically contribute to immune tolerance to the fetus.[7–9] In addition to the unique HLA expression pattern, trophoblast cells express immune inhibitory molecules—such as B7-H4 (this work), HLA-G, and PD-L1.[7,8,12,13,89] We find that B7-H4 is expressed in human EVTs which are exposed to the maternal immune system. We also find that $CD8^+$ T cells are in close contact with B7-$H4^+$ EVTs at the anchoring sites of villi and the EVT invasive front in the decidua with implantation. Notably, although murine and human placenta are structurally different and composed of different subsets of trophoblast cells, mouse TGCs, which resemble human EVTs, also express B7-H4. Consistent with previous reports,[64] limited $CD8^+$ T cells are found in normal mouse placental and decidual area. Interestingly, the deficiency of B7-H4 leads to more fetus resorption and increased $CD8^+$ T cells infiltrating the placental and decidual area of the resorbed fetuses. In line with this, we have detected elevated T cell-attracting chemokines, such as CXCL9 and CXCL10, and elevated IFN-γ and TNF-α, which can induce chemokine expression in myometrial and decidual stromal cells as previously reported.[64] These data suggest the possibility of B7-H4 as a "tolerogenic" molecule and the potential involvement of $CD8^+$ T cells in B7-H4-mediated tolerance, adding an additional layer of immune compartmentalization at cellular levels, to safeguard the fetus in both humans and mice. Further studies are warranted to investigate the functional outcomes of

(D–L) Syngeneic tumors were established as in (A). Mice were treated with BD-9136, anti-PD-L1, or their combination. B7-H4 expression in tumors treated with or without BD-9136 (D and E). Tumor growth (F), CyTOF analysis of tumor-infiltrating immune cells (H and I), IHC staining of CD8 (J and K), and cytokine production of tumor-infiltrating $CD8^+$ T cells (L) were presented.

Data are presented as mean ± SEM (A, F, and K) and violin plots (E, I, and L). Each dot represents an individual tumor sample (E, I, and L) or a high-magnification field (K). $^{****}p < 0.0001$; $^{***}p < 0.001$; $^{**}p < 0.01$; $^{*}p < 0.05$; ns, not significant; by two-way ANOVA (A, F), log rank test (C), unpaired t test (E), and one-way ANOVA (I, K, and L; compared to Vehicle + IgG). See also Figure S7.

the interactions between B7-H4$^+$ EVTs and maternal immune cells. Notably, the human trophoblast organoid culture system has been employed to investigate the impact of cytokines derived from immune cells on trophoblast cell differentiation.[90] Utilizing this system to directly simulate the immunobiological communication between trophoblast cells and specific maternal immune cell subsets (such as CD8$^+$ T cells) from the same placenta poses both technical and ethical challenges due to the inaccessibility of fresh maternal-fetal interface samples early in human gestation.[90] Nonetheless, the exploration of immune regulatory molecules in different cells shared by the TME and maternal-fetal interface not only provides insight into how different immune inhibitory pathways function in the TME but also provides the rationale for immune combination therapy.

Crosstalk between the immune system and other systems, including the endocrine system, modulates immune responses in infectious immunity, autoimmunity, and tumor immunity.[36–40] Recent studies examining the intersection of the endocrine and immune systems have shed light on the role of androgen, a male sex hormone, in regulating T cell exhaustion in the TME.[41–43] Along this line, we demonstrate that progesterone, a female sex hormone, dampens T cell immunity to both cancer and fetus via induction of B7-H4 expression. It appears that progesterone signaling promotes B7-H4 expression, contributing to T cell exhaustion and cancer progression. Thus, we fill an important knowledge gap regarding if and how a female sex hormone affects T cell function in the context of tumor and reproductive immune responses. Low levels of serum progesterone are associated with high risk for pregnancy loss and supplementation of progesterone may improve the pregnancy outcome in patients with a history of recurrent pregnancy loss.[91–93] Our work provides a possible immunological mechanism underlying these experimental and clinical observations. Thus, progesterone signaling controls B7-H4 expression and plays an immunological role in breast cancer progression and pregnancy.

B7-H4 acts as a negative regulator of T cell-mediated immune responses.[20–22] B7-H4 overexpression in tumors is often associated with poor prognosis and decreased patient survival.[23–29] Its expression on antigen-presenting cells can mediate immunosuppression and can be regulated by the tumor microenvironmental factors.[23] However, the functional receptor(s) of B7-H4 has not been identified. Prior to our current work, it was unknown if and how environmental cues, such as progesterone, regulate B7-H4 expression in non-immune cells, including tumor cells. Our observations suggest that B7-H4 expression can be regulated by different factors in different cell types in the TME. Furthermore, given the lack of understanding of tumor B7-H4 regulation, there was no well-established system to study an immune inhibitory role of autologous B7-H4 in tumor in the immune-competent model *in vivo*. These deficiencies impede the clinical development of agents that directly target B7-H4 and its related pathway. Hence, it may be unsurprising that clinical trials using potential monoclonal antibodies against B7-H4 have not produced an impactful anti-tumor effect.[94] An alternative translational strategy is to use B7-H4 as a molecular marker for delivery system to target B7-H4$^+$ tumor cells.[95,96] Our study has identified a *cis*-regulatory element, the −58 kb enhancer, and unraveled related *trans*-regulatory elements, which control B7-H4 transcription via the PR-P300-BRD4 axis. PR antagonist and BRD4 inhibitors are pursued clinically in different disease indications.[68,97] As proof of principle, we demonstrate that the PR antagonist RU486 and the BRD4 degrader BD-9136[82] can reduce B7-H4 expression in breast cancers *in vivo* and sensitize tumor response to ICB in a preclinical model. Thus, although it will not be specific to B7-H4, targeting the PR-P300-BRD4 axis, including repurposing PR antagonists and BRD4 inhibitors, may be a reasonable strategy to treat B7-H4$^+$ cancers, especially breast cancer and several types of gynecological cancers.

In summary, we demonstrate that B7-H4 acts as a previously unappreciated immune tolerance mechanism shared by cancer and pregnancy and is regulated by the PR-P300-BRD4 axis through a newly identified −58 kb enhancer. Thus, hormonal signal-mediated B7-H4 regulation and immunosuppression add a previously unknown component to the recently proposed onco-fetal ecosystem.[98,99] Our findings generate insight into how endocrine and immune systems cooperatively support physiological and pathological immune tolerance. We suggest that targeting the PR-P300-BRD4 axis is a potential modality to treat patients with B7-H4$^+$ cancers.

Limitations of this study

We have shown that loss of B7-H4 at the maternal-fetal interface causes immune activation and fetus resorption in mice. Since B7-H4 expression was observed in multiple cell subsets, further studies are needed to ascertain the contribution of B7-H4 expressed by different cell subsets in maternal-fetal immune tolerance. Given that the receptor(s) of B7-H4 are not identified yet, the direct cellular target of B7-H4 remains to be defined in both mice and humans. We demonstrate that genetic deficiency of B7-H4 leads to CD8$^+$ T cell activation at the maternal-fetal interface and that CD8$^+$ T cell depletion and removal of adaptive immunity (in RAG1$^{-/-}$ models) largely reverse fetal resorption caused by B7-H4 deficiency. Our work reveals the involvement and necessity of CD8$^+$ T cells in B7-H4-regulated fetal immune tolerance. However, despite years of extensive research showing that maternal CD8$^+$ T cells can respond to fetal antigen,[100–109] both our work and current literature have not determined whether endogenous alloantigen-specific CD8$^+$ T cells directly recognize and kill fetal antigen-expressing trophoblast cells, thereby causing fetal loss. Moreover, we have observed a close contact between CD8$^+$ T cells and B7-H4$^+$ EVTs in human POC tissues and enhanced CD8$^+$ T cell activation as well as high levels of IFN-γ and TNF-α in B7-H4$^{-/-}$ mouse placental and decidual tissues. Altogether, our mouse and human complementary and confirmatory results are in line with the notion that aberrant immune activation signals at the maternal-fetal interface can contribute to fetus resorption.[7,9,110–114]

STAR★METHODS

Detailed methods are provided in the online version of this paper and include the following:

- KEY RESOURCES TABLE
- RESOURCE AVAILABILITY
  - Lead contact

ACKNOWLEDGMENTS

This work was supported in part by the NIH/NCI R01 grants (CA217648, CA123088, CA099985, CA193136, and CA152470), by the NIH/NCI through the University of Michigan Rogel Cancer Center (CA46592) to W.Z. and by the UTC-Yale Endowment to L.C. We are grateful for the support from Drs. Rafal Tarkowski, Marcin Bobinski, and Alicja Rajtak at the Medical University of Lublin, Poland, for providing endometrial cancer tissues for this work. We thank the support of the University of Michigan CyTOF Core, Transgenic Animal Model Core, In Vivo Animal Core, and Microscopy Core.

AUTHOR CONTRIBUTIONS

J.Y., Y.Y., and W.Z. conceived the idea, designed the experiments, and composed the paper. J.Y. and Y.Y. conducted experiments. S.L., A.P., Y.Z., and X. Li contributed to bioinformatic analyses. S.R. and F.W. contributed to CyTOF experiments. Y.X., W.W., R.X., P.L., J.Z., H.L., X. Lin, S.G., S. Wei, and L.V. contributed to the *in vivo* and *in vitro* experiments. K.O., J.S., J.K., and I.K. contributed to human tumor samples. Z.T.F. contributed to embryo transfer experiments. S. Skala contributed to human first-trimester POCs. S. Schon contributed to human endometrial epithelial cells. S. Wang and J.H. provided BRD4 degrader. L.C. offered intellectual input and provided B7-H4$^{-/-}$ mice. M.W., K.R.C., A.M.C., and I.K. contributed to the interpretation of the results. W.Z. supervised the project.

DECLARATION OF INTERESTS

W.Z. has served as a scientific advisor or consultant for Cstone, NextCure, and Hanchorbio. S. Wang is a co-founder and paid consultant of Ascentage Pharma Group International and owns stock in Ascentage. L.C. has been a scientific founder, consultant, and/or board observer for NextCure, Normunity, Tayu, Zai Lab, Tpioneer, Vcanbio, OncoC4, and GenomiCare and has sponsored research funds from NextCure, Normunity, and DynamiCure. This research is conducted independently and has not received resources from and is unrelated to the scientific and commercial pursuits of these industrial entities, including NextCure.

Received: July 19, 2023
Revised: February 9, 2024
Accepted: June 9, 2024
Published: July 4, 2024

REFERENCES

1. Topalian, S.L., Drake, C.G., and Pardoll, D.M. (2015). Immune checkpoint blockade: a common denominator approach to cancer therapy. Cancer Cell *27*, 450–461. https://doi.org/10.1016/j.ccell.2015.03.001.
2. Zou, W., Wolchok, J.D., and Chen, L. (2016). PD-L1 (B7-H1) and PD-1 pathway blockade for cancer therapy: Mechanisms, response biomarkers, and combinations. Sci. Transl. Med. *8*, 328rv4. https://doi.org/10.1126/scitranslmed.aad7118.
3. Ribas, A., and Wolchok, J.D. (2018). Cancer immunotherapy using checkpoint blockade. Science *359*, 1350–1355. https://doi.org/10.1126/science.aar4060.
4. Sharma, P., Hu-Lieskovan, S., Wargo, J.A., and Ribas, A. (2017). Primary, Adaptive, and Acquired Resistance to Cancer Immunotherapy. Cell *168*, 707–723. https://doi.org/10.1016/j.cell.2017.01.017.
5. Zou, W. (2005). Immunosuppressive networks in the tumour environment and their therapeutic relevance. Nat. Rev. Cancer *5*, 263–274. https://doi.org/10.1038/nrc1586.
6. Hanahan, D. (2022). Hallmarks of Cancer: New Dimensions. Cancer Discov. *12*, 31–46. https://doi.org/10.1158/2159-8290.CD-21-1059.
7. Moffett, A., and Shreeve, N. (2023). Local immune recognition of trophoblast in early human pregnancy: controversies and questions. Nat. Rev. Immunol. *23*, 222–235. https://doi.org/10.1038/s41577-022-00777-2.
8. Erlebacher, A. (2013). Mechanisms of T cell tolerance towards the allogeneic fetus. Nat. Rev. Immunol. *13*, 23–33. https://doi.org/10.1038/nri3361.
9. Erlebacher, A. (2013). Immunology of the maternal-fetal interface. Annu. Rev. Immunol. *31*, 387–411. https://doi.org/10.1146/annurev-immunol-032712-100003.
10. Ander, S.E., Diamond, M.S., and Coyne, C.B. (2019). Immune responses at the maternal-fetal interface. Sci. Immunol. *4*, eaat6114. https://doi.org/10.1126/sciimmunol.aat6114.
11. Guleria, I., Khosroshahi, A., Ansari, M.J., Habicht, A., Azuma, M., Yagita, H., Noelle, R.J., Coyle, A., Mellor, A.L., Khoury, S.J., and Sayegh, M.H. (2005). A critical role for the programmed death ligand 1 in fetomaternal tolerance. J. Exp. Med. *202*, 231–237. https://doi.org/10.1084/jem.20050019.
12. Curigliano, G., Criscitiello, C., Gelao, L., and Goldhirsch, A. (2013). Molecular pathways: human leukocyte antigen G (HLA-G). Clin. Cancer Res. *19*, 5564–5571. https://doi.org/10.1158/1078-0432.Ccr-12-3697.
13. Apps, R., Gardner, L., and Moffett, A. (2008). A critical look at HLA-G. Trends Immunol. *29*, 313–321. https://doi.org/10.1016/j.it.2008.02.012.
14. Munn, D.H., Zhou, M., Attwood, J.T., Bondarev, I., Conway, S.J., Marshall, B., Brown, C., and Mellor, A.L. (1998). Prevention of Allogeneic Fetal Rejection by Tryptophan Catabolism. Science *281*, 1191–1193. https://doi.org/10.1126/science.281.5380.1191.
15. Munn, D.H., Sharma, M.D., Lee, J.R., Jhaver, K.G., Johnson, T.S., Keskin, D.B., Marshall, B., Chandler, P., Antonia, S.J., Burgess, R., et al. (2002). Potential regulatory function of human dendritic cells expressing indoleamine 2,3-dioxygenase. Science *297*, 1867–1870. https://doi.org/10.1126/science.1073514.
16. Spranger, S., Spaapen, R.M., Zha, Y., Williams, J., Meng, Y., Ha, T.T., and Gajewski, T.F. (2013). Up-regulation of PD-L1, IDO, and T(regs) in the melanoma tumor microenvironment is driven by CD8(+) T cells. Sci. Transl. Med. *5*, 200ra116. https://doi.org/10.1126/scitranslmed.3006504.

17. Aluvihare, V.R., Kallikourdis, M., and Betz, A.G. (2004). Regulatory T cells mediate maternal tolerance to the fetus. Nat. Immunol. *5*, 266–271. https://doi.org/10.1038/ni1037.

18. Rowe, J.H., Ertelt, J.M., Xin, L., and Way, S.S. (2012). Pregnancy imprints regulatory memory that sustains anergy to fetal antigen. Nature *490*, 102–106. https://doi.org/10.1038/nature11462.

19. Samstein, R.M., Josefowicz, S.Z., Arvey, A., Treuting, P.M., and Rudensky, A.Y. (2012). Extrathymic generation of regulatory T cells in placental mammals mitigates maternal-fetal conflict. Cell *150*, 29–38. https://doi.org/10.1016/j.cell.2012.05.031.

20. Sica, G.L., Choi, I.H., Zhu, G., Tamada, K., Wang, S.D., Tamura, H., Chapoval, A.I., Flies, D.B., Bajorath, J., and Chen, L. (2003). B7-H4, a molecule of the B7 family, negatively regulates T cell immunity. Immunity *18*, 849–861. https://doi.org/10.1016/s1074-7613(03)00152-3.

21. Prasad, D.V.R., Richards, S., Mai, X.M., and Dong, C. (2003). B7S1, a novel B7 family member that negatively regulates T cell activation. Immunity *18*, 863–873. https://doi.org/10.1016/s1074-7613(03)00147-x.

22. Zang, X., Loke, P., Kim, J., Murphy, K., Waitz, R., and Allison, J.P. (2003). B7x: A widely expressed B7 family member that inhibits T cell activation. Proc. Natl. Acad. Sci. USA *100*, 10388–10392. https://doi.org/10.1073/pnas.1434299100.

23. Kryczek, I., Zou, L., Rodriguez, P., Zhu, G., Wei, S., Mottram, P., Brumlik, M., Cheng, P., Curiel, T., Myers, L., et al. (2006). B7-H4 expression identifies a novel suppressive macrophage population in human ovarian carcinoma. J. Exp. Med. *203*, 871–881. https://doi.org/10.1084/jem.20050930.

24. Li, J., Lee, Y., Li, Y., Jiang, Y., Lu, H., Zang, W., Zhao, X., Liu, L., Chen, Y., Tan, H., et al. (2018). Co-inhibitory Molecule B7 Superfamily Member 1 Expressed by Tumor-Infiltrating Myeloid Cells Induces Dysfunction of Anti-tumor CD8(+) T Cells. Immunity *48*, 773–786.e5. https://doi.org/10.1016/j.immuni.2018.03.018.

25. Schalper, K.A., Carvajal-Hausdorf, D., McLaughlin, J., Altan, M., Velcheti, V., Gaule, P., Sanmamed, M.F., Chen, L., Herbst, R.S., and Rimm, D.L. (2017). Differential Expression and Significance of PD-L1, IDO-1, and B7-H4 in Human Lung Cancer. Clin. Cancer Res. *23*, 370–378. https://doi.org/10.1158/1078-0432.Ccr-16-0150.

26. Song, X., Zhou, Z., Li, H., Xue, Y., Lu, X., Bahar, I., Kepp, O., Hung, M.-C., Kroemer, G., and Wan, Y. (2020). Pharmacologic Suppression of B7-H4 Glycosylation Restores Antitumor Immunity in Immune-Cold Breast Cancers. Cancer Discov. *10*, 1872–1893. https://doi.org/10.1158/2159-8290.Cd-20-0402.

27. Kryczek, I., Wei, S., Zhu, G., Myers, L., Mottram, P., Cheng, P., Chen, L., Coukos, G., and Zou, W. (2007). Relationship between B7-H4, Regulatory T Cells, and Patient Outcome in Human Ovarian Carcinoma. Cancer Res. *67*, 8900–8905. https://doi.org/10.1158/0008-5472.Can-07-1866.

28. Podojil, J.R., and Miller, S.D. (2017). Potential targeting of B7-H4 for the treatment of cancer. Immunol. Rev. *276*, 40–51. https://doi.org/10.1111/imr.12530.

29. Smith, J.B., Stashwick, C., and Powell, D.J. (2014). B7-H4 as a potential target for immunotherapy for gynecologic cancers: a closer look. Gynecol. Oncol. *134*, 181–189. https://doi.org/10.1016/j.ygyno.2014.03.553.

30. Duan, L., Reisch, B., Iannaccone, A., Hadrovic, E., Wu, Y., Vogtmann, R., Winterhager, E., Kimmig, R., Köninger, A., Mach, P., and Gellhaus, A. (2021). Abnormal expression of the costimulatory molecule B7-H4 in placental chorionic villous and decidual basalis tissues of patients with preeclampsia and HELLP syndrome. Am. J. Reprod. Immunol. *86*, e13430. https://doi.org/10.1111/aji.13430.

31. Karvas, R.M., McInturf, S., Zhou, J., Ezashi, T., Schust, D.J., Roberts, R.M., and Schulz, L.C. (2020). Use of a human embryonic stem cell model to discover GABRP, WFDC2, VTCN1 and ACTC1 as markers of early first trimester human trophoblast. Mol. Hum. Reprod. *26*, 425–440. https://doi.org/10.1093/molehr/gaaa029.

32. Zhou, J., Tian, Y., Qu, Y., Williams, M., Yuan, Y., Karvas, R.M., Sheridan, M.A., Schulz, L.C., Ezashi, T., Roberts, M.R., and Schust, D.J. (2023). The immune checkpoint molecule, VTCN1/B7-H4, guides differentiation and suppresses proinflammatory responses and MHC class I expression in an embryonic stem cell-derived model of human trophoblast. Front. Endocrinol. *14*, 1069395. https://doi.org/10.3389/fendo.2023.1069395.

33. Cui, L., Wang, Y., Ren, L., Li, Z., Jiang, Y., Wang, C., Liu, X., Ren, Y., and Hu, X. (2022). Effect of B7-H4 downregulation induced by Toxoplasma gondii infection on dysfunction of decidual macrophages contributes to adverse pregnancy outcomes. Parasit. Vectors *15*, 464. https://doi.org/10.1186/s13071-022-05560-9.

34. Galazka, K., Wicherek, L., Pitynski, K., Kijowski, J., Zajac, K., Bednarek, W., Dutsch-Wicherek, M., Rytlewski, K., Kalinka, J., Basta, A., and Majka, M. (2009). Changes in the subpopulation of CD25+ CD4+ and FOXP3+ regulatory T cells in decidua with respect to the progression of labor at term and the lack of analogical changes in the subpopulation of suppressive B7-H4 macrophages-a preliminary report. Am. J. Reprod. Immunol. *61*, 136–146. https://doi.org/10.1111/j.1600-0897.2008.00674.x.

35. Mach, P., Nolte-Boenigk, L., Droste, L., Fox, L., Frank, M., Schmidt, B., Herse, F., Verlohren, S., Wicherek, L., Iannaccone, A., et al. (2018). Soluble B7-H4 blood serum levels are elevated in women at high risk for preeclampsia in the first trimester, as well as in patients with confirmed preeclampsia. Am. J. Reprod. Immunol. *80*, e12988. https://doi.org/10.1111/aji.12988.

36. Zhang, X., Lei, B., Yuan, Y., Zhang, L., Hu, L., Jin, S., Kang, B., Liao, X., Sun, W., Xu, F., et al. (2020). Brain control of humoral immune responses amenable to behavioural modulation. Nature *581*, 204–208. https://doi.org/10.1038/s41586-020-2235-7.

37. Huang, S., Ziegler, C.G.K., Austin, J., Mannoun, N., Vukovic, M., Ordovas-Montanes, J., Shalek, A.K., and von Andrian, U.H. (2021). Lymph nodes are innervated by a unique population of sensory neurons with immunomodulatory potential. Cell *184*, 441–459.e25. https://doi.org/10.1016/j.cell.2020.11.028.

38. Zhao, R., Chen, X., Ma, W., Zhang, J., Guo, J., Zhong, X., Yao, J., Sun, J., Rubinfien, J., Zhou, X., et al. (2020). A GPR174-CCL21 module imparts sexual dimorphism to humoral immunity. Nature *577*, 416–420. https://doi.org/10.1038/s41586-019-1873-0.

39. Quatrini, L., Wieduwild, E., Escaliere, B., Filtjens, J., Chasson, L., Laprie, C., Vivier, E., and Ugolini, S. (2018). Endogenous glucocorticoids control host resistance to viral infection through the tissue-specific regulation of PD-1 expression on NK cells. Nat. Immunol. *19*, 954–962. https://doi.org/10.1038/s41590-018-0185-0.

40. Ozdemir, B.C., and Dotto, G.P. (2019). Sex Hormones and Anticancer Immunity. Clin. Cancer Res. *25*, 4603–4610. https://doi.org/10.1158/1078-0432.CCR-19-0137.

41. Guan, X., Polesso, F., Wang, C., Sehrawat, A., Hawkins, R.M., Murray, S.E., Thomas, G.V., Caruso, B., Thompson, R.F., Wood, M.A., et al. (2022). Androgen receptor activity in T cells limits checkpoint blockade efficacy. Nature *606*, 791–796. https://doi.org/10.1038/s41586-022-04522-6.

42. Yang, C., Jin, J., Yang, Y., Sun, H., Wu, L., Shen, M., Hong, X., Li, W., Lu, L., Cao, D., et al. (2022). Androgen receptor-mediated CD8(+) T cell stemness programs drive sex differences in antitumor immunity. Immunity *55*, 1268–1283.e9. https://doi.org/10.1016/j.immuni.2022.05.012.

43. Kwon, H., Schafer, J.M., Song, N.J., Kaneko, S., Li, A., Xiao, T., Ma, A., Allen, C., Das, K., Zhou, L., et al. (2022). Androgen conspires with the CD8(+) T cell exhaustion program and contributes to sex bias in cancer. Sci. Immunol. *7*, eabq2630. https://doi.org/10.1126/sciimmunol.abq2630.

44. Guo, Y.E., Li, Y., Cai, B., He, Q., Chen, G., Wang, M., Wang, K., Wan, X., and Yan, Q. (2021). Phenotyping of immune and endometrial epithelial cells in endometrial carcinomas revealed by single-cell RNA sequencing.

Aging (Albany NY) *13*, 6565–6591. https://doi.org/10.18632/aging.202288.

45. Qian, J., Olbrecht, S., Boeckx, B., Vos, H., Laoui, D., Etlioglu, E., Wauters, E., Pomella, V., Verbandt, S., Busschaert, P., et al. (2020). A pan-cancer blueprint of the heterogeneous tumor microenvironment revealed by single-cell profiling. Cell Res. *30*, 745–762. https://doi.org/10.1038/s41422-020-0355-0.

46. Pal, B., Chen, Y., Vaillant, F., Capaldo, B.D., Joyce, R., Song, X., Bryant, V.L., Penington, J.S., Di Stefano, L., Tubau Ribera, N., et al. (2021). A single-cell RNA expression atlas of normal, preneoplastic and tumorigenic states in the human breast. EMBO J. *40*, e107333. https://doi.org/10.15252/embj.2020107333.

47. Zilionis, R., Engblom, C., Pfirschke, C., Savova, V., Zemmour, D., Saatcioglu, H.D., Krishnan, I., Maroni, G., Meyerovitz, C.V., Kerwin, C.M., et al. (2019). Single-Cell Transcriptomics of Human and Mouse Lung Cancers Reveals Conserved Myeloid Populations across Individuals and Species. Immunity *50*, 1317–1334.e10. https://doi.org/10.1016/j.immuni.2019.03.009.

48. Gao, R., Bai, S., Henderson, Y.C., Lin, Y., Schalck, A., Yan, Y., Kumar, T., Hu, M., Sei, E., Davis, A., et al. (2021). Delineating copy number and clonal substructure in human tumors from single-cell transcriptomes. Nat. Biotechnol. *39*, 599–608. https://doi.org/10.1038/s41587-020-00795-2.

49. Bassez, A., Vos, H., Van Dyck, L., Floris, G., Arijs, I., Desmedt, C., Boeckx, B., Vanden Bempt, M., Nevelsteen, I., Lambein, K., et al. (2021). A single-cell map of intratumoral changes during anti-PD1 treatment of patients with breast cancer. Nat. Med. *27*, 820–832. https://doi.org/10.1038/s41591-021-01323-8.

50. Lambrechts, D., Wauters, E., Boeckx, B., Aibar, S., Nittner, D., Burton, O., Bassez, A., Decaluwé, H., Pircher, A., Van den Eynde, K., et al. (2018). Phenotype molding of stromal cells in the lung tumor microenvironment. Nat. Med. *24*, 1277–1289. https://doi.org/10.1038/s41591-018-0096-5.

51. Shih, A.J., Menzin, A., Whyte, J., Lovecchio, J., Liew, A., Khalili, H., Bhuiya, T., Gregersen, P.K., and Lee, A.T. (2018). Identification of grade and origin specific cell populations in serous epithelial ovarian cancer by single cell RNA-seq. PLoS One *13*, e0206785. https://doi.org/10.1371/journal.pone.0206785.

52. Vento-Tormo, R., Efremova, M., Botting, R.A., Turco, M.Y., Vento-Tormo, M., Meyer, K.B., Park, J.-E., Stephenson, E., Polański, K., Goncalves, A., et al. (2018). Single-cell reconstruction of the early maternal–fetal interface in humans. Nature *563*, 347–353. https://doi.org/10.1038/s41586-018-0698-6.

53. Suryawanshi, H., Morozov, P., Straus, A., Sahasrabudhe, N., Max, K.E.A., Garzia, A., Kustagi, M., Tuschl, T., and Williams, Z. (2018). A single-cell survey of the human first-trimester placenta and decidua. Sci. Adv. *4*, eaau4788. https://doi.org/10.1126/sciadv.aau4788.

54. Sun, T., Gonzalez, T.L., Deng, N., DiPentino, R., Clark, E.L., Lee, B., Tang, J., Wang, Y., Stripp, B.R., Yao, C., et al. (2020). Sexually Dimorphic Crosstalk at the Maternal-Fetal Interface. J. Clin. Endocrinol. Metab. *105*, e4831–e4847. https://doi.org/10.1210/clinem/dgaa503.

55. Han, X., Zhou, Z., Fei, L., Sun, H., Wang, R., Chen, Y., Chen, H., Wang, J., Tang, H., Ge, W., et al. (2020). Construction of a human cell landscape at single-cell level. Nature *581*, 303–309. https://doi.org/10.1038/s41586-020-2157-4.

56. Zheng, Y., Pan, J., Xia, C., Chen, H., Zhou, H., Ju, W., Wegiel, J., Myatt, L., Roberts, J.M., Guo, X., and Zhong, N. (2022). Characterization of placental and decidual cell development in early pregnancy loss by single-cell RNA sequencing. Cell Biosci. *12*, 168. https://doi.org/10.1186/s13578-022-00904-5.

57. Shannon, M.J., Baltayeva, J., Castellana, B., Wächter, J., McNeill, G.L., Yoon, J.S., Treissman, J., Le, H.T., Lavoie, P.M., and Beristain, A.G. (2022). Cell trajectory modeling identifies a primitive trophoblast state defined by BCAM enrichment. Development *149*, dev199840. https://doi.org/10.1242/dev.199840.

58. Wang, J., Sanmamed, M.F., Datar, I., Su, T.T., Ji, L., Sun, J., Chen, L., Chen, Y., Zhu, G., Yin, W., et al. (2019). Fibrinogen-like Protein 1 Is a Major Immune Inhibitory Ligand of LAG-3. Cell *176*, 334–347.e12. https://doi.org/10.1016/j.cell.2018.11.010.

59. Sun, D., Wang, J., Han, Y., Dong, X., Ge, J., Zheng, R., Shi, X., Wang, B., Li, Z., Ren, P., et al. (2021). TISCH: a comprehensive web resource enabling interactive single-cell transcriptome visualization of tumor microenvironment. Nucleic Acids Res. *49*, D1420–D1430. https://doi.org/10.1093/nar/gkaa1020.

60. Bergmann, S., Penfold, C.A., Slatery, E., Siriwardena, D., Drummer, C., Clark, S., Strawbridge, S.E., Kishimoto, K., Vickers, A., Tewary, M., et al. (2022). Spatial profiling of early primate gastrulation in utero. Nature *609*, 136–143. https://doi.org/10.1038/s41586-022-04953-1.

61. Marsh, B., and Blelloch, R. (2020). Single nuclei RNA-seq of mouse placental labyrinth development. Elife *9*, e60266. https://doi.org/10.7554/eLife.60266.

62. Uhlén, M., Fagerberg, L., Hallström, B.M., Lindskog, C., Oksvold, P., Mardinoglu, A., Sivertsson, Å., Kampf, C., Sjöstedt, E., Asplund, A., et al. (2015). Proteomics. Tissue-based map of the human proteome. Science *347*, 1260419. https://doi.org/10.1126/science.1260419.

63. Zhu, G., Augustine, M.M., Azuma, T., Luo, L., Yao, S., Anand, S., Rietz, A.C., Huang, J., Xu, H., Flies, A.S., et al. (2009). B7-H4-deficient mice display augmented neutrophil-mediated innate immunity. Blood *113*, 1759–1767. https://doi.org/10.1182/blood-2008-01-133223.

64. Nancy, P., Tagliani, E., Tay, C.S., Asp, P., Levy, D.E., and Erlebacher, A. (2012). Chemokine gene silencing in decidual stromal cells limits T cell access to the maternal-fetal interface. Science *336*, 1317–1321. https://doi.org/10.1126/science.1220030.

65. Yadi, H., Burke, S., Madeja, Z., Hemberger, M., Moffett, A., and Colucci, F. (2008). Unique receptor repertoire in mouse uterine NK cells. J. Immunol. *181*, 6140–6147. https://doi.org/10.4049/jimmunol.181.9.6140.

66. Madeja, Z., Yadi, H., Apps, R., Boulenouar, S., Roper, S.J., Gardner, L., Moffett, A., Colucci, F., and Hemberger, M. (2011). Paternal MHC expression on mouse trophoblast affects uterine vascularization and fetal growth. Proc. Natl. Acad. Sci. USA *108*, 4012–4017. https://doi.org/10.1073/pnas.1005342108.

67. Spearow, J.L. (1988). Major genes control hormone-induced ovulation rate in mice. J. Reprod. Fertil. *82*, 787–797. https://doi.org/10.1530/jrf.0.0820787.

68. Elía, A., Saldain, L., Vanzulli, S.I., Helguero, L.A., Lamb, C.A., Fabris, V., Pataccini, G., Martínez-Vazquez, P., Burruchaga, J., Caillet-Bois, I., et al. (2023). Beneficial Effects of Mifepristone Treatment in Patients with Breast Cancer Selected by the Progesterone Receptor Isoform Ratio: Results from the MIPRA Trial. Clin. Cancer Res. *29*, 866–877. https://doi.org/10.1158/1078-0432.Ccr-22-2060.

69. Mørch, L.S., Skovlund, C.W., Hannaford, P.C., Iversen, L., Fielding, S., and Lidegaard, Ø. (2017). Contemporary Hormonal Contraception and the Risk of Breast Cancer. N. Engl. J. Med. *377*, 2228–2239. https://doi.org/10.1056/NEJMoa1700732.

70. Collaborative Group on Hormonal Factors in Breast Cancer (2019). Type and timing of menopausal hormone therapy and breast cancer risk: individual participant meta-analysis of the worldwide epidemiological evidence. Lancet *394*, 1159–1168. https://doi.org/10.1016/s0140-6736(19)31709-x.

71. Aldaz, C.M., Liao, Q.Y., LaBate, M., and Johnston, D.A. (1996). Medroxyprogesterone acetate accelerates the development and increases the incidence of mouse mammary tumors induced by dimethylbenzanthracene. Carcinogenesis *17*, 2069–2072. https://doi.org/10.1093/carcin/17.9.2069.

72. Buqué, A., Bloy, N., Perez-Lanzón, M., Iribarren, K., Humeau, J., Pol, J.G., Levesque, S., Mondragon, L., Yamazaki, T., Sato, A., et al. (2020). Immunoprophylactic and immunotherapeutic control of hormone receptor-positive breast cancer. Nat. Commun. *11*, 3819. https://doi.org/10.1038/s41467-020-17644-0.

73. Kim, M.H., Kim, C.G., Kim, S.-K., Shin, S.J., Choe, E.A., Park, S.-H., Shin, E.-C., and Kim, J. (2018). YAP-Induced PD-L1 Expression Drives Immune Evasion in BRAFi-Resistant Melanoma. Cancer Immunol. Res. *6*, 255–266. https://doi.org/10.1158/2326-6066.Cir-17-0320.

74. Xu, Y., Wu, Y., Zhang, S., Ma, P., Jin, X., Wang, Z., Yao, M., Zhang, E., Tao, B., Qin, Y., et al. (2019). A Tumor-Specific Super-Enhancer Drives Immune Evasion by Guiding Synchronous Expression of PD-L1 and PD-L2. Cell Rep. *29*, 3435–3447.e4. https://doi.org/10.1016/j.celrep.2019.10.093.

75. Green, M.R., Rodig, S., Juszczynski, P., Ouyang, J., Sinha, P., O'Donnell, E., Neuberg, D., and Shipp, M.A. (2012). Constitutive AP-1 Activity and EBV Infection Induce PD-L1 in Hodgkin Lymphomas and Posttransplant Lymphoproliferative Disorders: Implications for Targeted Therapy. Clin. Cancer Res. *18*, 1611–1618. https://doi.org/10.1158/1078-0432.Ccr-11-1942.

76. Zhang, K., Hocker, J.D., Miller, M., Hou, X., Chiou, J., Poirion, O.B., Qiu, Y., Li, Y.E., Gaulton, K.J., Wang, A., et al. (2021). A single-cell atlas of chromatin accessibility in the human genome. Cell *184*, 5985–6001.e19. https://doi.org/10.1016/j.cell.2021.10.024.

77. Domcke, S., Hill, A.J., Daza, R.M., Cao, J., O'Day, D.R., Pliner, H.A., Aldinger, K.A., Pokholok, D., Zhang, F., Milbank, J.H., et al. (2020). A human cell atlas of fetal chromatin accessibility. Science *370*, eaba7612. https://doi.org/10.1126/science.aba7612.

78. Pliner, H.A., Packer, J.S., McFaline-Figueroa, J.L., Cusanovich, D.A., Daza, R.M., Aghamirzaie, D., Srivatsan, S., Qiu, X., Jackson, D., Minkina, A., et al. (2018). Cicero Predicts cis-Regulatory DNA Interactions from Single-Cell Chromatin Accessibility Data. Mol. Cell *71*, 858–871.e8. https://doi.org/10.1016/j.molcel.2018.06.044.

79. Beato, M., Wright, R.H.G., and Dily, F.L. (2020). 90 YEARS OF PROGESTERONE: Molecular mechanisms of progesterone receptor action on the breast cancer genome. J. Mol. Endocrinol. *65*. T65–t79. https://doi.org/10.1530/jme-19-0266.

80. Filippakopoulos, P., and Knapp, S. (2014). Targeting bromodomains: epigenetic readers of lysine acetylation. Nat. Rev. Drug Discov. *13*, 337–356. https://doi.org/10.1038/nrd4286.

81. Lu, J., Qian, Y., Altieri, M., Dong, H., Wang, J., Raina, K., Hines, J., Winkler, J.D., Crew, A.P., Coleman, K., and Crews, C.M. (2015). Hijacking the E3 Ubiquitin Ligase Cereblon to Efficiently Target BRD4. Chem. Biol. *22*, 755–763. https://doi.org/10.1016/j.chembiol.2015.05.009.

82. Hu, J., Hu, B., Xu, F., Wang, M., Qin, C., McEachern, D., Stuckey, J., and Wang, S. (2023). Precise Conformational Control Yielding Highly Potent and Exceptionally Selective BRD4 Degraders with Strong Antitumor Activity. J. Med. Chem. *66*, 8222–8237. https://doi.org/10.1021/acs.jmedchem.3c00520.

83. Kinder, J.M., Jiang, T.T., Ertelt, J.M., Xin, L., Strong, B.S., Shaaban, A.F., and Way, S.S. (2015). Cross-Generational Reproductive Fitness Enforced by Microchimeric Maternal Cells. Cell *162*, 505–515. https://doi.org/10.1016/j.cell.2015.07.006.

84. Moffett-King, A. (2002). Natural killer cells and pregnancy. Nat. Rev. Immunol. *2*, 656–663. https://doi.org/10.1038/nri886.

85. Fu, B., Li, X., Sun, R., Tong, X., Ling, B., Tian, Z., and Wei, H. (2013). Natural killer cells promote immune tolerance by regulating inflammatory TH17 cells at the human maternal-fetal interface. Proc. Natl. Acad. Sci. USA *110*, E231–E240. https://doi.org/10.1073/pnas.1206322110.

86. Wang, F., Qualls, A.E., Marques-Fernandez, L., and Colucci, F. (2021). Biology and pathology of the uterine microenvironment and its natural killer cells. Cell. Mol. Immunol. *18*, 2101–2113. https://doi.org/10.1038/s41423-021-00739-z.

87. Mellor, A.L., and Munn, D.H. (2004). Ido expression by dendritic cells: tolerance and tryptophan catabolism. Nat. Rev. Immunol. *4*, 762–774. https://doi.org/10.1038/nri1457.

88. True, H., Blanton, M., Sureshchandra, S., and Messaoudi, I. (2022). Monocytes and macrophages in pregnancy: The good, the bad, and the ugly. Immunol. Rev. *308*, 77–92. https://doi.org/10.1111/imr.13080.

89. Petroff, M.G., Chen, L., Phillips, T.A., Azzola, D., Sedlmayr, P., and Hunt, J.S. (2003). B7 family molecules are favorably positioned at the human maternal-fetal interface. Biol. Reprod. *68*, 1496–1504. https://doi.org/10.1095/biolreprod.102.010058.

90. Li, Q., Sharkey, A., Sheridan, M., Magistrati, E., Arutyunyan, A., Huhn, O., Sancho-Serra, C., Anderson, H., McGovern, N., Esposito, L., et al. (2024). Human uterine natural killer cells regulate differentiation of extravillous trophoblast early in pregnancy. Cell Stem Cell *31*, 181–195.e9. https://doi.org/10.1016/j.stem.2023.12.013.

91. Arck, P.C., Rücke, M., Rose, M., Szekeres-Bartho, J., Douglas, A.J., Pritsch, M., Blois, S.M., Pincus, M.K., Bärenstrauch, N., Dudenhausen, J.W., et al. (2008). Early risk factors for miscarriage: a prospective cohort study in pregnant women. Reprod. Biomed. Online *17*, 101–113. https://doi.org/10.1016/s1472-6483(10)60300-8.

92. Coomarasamy, A., Devall, A.J., Brosens, J.J., Quenby, S., Stephenson, M.D., Sierra, S., Christiansen, O.B., Small, R., Brewin, J., Roberts, T.E., et al. (2020). Micronized vaginal progesterone to prevent miscarriage: a critical evaluation of randomized evidence. Am. J. Obstet. Gynecol. *223*, 167–176. https://doi.org/10.1016/j.ajog.2019.12.006.

93. Coomarasamy, A., Devall, A.J., Cheed, V., Harb, H., Middleton, L.J., Gallos, I.D., Williams, H., Eapen, A.K., Roberts, T., Ogwulu, C.C., et al. (2019). A Randomized Trial of Progesterone in Women with Bleeding in Early Pregnancy. N. Engl. J. Med. *380*, 1815–1824. https://doi.org/10.1056/NEJMoa1813730.

94. Sachdev, J.C., Bauer, T.M., Chawla, S.P., Pant, S., Patnaik, A., Wainberg, Z.A., Inamdar, S.P., Marina, N., Sun, S., Schmidt, M., et al. (2019). Phase 1a/1b study of first-in-class B7-H4 antibody, FPA150, as monotherapy in patients with advanced solid tumors. J. Clin. Oncol. *37*, 2529. https://doi.org/10.1200/JCO.2019.37.15_suppl.2529.

95. Kinneer, K., Wortmann, P., Cooper, Z.A., Dickinson, N.J., Masterson, L., Cailleau, T., Hutchinson, I., Vijayakrishnan, B., McFarlane, M., Ball, K., et al. (2023). Design and Preclinical Evaluation of a Novel B7-H4-Directed Antibody-Drug Conjugate, AZD8205, Alone and in Combination with the PARP1-Selective Inhibitor AZD5305. Clin. Cancer Res. *29*, 1086–1101. https://doi.org/10.1158/1078-0432.Ccr-22-2630.

96. Iizuka, A., Nonomura, C., Ashizawa, T., Kondou, R., Ohshima, K., Sugino, T., Mitsuya, K., Hayashi, N., Nakasu, Y., Maruyama, K., et al. (2019). A T-cell–engaging B7-H4/CD3-bispecific Fab-scFv Antibody Targets Human Breast Cancer. Clin. Cancer Res. *25*, 2925–2934. https://doi.org/10.1158/1078-0432.Ccr-17-3123.

97. Trojer, P. (2022). Targeting BET Bromodomains in Cancer. Annu. Rev. Cancer Biol. *6*, 313–336. https://doi.org/10.1146/annurev-cancerbio-070120-103531.

98. Sharma, A., Seow, J.J.W., Dutertre, C.A., Pai, R., Blériot, C., Mishra, A., Wong, R.M.M., Singh, G.S.N., Sudhagar, S., Khalilnezhad, S., et al. (2020). Onco-fetal Reprogramming of Endothelial Cells Drives Immunosuppressive Macrophages in Hepatocellular Carcinoma. Cell *183*, 377–394.e21. https://doi.org/10.1016/j.cell.2020.08.040.

99. Sharma, A., Blériot, C., Currenti, J., and Ginhoux, F. (2022). Oncofetal reprogramming in tumour development and progression. Nat. Rev. Cancer *22*, 593–602. https://doi.org/10.1038/s41568-022-00497-8.

100. Tafuri, A., Alferink, J., Möller, P., Hämmerling, G.J., and Arnold, B. (1995). T cell awareness of paternal alloantigens during pregnancy. Science *270*, 630–633. https://doi.org/10.1126/science.270.5236.630.

101. Mellor, A.L., Sivakumar, J., Chandler, P., Smith, K., Molina, H., Mao, D., and Munn, D.H. (2001). Prevention of T cell-driven complement activation and inflammation by tryptophan catabolism during pregnancy. Nat. Immunol. *2*, 64–68. https://doi.org/10.1038/83183.

102. Erlebacher, A., Vencato, D., Price, K.A., Zhang, D., and Glimcher, L.H. (2007). Constraints in antigen presentation severely restrict T cell recognition of the allogeneic fetus. J. Clin. Invest. *117*, 1399–1411. https://doi.org/10.1172/JCI28214.

103. Lissauer, D., Piper, K., Goodyear, O., Kilby, M.D., and Moss, P.A.H. (2012). Fetal-specific CD8+ cytotoxic T cell responses develop during normal human pregnancy and exhibit broad functional capacity. J. Immunol. *189*, 1072–1080. https://doi.org/10.4049/jimmunol.1200544.

104. Chaturvedi, V., Ertelt, J.M., Jiang, T.T., Kinder, J.M., Xin, L., Owens, K.J., Jones, H.N., and Way, S.S. (2015). CXCR3 blockade protects against Listeria monocytogenes infection-induced fetal wastage. J. Clin. Invest. *125*, 1713–1725. https://doi.org/10.1172/JCI78578.

105. Moldenhauer, L.M., Diener, K.R., Hayball, J.D., and Robertson, S.A. (2017). An immunogenic phenotype in paternal antigen-specific CD8+ T cells at embryo implantation elicits later fetal loss in mice. Immunol. Cell Biol. *95*, 705–715. https://doi.org/10.1038/icb.2017.41.

106. Barton, B.M., Xu, R., Wherry, E.J., and Porrett, P.M. (2017). Pregnancy promotes tolerance to future offspring by programming selective dysfunction in long-lived maternal T cells. J. Leukoc. Biol. *101*, 975–987. https://doi.org/10.1189/jlb.1A0316-135R.

107. Kinder, J.M., Turner, L.H., Stelzer, I.A., Miller-Handley, H., Burg, A., Shao, T.Y., Pham, G., and Way, S.S. (2020). CD8+ T Cell Functional Exhaustion Overrides Pregnancy-Induced Fetal Antigen Alloimmunization. Cell Rep. *31*, 107784. https://doi.org/10.1016/j.celrep.2020.107784.

108. Lewis, E.L., Xu, R., Beltra, J.C., Ngiow, S.F., Cohen, J., Telange, R., Crane, A., Sawinski, D., Wherry, E.J., and Porrett, P.M. (2022). NFAT-dependent and -independent exhaustion circuits program maternal CD8 T cell hypofunction in pregnancy. J. Exp. Med. *219*, e20201599. https://doi.org/10.1084/jem.20201599.

109. Miller, D., Romero, R., Myers, L., Xu, Y., Arenas-Hernandez, M., Galaz, J., Soto, C., Done, B., Quiroz, A., Awonuga, A.O., et al. (2023). Immunosequencing and Profiling of T Cells at the Maternal-Fetal Interface of Women with Preterm Labor and Chronic Chorioamnionitis. J. Immunol. *211*, 1082–1098. https://doi.org/10.4049/jimmunol.2300201.

110. Otun, H.A., Lash, G.E., Innes, B.A., Bulmer, J.N., Naruse, K., Hannon, T., Searle, R.F., and Robson, S.C. (2011). Effect of tumour necrosis factor-α in combination with interferon-γ on first trimester extravillous trophoblast invasion. J. Reprod. Immunol. *88*, 1–11. https://doi.org/10.1016/j.jri.2010.10.003.

111. Lash, G.E., Otun, H.A., Innes, B.A., Kirkley, M., De Oliveira, L., Searle, R.F., Robson, S.C., and Bulmer, J.N. (2006). Interferon-gamma inhibits extravillous trophoblast cell invasion by a mechanism that involves both changes in apoptosis and protease levels. FASEB J *20*, 2512–2518. https://doi.org/10.1096/fj.06-6616com.

112. Xiong, S., Sharkey, A.M., Kennedy, P.R., Gardner, L., Farrell, L.E., Chazara, O., Bauer, J., Hiby, S.E., Colucci, F., and Moffett, A. (2013). Maternal uterine NK cell-activating receptor KIR2DS1 enhances placentation. J. Clin. Invest. *123*, 4264–4272. https://doi.org/10.1172/JCI68991.

113. Sotnikova, N., Voronin, D., Antsiferova, Y., and Bukina, E. (2014). Interaction of decidual CD56+ NK with trophoblast cells during normal pregnancy and recurrent spontaneous abortion at early term of gestation. Scand. J. Immunol. *80*, 198–208. https://doi.org/10.1111/sji.12196.

114. Sliz, A., Locker, K.C.S., Lampe, K., Godarova, A., Plas, D.R., Janssen, E.M., Jones, H., Herr, A.B., and Hoebe, K. (2019). Gab3 is required for IL-2- and IL-15-induced NK cell expansion and limits trophoblast invasion during pregnancy. Sci. Immunol. *4*, eaav3866. https://doi.org/10.1126/sciimmunol.aav3866.

115. Mohammed, H., Russell, I.A., Stark, R., Rueda, O.M., Hickey, T.E., Tarulli, G.A., Serandour, A.A., Birrell, S.N., Bruna, A., Saadi, A., et al. (2015). Progesterone receptor modulates ERα action in breast cancer. Nature *523*, 313–317. https://doi.org/10.1038/nature14583.

116. Chan, H.L., Beckedorff, F., Zhang, Y., Garcia-Huidobro, J., Jiang, H., Colaprico, A., Bilbao, D., Figueroa, M.E., LaCava, J., Shiekhattar, R., and Morey, L. (2018). Polycomb complexes associate with enhancers and promote oncogenic transcriptional programs in cancer through multiple mechanisms. Nat. Commun. *9*, 3377. https://doi.org/10.1038/s41467-018-05728-x.

117. Le Dily, F., Baù, D., Pohl, A., Vicent, G.P., Serra, F., Soronellas, D., Castellano, G., Wright, R.H.G., Ballare, C., Filion, G., et al. (2014). Distinct structural transitions of chromatin topological domains correlate with coordinated hormone-induced gene regulation. Genes Dev. *28*, 2151–2162. https://doi.org/10.1101/gad.241422.114.

118. Bi, M., Zhang, Z., Jiang, Y.Z., Xue, P., Wang, H., Lai, Z., Fu, X., De Angelis, C., Gong, Y., Gao, Z., et al. (2020). Enhancer reprogramming driven by high-order assemblies of transcription factors promotes phenotypic plasticity and breast cancer endocrine resistance. Nat. Cell Biol. *22*, 701–715. https://doi.org/10.1038/s41556-020-0514-z.

119. Need, E.F., Selth, L.A., Trotta, A.P., Leach, D.A., Giorgio, L., O'Loughlin, M.A., Smith, E., Gill, P.G., Ingman, W.V., Graham, J.D., and Buchanan, G. (2015). The unique transcriptional response produced by concurrent estrogen and progesterone treatment in breast cancer cells results in upregulation of growth factor pathways and switching from a Luminal A to a Basal-like subtype. BMC Cancer *15*, 791. https://doi.org/10.1186/s12885-015-1819-3.

120. Singh, A.A., Schuurman, K., Nevedomskaya, E., Stelloo, S., Linder, S., Droog, M., Kim, Y., Sanders, J., van der Poel, H., Bergman, A.M., et al. (2019). Optimized ChIP-seq method facilitates transcription factor profiling in human tumors. Life Sci. Alliance *2*, e201800115. https://doi.org/10.26508/lsa.201800115.

121. Reddy, J., Fonseca, M.A.S., Corona, R.I., Nameki, R., Segato Dezem, F., Klein, I.A., Chang, H., Chaves-Moreira, D., Afeyan, L.K., Malta, T.M., et al. (2021). Predicting master transcription factors from pan-cancer expression data. Sci. Adv. *7*, eabf6123. https://doi.org/10.1126/sciadv.abf6123.

122. Schultz, M.D., He, Y., Whitaker, J.W., Hariharan, M., Mukamel, E.A., Leung, D., Rajagopal, N., Nery, J.R., Urich, M.A., Chen, H., et al. (2015). Human body epigenome maps reveal noncanonical DNA methylation variation. Nature *523*, 212–216. https://doi.org/10.1038/nature14465.

123. La Greca, A., Bellora, N., Le Dily, F., Jara, R., Nacht, A.S., Quilez Oliete, J., Villanueva, J.L., Vidal, E., Merino, G., Fresno, C., et al. (2022). Chromatin topology defines estradiol-primed progesterone receptor and PAX2 binding in endometrial cancer cells. Elife *11*, e66034. https://doi.org/10.7554/eLife.66034.

124. Takaku, M., Grimm, S.A., De Kumar, B., Bennett, B.D., and Wade, P.A. (2020). Cancer-specific mutation of GATA3 disrupts the transcriptional regulatory network governed by Estrogen Receptor alpha, FOXA1 and GATA3. Nucleic Acids Res. *48*, 4756–4768. https://doi.org/10.1093/nar/gkaa179.

125. Shu, S., Lin, C.Y., He, H.H., Witwicki, R.M., Tabassum, D.P., Roberts, J.M., Janiszewska, M., Huh, S.J., Liang, Y., Ryan, J., et al. (2016). Response and resistance to BET bromodomain inhibitors in triple-negative breast cancer. Nature *529*, 413–417. https://doi.org/10.1038/nature16508.

126. Kallol, S., Martin-Sancho, L., Morey, R., Aisagbonhi, O., Pizzo, D., Meads, M., Chanda, S.K., and Soncin, F. (2023). Activation of the Interferon Pathway in Trophoblast Cells Productively Infected with SARS-CoV-2. Stem Cells Dev. *32*, 225–236. https://doi.org/10.1089/scd.2022.0255.

127. Liu, X., Ouyang, J.F., Rossello, F.J., Tan, J.P., Davidson, K.C., Valdes, D.S., Schröder, J., Sun, Y.B.Y., Chen, J., Knaupp, A.S., et al. (2020). Reprogramming roadmap reveals route to human induced trophoblast stem cells. Nature *586*, 101–107. https://doi.org/10.1038/s41586-020-2734-6.128.

128. Satija, R., Farrell, J.A., Gennert, D., Schier, A.F., and Regev, A. (2015). Spatial reconstruction of single-cell gene expression data. Nat Biotechnol *33*, 495–502. https://doi.org/10.1038/nbt.3192.

129. McInnes, et al. (2018). UMAP: Uniform Manifold Approximation and Projection. Journal of Open Source Software *3* (29), 861. https://doi.org/10.21105/joss.00861.

130. Kuleshov, M.V., Jones, M.R., Rouillard, A.D., Fernandez, N.F., Duan, Q., Wang, Z., Koplev, S., Jenkins, S.L., Jagodnik, K.M., Lachmann, A., McDermott, M.G., Monteiro, C.D., Gundersen, G.W., and Ma'ayan, A. (2016). Enrichr: a comprehensive gene set enrichment analysis web server 2016 update. Nucleic Acids Res *44*. W90–7. https://doi.org/10.1093/nar/gkw377.

131. Subramanian, A., Tamayo, P., Mootha, V.K., Mukherjee, S., Ebert, B.L., Gillette, M.A., Paulovich, A., Pomeroy, S.L., Golub, T.R., Lander, E.S., and Mesirov, J.P. (2005). Gene set enrichment analysis: a knowledge-based approach for interpreting genome-wide expression profiles. Proc. Natl. Acad. Sci. USA *102*, 15545–15550. https://doi.org/10.1073/pnas.0506580102.

132. Schindelin, J., Arganda-Carreras, I., Frise, E., Kaynig, V., Longair, M., Pietzsch, T., Preibisch, S., Rueden, C., Saalfeld, S., Schmid, B., Tinevez, J.Y., White, D.J., Hartenstein, V., Eliceiri, K., Tomancak, P., and Cardona, A. (2012). Fiji: an open-source platform for biological-image analysis. Nat Methods. *9*. 676–82. https://doi.org/10.1038/nmeth.2019.

133. Peng, D., Tanikawa, T., Li, W., Zhao, L., Vatan, L., Szeliga, W., Wan, S., Wei, S., Wang, Y., Liu, Y., et al. (2016). Myeloid-Derived Suppressor Cells Endow Stem-like Qualities to Breast Cancer Cells through IL6/STAT3 and NO/NOTCH Cross-talk Signaling. Cancer Res. *76*, 3156–3165. https://doi.org/10.1158/0008-5472.Can-15-2528.

134. Van Keuren, M.L., and Saunders, T.L. (2004). Rederivation of transgenic and gene-targeted mice by embryo transfer. Transgenic Res. *13*, 363–371. https://doi.org/10.1023/b:trag.0000040040.82536.a5.

135. Yu, J., Green, M.D., Li, S., Sun, Y., Journey, S.N., Choi, J.E., Rizvi, S.M., Qin, A., Waninger, J.J., Lang, X., et al. (2021). Liver metastasis restrains immunotherapy efficacy via macrophage-mediated T cell elimination. Nat. Med. *27*, 152–164. https://doi.org/10.1038/s41591-020-1131-x.

136. De Clercq, K., Hennes, A., and Vriens, J. (2017). Isolation of Mouse Endometrial Epithelial and Stromal Cells for In Vitro Decidualization. J. Vis. Exp. 55168. https://doi.org/10.3791/55168.

137. Ran, F.A., Hsu, P.D., Wright, J., Agarwala, V., Scott, D.A., and Zhang, F. (2013). Genome engineering using the CRISPR-Cas9 system. Nat. Protoc. *8*, 2281–2308. https://doi.org/10.1038/nprot.2013.143.

138. Dekker, J., Rippe, K., Dekker, M., and Kleckner, N. (2002). Capturing chromosome conformation. Science *295*, 1306–1311. https://doi.org/10.1126/science.1067799.

139. Hagège, H., Klous, P., Braem, C., Splinter, E., Dekker, J., Cathala, G., de Laat, W., and Forné, T. (2007). Quantitative analysis of chromosome conformation capture assays (3C-qPCR). Nat. Protoc. *2*, 1722–1733. https://doi.org/10.1038/nprot.2007.243.

140. Hao, Y., Hao, S., Andersen-Nissen, E., Mauck, W.M., 3rd, Zheng, S., Butler, A., Lee, M.J., Wilk, A.J., Darby, C., Zager, M., et al. (2021). Integrated analysis of multimodal single-cell data. Cell *184*, 3573–3587.e29. https://doi.org/10.1016/j.cell.2021.04.048.

STAR★METHODS

KEY RESOURCES TABLE

REAGENT or RESOURCE	SOURCE	IDENTIFIER
Antibodies		
Anti-human HLA-G	Abcam	Clone MEM-G/1; RRID: AB_306053
Anti-human CDH1	GeneTex	GTX100443; RRID: AB_10729586
Anti-human SDC1	Biolegend	Clone MI15; RRID: AB_2561790
Anti-human CD3	Agilent	A0452; RRID: AB_2335677
Anti-human CD8	Agilent	M7103; RRID: AB_2075537
Anti-human HLA-G	Abcam	Clone 4H84; RRID: AB_880552
Anti-mouse CD8 AF700	BD Biosciences	Clone 53–6.7; RRID: AB_396959
Anti-mouse CD90 FITC	BD Biosciences	Clone 53–2.1; RRID: AB_465151
Anti- mouse CD4 APC	Thermo Fisher	Cat# 551980; RRID: AB_398521
Anti- mouse CD44 BV786	BD Biosciences	Clone IM7; RRID: AB_2738395
Anti- mouse CD69 PE/CY7	Thermo Fisher	Cat# 561930; RRID: AB_394508
Anti- mouse CD25 APC	BD Biosciences	Clone PC61.5; RRID: AB_469366
Anti- mouse CD45 BUV395	BD Biosciences	Cat#564279; RRID: AB_2651134
Anti-mouse CD3 FITC	Thermo Fisher	Cat#16-0031-82; RRID: AB_464882
Anti-mouse IFN-γ BV786	BD Biosciences	Cat#563773; RRID: AB_2738419
Anti-mouse TNF-α PE/Cy7	BD Biosciences	Cat#557644; RRID: AB_396761
Anti-mouse NK1.1 BV605	BD Biosciences	Cat#563220; RRID: AB_2738077
Anti-mouse Ly49D FITC	Biolegend	Cat#138303; RRID: AB_10588709
Anti-mouse Ly49H PE-Cy7	Biolegend	Cat#144706; RRID: AB_2561674
Anti-mouse Ly49A PE	Thermo Fisher	Cat#12-5856-82; RRID: AB_1311270
Anti-mouse Ly49C FITC	Leinco	Clone 4LO3311; RRID: N/A
Anti-mouse Ly49G2 PE/Cy7	BD Biosciences	Cat#560730; RRID: AB_1727551
Anti-mouse H-2D^{b} PE/Cy7	Biolegend	Cat#111516; RRID: AB_2565863
Anti-mouse H-2D^{d} APC	Biolegend	Cat#114714; RRID: AB_2734174
Anti-mouse H-2K^{b} APC	Biolegend	Cat#116518; RRID: AB_10568693
Anti-mouse H2K^{d} PE-Cy7	Biolegend	Cat#116622; RRID: AB_2562733
Anti-mouse CK7 PE	Abcam	Cat#ab213193; RRID: N/A
Anti-B7-H4 Alexa Fluor 594	Abcam	Cat#ab277937; RRID: N/A
Anti-mouse TCF-1 PE	BD Biosciences	Cat#564217; RRID: AB_2687845
Anti-TOX BV515	Miltenyi Biotec	Cat#130-129-208; RRID: AB_2922006
Anti-human Granzyme B PE	Thermo Fisher	Cat#25-8898-82; RRID: AB_10853339
Anti-mouse Foxp3	BD Biosciences	Cat#563101; RRID: AB_2738006
IgG (Blocking)	BioXCell	Cat#BE0090; RRID: AB_1107780
Anti-mouse PD-L1 (Blocking)	BioXCell	Cat#BE0101; RRID: AB_10949073
Anti-mouse CD4 (Depleting)	BioXCell	Cat#BE0003-1; RRID: AB_1107636
Anti-mouse CD8 (Depleting)	BioXCell	Cat#BE0117; RRID: AB_10950145
Anti-mouse Foxp3	Cell Signaling Technology	Cat#12653; RRID: AB_2797979
Anti-mouse CD8 (IHC)	Cell Signaling Technology	Cat#98941; RRID: AB_2756376
Anti-human CD8 (IHC)	Abcam	Cat# ab17147; RRID: AB_443686
Anti-B7-H4	Abcam	Cat#ab209242; RRID: AB_2801513
Anti-human PD-L1	Thermo Fisher	Cat#PA5-20343; RRID: AB_11153819
Anti-human BRD4	Cell Signaling Technology	Cat#13440; RRID: AB_2687578
Actin	Cell Signaling Technology	Cat#4967s; RRID: AB_330288

(*Continued on next page*)

Continued

REAGENT or RESOURCE	SOURCE	IDENTIFIER
GAPDH	Cell Signaling Technology	Cat#97166; RRID: AB_627678
Anti-mouse Progesterone receptor	Santa Cruz	Cat#sc-810; RRID: AB_628172
Anti-human Progesterone receptor	Cell Signaling Technology	Cat#8757s; RRID: AB_2797144
Chemicals, peptides, and recombinant proteins		
Phorbol 12-myristate 13-acetate (PMA)	STEMCELL Technologies	Cat#74042
Ionomycin	STEMCELL Technologies	Cat#73724
Brefeldin A	STEMCELL Technologies	Cat#73014
Monensin	STEMCELL Technologies	Cat#100-1162
Progesterone	Cayman Chemical	Cat#15876
β-Estradiol	Cayman Chemical	Cat#10006315
Follicle-stimulating hormone (FSH)	Sigma	Cat#F4021
Luteinizing hormone (LH)	Sigma	Cat#L6420
Human chorionic gonadotropin (hCG)	Sigma	Cat#CG10
Human placental lactogen (hPL)	Sigma	Cat#SRP4869
Medroxyprogesterone (MPA)	Cayman Chemical	Cat#23664
MPA pellet	Innovative Research of America	Cat#NP-161
RU486 pellet	Innovative Research of America	Cat#X-999
Levonorgestrel (LNG)	Cayman Chemical	Cat#10006318
RU486	Cayman Chemical	Cat#10006317
Dimethyl Benz anthracene (DMBA)	Sigma	Cat#D3254
L002	Cayman Chemical	Cat#17778
CCS1477	Cayman Chemical	Cat#34546
JQ1	Cayman Chemical	Cat#11187
ARV-825	Sigma	Cat#SML-3423
BD-9136	Hu et al.[79]	N/A
Critical commercial assays		
Mouse CXCL9/MIG DuoSet ELISA	R&D Systems	Cat#DY492
Mouse CXCL10/IP-10/CRG-2 DuoSet ELISA	R&D Systems	Cat#DY466
Mouse IFN-γ DuoSet ELISA	R&D Systems	Cat#DY485
Mouse TNF-α DuoSet ELISA	R&D Systems	Cat#DY410
Mouse/Rat B7-H4 ELISA Kit	Abcam	Cat#ab263879
Simple ChIP Enzymatic Chromatin IP Kit (Magnetic Beads)	Cell Signaling Technology	Cat#9003
Rapid Detection of Firefly Luciferase Activity	Promega	Cat#E1500
OPAL-3-plex detection kit	AKOYA	NEL810001KT
OPAL 620 reagent	AKOYA	FP1495001KT
Deposited Data		
Human breast cancer (BRCA) scRNA-seq dataset I	Gao et al.[48]	GSE148673
Human BRCA scRNA-seq dataset II	Bhupinder et al.[46]	GSE161529
Human BRCA scRNA-seq and bulk RNA-seq dataset	Bassez et al.[49]	EGAD00001006608
Human ovarian, colorectal and breast cancer scRNA-seq dataset	Qian et al.[45]	E-MTAB-8107
Human endometrial cancer scRNA-seq dataset	Guo et al.[44]	PRJNA650549
Human ovarian cancer scRNA-seq dataset	Shih et al.[51]	GSE118828
Human lung carcinoma scRNA-seq dataset	Lambrechts et al.[50]	E-MTAB-6149
Human and mouse lung carcinoma scRNA-seq dataset	Zilionis et al.[47]	GSE127465
scRNA-seq of fetal-maternal interface in human first trimester	Vento-Tormo et al.[52]	E-MTAB-6701
Human first trimester placenta and decidua scRNA-seq dataset	Suryawanshi et al.[53]	PRJNA492324
Human first trimester placenta villi scRNA-seq dataset	Sun et al.[54]	GSE131696
Human first trimester placenta scRNA-seq dataset	Han et al.[55]	GSE134355
Human first trimester placenta and decidua scRNA-seq dataset	Zheng et al.[56]	GSE174399

(*Continued on next page*)

Continued

REAGENT or RESOURCE	SOURCE	IDENTIFIER
Human first trimester placenta villi scRNA-seq dataset	Shannon et al.[57]	GSE174481
Bulk RNA-seq human breast cancer treated with RU486	Elia et al.[68]	GSE212690
PR ChIP-seq in T-47D	Mohammed et al.[115]	GSE68359
ATAC-seq and H3K ChIP-seq in T-47D	Chan et al.[116]	GSE107176
Hi-C of T-47D	Le Dily et al.[117]	GSE53463
H3K27ac ChIP-Seq in ZR-75-1	Bi et al.[118]	GSE128460
PR ChIP-Seq in ZR-75-1	Need et al.[119]	PRJNA252531
H3K27ac ChIP-Seq in human tumor tissues	Singh et al.[120]	GSE114737
H3K27ac ChIP-Seq in human tumor tissues	Reddy et al.[121]	GSE152885
H3K27ac and H3K4me1 ChIP-Seq in Human placenta	Schultz et al.[122]	GSE18927
PR ChIP-Seq in human endometrium	La Greca et al.[123]	GSE132713
H3K27ac ChIP-seq in T-47D	Takaku et al.[124]	GSE130703
BRD4 ChIP-Seq in T47D	Shu et al.[125]	GSE63584
Bulk RNA-seq of trophoblast cells	Kallol et al.[126]	GSE216484
Bulk RNA-seq of trophoblast cells	Liu et al.[127]	GSE150616
Single nuclei RNA-seq of mouse placental labyrinth	Marsh et al.[61]	GSE152248
Experimental Models: Cell Lines		
HEK293T	ATCC	CRL-3126
JEG-3	ATCC	HTB-36
T-47D	ATCC	HTB-133
ZR-75-1	ATCC	CRL-1500
UACC-812	ATCC	CRL-1897
CAMA-1	ATCC	HTB-21
MDA-MB-231	ATCC	CRM-HTB-26
4T-1	ATCC	CRL-2539
OVKATE	AcceGen	ABC-TC0882
OVCAR-3	ATCC	HTB-161
LNCaP	ATCC	CRL-1740
3E10	This paper	N/A
4H11	This paper	N/A
4H11 sgCTRL	This paper	N/A
4H11 B7-H4$^{-/-}$	This paper	N/A
Experimental Models: Organisms/Strains		
Mouse: C57BL/6J	The Jackson Laboratory	Stock No: 000664
Mouse: OT-I	The Jackson Laboratory	Stock No: 003831
Mouse: BALB/c	The Jackson Laboratory	Stock No: 000651
Mouse: B7-H4$^{-/-}$	Zhu et al.[60]	N/A
Mouse: RAG1$^{-/-}$	The Jackson Laboratory	Stock No: 002216
Mouse: CBA/J	The Jackson Laboratory	Stock No: 000656
Mouse: RAG1$^{-/-}$B7-H4$^{-/-}$	This paper	N/A
Mouse: CBA/J B7-H4$^{-/-}$	This paper	N/A
Software and Algorithms		
Prism 9.0	https://www.graphpad.com	Commercial
Rstudio 3.6.0	https://rstudio.com	RStudio Team (2020). RStudio: Integrated Development for R. RStudio, PBC, Boston, MA
Seurat 2.3.4	https://satijalab.org/seurat/	Satija et al.[128]
UMAP 0.3.9	https://github.com/lmcinnes/umap	McInnes et al.[129]
Enrichr	https://maayanlab.cloud/Enrichr/	Kuleshov et al.[130]

(*Continued on next page*)

Continued

REAGENT or RESOURCE	SOURCE	IDENTIFIER
GSEA 3.0	https://www.gsea-msigdb.org/gsea/index.jsp	Subramanian et al.[131]
QuPath	https://qupath.github.io/	N/A
Fiji	https://imagej.net/software/fiji/	Schindelin et al.[132]
Flowjo 10.8.1	https://www.flowjo.com/	Commercial
Cytobank	https://premium.cytobank.org	Commercial
Image Lab Software	https://www.bio-rad.com/en-us/product/image-lab-software?ID=KRE6P5E8Z	Commercial
IGV 2.16.1	https://www.igv.org/	Commercial
BioRender	https://www.biorender.com/	Commercial

RESOURCE AVAILABILITY

Lead contact

Further information and requests for materials should be directed to the lead contact: Weiping Zou (wzou@umich.edu).

Materials availability

Request for cell lines and plasmids generated from this manuscript should be directed to the lead contact.

Data and code availability

- Data used in this manuscript are all publicly available with accession number indicated in the key resources table.
- This paper does not report original code.
- Any additional information is available from the lead contact upon reasonable request.

EXPERIMENTAL MODEL AND STUDY PARTICIPANT DETAILS

Human studies

Human breast cancer tissues were reported before.[133] Human endometrial cancer tissue samples used for initial diagnosis were collected from patients recruited at the First Department of Oncologic Gynecology and Gynecology, Medical University of Lublin, Poland. Declaration of Helsinki and approved by the Institutional Ethics Committee of the Medical University of Lublin (registration no. KE-0254/270/2021). Human endometrial epithelial cells (HEECs) were collected for Reproductive Subject Registry and Sample Repository (RSRSR) study managed by the Department of Obstetrics and Gynecology in Michigan Medicine, under the IRB#REP00000077 and HUM00195340. Human amniotic epithelial cells (7110) and human amniotic mesenchymal stromal cells (7140) were purchased from ScienCell. The human products of conception (POCs) were collected for ''Biomarker analysis and molecular characterization of gynecologic neoplasms and non-neoplastic processes of interest'' study managed by the Department of Pathology in Michigan Medicine, under the IRB#HUM00054493. POCs from elective abortion in first trimester were used for the present study.

Animals

C57BL/6 (Stock#000664), BALB/c (Stock#000651), CBA/J (Stock#000656), Rag1 KO (Stock#002216), and OT-1 (Stock#003831) mice (aged 6–8 weeks) were obtained from the Jackson Laboratory. B7-H4$^{-/-}$ mice on B6 background were reported previously.[63] C57BL/6 mice were bred in-house to generate age-matched wild-type (WT) control mice for B7-H4$^{-/-}$ mice. B7-H4$^{-/-}$ mice were bred with CBA/J mice to generate B7-H4$^{-/-}$ mice on CBA/J background. B7-H4$^{-/-}$ mice were bred with RAG1 KO mice to generate RAG1$^{-/-}$B7-H4$^{-/-}$ mice. RAG1$^{-/-}$ mice were bred in-house to get age-matched control (RAG1$^{-/-}$B7-H4$^{+/+}$) mice for RAG1$^{-/-}$B7-H4$^{-/-}$ mice. Six- to twenty-week-old female mice were age-matched in different groups and used for pregnancy and tumor models. All mice were maintained under pathogen-free conditions and housing with a maximum of five mice per cage. Animal studies were conducted under the approval of the Institutional Animal Care & Use Committee (IACUC) at the University of Michigan (PRO00010169).

Cell lines

Human breast cancer cell lines T-47D, ZR-75-1, CAMA-1, UACC-812, MDA-MB-231, mouse breast cancer cell line 4T1, human trophoblast cell line JEG-3, human embryonic cell line HEK293T, human ovarian cell line OVCAR-3 and OVKATE, and human prostate

cancer cell line LNCaP were purchased from the American Type Culture Collection (ATCC). 4H11 and 3E10 cells were two clones isolated from spontaneous breast tumor induced by MPA plus DMBA in C57BL/6 mice. HEK293T luciferase expression cells were established by transfection with the pGL3-basic or modified plasmids. All the cell lines in culture were regularly tested to be mycoplasma-free every 2 weeks.

Pregnancy models

Female and male mice were mated late in the afternoon. Vaginal plug check was performed in the morning of the following day. If the plug was present, the mouse was considered as gestational day 0.5. To examine the fetus resorption, pregnant mice were euthanized at indicated gestational days. Embryo transfer experiments were performed in the Transgenic Animal Model Core as previously described.[134] 3-4 week-old female mice were treated with PMSG and hCG, and then mated with male mice. Embryos were collected and transferred to pseudo-pregnant CBA/J mice. Pregnancy outcome was evaluated 13.5–14.5 days post embryo transfer.

Tumor models

The spontaneous breast cancer model was induced by MPA plus DMBA as reported previously.[71,72] Number of evaluable tumor nodules, tumor size, tumor-free survival and overall survival of mice were monitored. Transplant mouse tumor model was established using primary tumor cells derived from spontaneous breast tumor induced by MPA plus DMBA. Primary tumor cells were first isolated from the spontaneous tumor induced in C57BL/6 mice and then passaged *in vivo* in C57BL/6 mice for further expansion. Primary tumor cells from the second *in vivo* passage were used to establish transplant tumors for therapy models.

METHOD DETAILS

Animal studies

The spontaneous tumor model was induced by MPA plus DMBA as reported.[71,72] Briefly, age-matched female WT and B7-H4$^{-/-}$ mice were implanted with a pellet containing 50-mg-90 days-slow-releasing MPA (Innovative Research of America, NP-161) subcutaneously. Then, mice were administered 6 doses of 1 mg 7,12-dimethylbenz[*a*]anthracene (DMBA; Millipore Sigma, D3254) weekly by oral gavage. DMBA was dissolved in corn oil (Millipore Sigma, C8267) at 5 mg/mL. After the last dose of DMBA, the mice were routinely checked for the appearance of tumor growth. Evaluable tumor numbers were recorded. Tumor length and width were measured with a caliper. The tumor area was calculated as (length x width) x π/4. Tumor-free survival and overall survival of mice were monitored. To establish transplantable tumors, primary cells were isolated from 9 individual tumor nodules from 2 tumor-bearing WT mice through enzymatic digestion. Freshly isolated primary cells (1 x 10^7 cells) were inoculated into WT mice subcutaneously for *in vivo* passage and expansion. Primary cells (1 x 10^7 cells) from the second passage were used to establish subcutaneous transplant tumors for therapy models using RU486, BD-9136 or anti-PD-L1. For RU486 and anti-PD-L1 combination therapy, mice were randomized to 4 experimental groups (Placebo and IgG, RU486 and IgG, Placebo and anti-PD-L1, RU486 and anti-PD-L1) 7 days post-tumor inoculation. Each treatment group has 8 mice with bilateral subcutaneous tumors. Anti-PD-L1 (100 μg, BioXCell, BE0101) was given to mice intraperitoneally every 3 days, starting from 7 days post-inoculation. Placebo or RU486 pellets were implanted on 8 days post-inoculation. For BD-9136 and anti-PD-L1 combination therapy, mice were randomized to 4 experimental groups (vehicle and IgG, BD-9136 and IgG, vehicle and anti-PD-L1, BD9136 and anti-PD-L1) at 3 days post-tumor inoculation. Each treatment group had 5 mice with bilateral subcutaneous tumors. BD-9136 was dissolved at 2 mg/mL in 20% PEG400 (Sigma,91893), 6% Kolliphor EL (Sigma, C5135), and 74% PBS. BD-9136 (20 mg/kg) was given to tumor-bearing mice intraperitoneally 3 times per week, starting from 3 days post-inoculation. Anti-PD-L1 (100 μg, BioXCell, BE0101) was given to mice intraperitoneally every 3 days, starting from 4 days post-inoculation. Tumor-free survival and overall survival of mice were monitored. To examine B7-H4 expression on mouse endometrial epithelial cells (MEECs), RU486 (10 mg/kg) was given to WT mice subcutaneously every two days. Mice were euthanized 6 days after the first dose and the uteri were harvested for isolation of MEECs.

Pregnancy models

Female and male mice were mated late in the afternoon. Age-matched female C57BL/6 (WT) and B7-H4$^{-/-}$ mice were mated with male BALB/c mice for allogeneic mating. Age-matched female C57BL/6 (WT) and B7-H4$^{-/-}$ mice were mated with male C57BL/6 mice for syngeneic mating. Age-matched female RAG1$^{-/-}$B7-H4$^{+/+}$ and RAG1$^{-/-}$B7-H4$^{-/-}$ mice were mated with male BALB/c mice for allogeneic mating. Female B7-H4$^{-/-}$ CBA/J mice were mated with male B7-H4$^{+/-}$ C57BL/6 mice to examine the role of fetal B7-H4. Vaginal plug check was performed in the morning of the following day. If the plug check was positive, the mouse was considered as gestational day 0.5. To examine the fetus resorption, pregnant mice were euthanized at gestational day 13.5 unless otherwise specified. The number of all fetuses and resorbed fetuses were recorded. The fetus resorption rate was calculated as (Number of resorbed fetuses)/(Number of all fetuses) x 100. For depletion of CD4 and CD8 T cells, anti-CD4 (200 μg, BioXCell, BE0003-1) and anti-CD8 (200 μg, BioXCell, BE0117) were given intraperitoneally on gestational days 3.5 and 8.5. The depletion efficiency was confirmed at gestational day 13.5 by flow cytometry in spleen, uterus-draining lymph nodes (LNs), and placental and decidual tissues. Embryo transfer was done as described previously.[116] Briefly, 3-4 week-old age-matched WT and B7-H4$^{-/-}$ female mice (C57BL/6 background) were treated with PMSG (5 I.U., intraperitoneally, 3 days before embryo collection) and hCG (5 I.U., intraperitoneally, 1 day before embryo collection), and then mated with WT and B7-H4$^{-/-}$ male mice (CBA/J background) respectively.

Two-cell embryos from the donors of the indicated genetic backgrounds were collected by dissecting oviducts and ampullae. The eggs were transferred to a dish with M2 medium (MR-106, Sigma). After anesthesia of the recipient mice at the 0.5-day pseudopregnant stage, a standard surgical procedure was implemented in which 20 eggs were microinjected into the oviduct of the recipient. The transfer was done bi-laterally. The pregnancy outcome was examined at gestational day 13.5 or 14.5.

Cell culture

T-47D, ZR-75-1, CAMA-1, UACC-812, OVKATE, OVCAR-3, LNCaP, 4T1 cells, primary tumor cells and isolated mouse breast cancer clones 4H11 and 3E10 were cultured in RPMI 1640 medium. MDA-MB-231 was cultured in DMEM medium. JEG-3 cells were cultured in EMEM medium. HEK293T cells were cultured in DMEM medium. Human Endometrium Epithelial Cells (HEECs) and Mouse Endometrial Epithelial Cells (MEECs) were cultured in DMEM/F12 medium. Primary human amniotic epithelial cells were cultured in Epithelial Cell medium (ScienCell, 4101) and amniotic mesenchymal stromal cells were cultured in Mesenchymal Stem Cell Medium (ScienCell, 7501). For OVCAR-3 cells, the culture medium was supplemented with 20% fetal bovine serum (FBS) and Penicillin-Streptomycin (1x). For other cells, the culture medium was supplemented with 10% FBS and Penicillin-Streptomycin (1x). HEK293T luciferase expression cells were established by transfection with the pGL3-basic plasmid (Promega, E1751). For *in vitro* treatments, ZR-75-1, UACC-812, CAMA-1, JEG-3, OVKATE and primary MEECs were treated with progesterone in RPMI 1640 medium without phenol red supplemented with 10% charcoal-stripped FBS. 4H11 cells were treated with MPA in RPMI 1640 medium without phenol red supplemented with 10% charcoal stripped FBS. All cell lines were regularly tested to be mycoplasma-free every 2 weeks.

Flow cytometry

To prepare cells for flow cytometric analysis, tumor tissues, LNs, spleen, placental and decidual tissues were cut into small pieces and physically passed through 100 μm strainers. Immune cells were enriched by density gradient centrifugation with Ficoll (StemCell, 07851). Cells were collected, washed and then stained with fluorescently conjugated antibodies. For cytokine detection, cell suspensions were incubated in culture medium containing PMA (5 ng/mL), ionomycin (500 ng/mL), Brefeldin A (1:1,000) and Monensin (1:1,000) at 37 °C for 4 h. Extracellular staining using the antibodies listed below was performed for 30 min, then the cells were washed and resuspended in 500 μL of freshly prepared Fixation/Permeabilization solution (Invitrogen, 00-5523-00) at 4 °C overnight. After being washed with Permeabilization/Wash buffer the cells were stained with intracellular antibodies listed below. Data collection and analysis were performed on a LSRFortessa using BD FACS Diva software. Fixable viability stain 575V was purchased from BD Biosciences (565694). The following antibodies were used: CD45 (Clone 30-F11, BD Biosciences), CD90 (Clone 53–2.1, BD Biosciences), CD3 (Clone 145-2C11, Thermo Fisher Scientific), CD8 (Clone 53–6.7, BD Biosciences), CD4 (Clone RM4-5, Thermo Fisher Scientific), CD44 (Clone IM7, BD Biosciences), CD69 (Clone H1.2F3, Thermo Fisher Scientific), CD25 (Clone 7D4, BD Biosciences), IFN-γ (Clone XMG1.2, BD Biosciences), TNF-α (Clone MP6-XT22, BD Biosciences), granzyme B (Clone GB11, BD Biosciences), TCF-1 (Clone S33-966, BD Biosciences), TOX (Clone REA473, Miltenyi), NK1.1 (PK136, BD Biosciences), Ly49A (A1/Ly49A, Biolegend), Ly49C (4LO3311, Leinco Technologies), Ly49D (4E5, Biolegend), Ly49H (3D10, Biolegend), Ly49G2 (4D11, eBioscience), CK7 (EPR17078, Abcam), H-2K^{b} (AF6-88.5.5.3, eBioscience), H-2D^{b} (KH95, Biolegend), H-2K^{d} (SF1-1.1, Biolegend), H-2D^{d} (34-2-12, Biolegend).

Mass cytometry CyTOF

CyTOF procedures, including antibody generation, antibody staining and data acquisition were performed as previously reported.[135] CD11c (N418), CD69 (H1.2F3), CD45 (30-F11), CD11b (M1/70), CD19 (6D5), CD25 (3C7), CD3 (145-2C11), TER-119 (TER119), CD62L (MEL-14), CD8α (53–6.7), TCRβ (H57-597), NK1.1 (PK136), CD44 (IM7), CD4 (RM4-5), B220 (RA3-6B2) were purchased from Fluidigm. Ly6G (1A8), Ly6C (HK1.4), I-A/I-E (M5/114.15.2), Ly49 (14B11), NKp46 (29A1.4), TIM-3 (RMT3-23), NKG2D (CX5), PD-1 (RMP1-30), F4/80 (BM8) were conjugated with metal in house. CyTOF data analyses were performed using the Cytobank platform.

ELISA

Mouse placental and decidual tissues were collected after the pregnant mice were euthanized, weighed, and stored at −80°C. Tissues were homogenized with Dounce homogenizer in RIPA buffer to extract total tissue protein. The lysates were then centrifuged at 8,000 g at 4°C to remove cell debris and dead cells, and supernatants were collected. CXCL9 (DY492), CXCL10 (DY466), IFN-γ (DY485), and TNF-α (DY410) ELISA sets from R&D Systems were used according to the manufacturer's instructions. Mouse B7-H4 ELISA set (ab263879) was used to detect the soluble B7-H4 in the culture supernatant of OT-I and 4H11 cells.

OT-I coculture experiments

OT-I splenocytes were isolated by passing through 100 μm strainers and subsequent density gradient centrifugation with Ficoll. OT-I splenocytes (2 x 10^{5}) were cocultured with 4H11 tumor cells (1 x 10^{4}) in the presence of 1 μM ovalbumin peptide (SIINFEKL), 5 ng/mL IL-2, and 55 μM β-mercaptoethanol (β-ME) in 96-well plates for 3 days. To evaluate the proliferation of OT-I cells, OT-I splenocytes were stained with 1 μM CFSE prior to coculture with tumor cells and examined for proliferation based on CFSE dilution on day 2. To evaluate transcription factor expression and cytokine production, cells were stained for flow cytometry on day 3. For transwell

experiments, a 6.5-mm insert in 24-well plate with a pore size of 0.4 μm was used (Sigma, CLS3397). OT-1 splenocytes (2 x 10^5) were seeded in the insert, and 4H11 tumor cells (1 x 10^4) were seeded in the bottom plate.

Reagents

Follicle-Stimulating Hormone (FSH, F4021), Luteinizing Hormone (LH, L6420), Chorionic gonadotropin human (hCG, CG10), Placental Lactogen human (hPL, SRP4869), 7,12-Dimethylbenz[*a*]anthracene (DMBA, D3254), OVA peptide (SIINFEKL; S7951), ARV-825 (SML-3423), PMSG (G-4877), and HCG (CG-5) were purchased from Sigma. MPA pellets (50 mg, 90 days slow-releasing, NP-161), RU486 pellets (15 mg, 21 days slow-releasing, X-999) and placebo pellets (C-111) were purchased from Innovative Research of America. Progesterone (15876), Medroxyprogesterone 17-acetate (MPA, 23664), Levonorgestrel (LNG, 10006318), 17β-Estradiol (10006315), Mifepristone (RU486, 10006317), CCS1477 (34546), JQ1 (11187), and L002 (17778) were purchased from Cayman Chemical. BD-9136 was provided by Dr. Shaomeng Wang. CFSE was purchased from Invitrogen (C34570). IgG (BE0090), anti-mouse PD-L1 (BE0101), anti-mouse CD4 (BE0003-1), and anti-mouse CD8 (BE0117) were purchased from BioXCell.

Isolation of mouse endometrial epithelial cells (MEECs)

Isolation of MEECs was performed as described previously.[136] Briefly, mouse uterine horns were harvested after euthanasia. Adipose and connective tissues were removed carefully in HBSS buffer. The uterine horns were cut open longitudinally to expose the uterine lumen, washed in HBSS gently, and then transferred to a 15 mL canonical tube containing 2.5% pancreatin (Sigma, P3292) and 0.25% trypsin in 5 mL HBSS. These were incubated on an orbital shaker for 60 min at 4 °C at 50 rpm, 45 min at room temperature, and then 15 min at 37°C. After incubation, the uteri were carefully transferred into the cold DMEM/F12 medium with 10% FBS for 5 min to stop digestion. Then the uteri were transferred to cold HBSS, and vortexed to release the epithelial sheets. Epithelial cells were then collected by centrifuging at 500 x g for 5 min and cultured in DMEM/F12 medium with 10% FBS for further use.

Immunohistochemistry

Tumor and fetal tissues were fixed in formalin and embedded in paraffin. Tissues were sectioned on a rotary microtome at 4 μm thickness and mounted on glass slides. Slides from the embedded tissues were baked for 60 min at 60°C, deparaffinized in xylene, and rehydrated in graded concentrations of ethanol in water. Heat-induced antigen epitope retrieval was performed. AR9 Buffer (pH 9, AKOYA) was used for B7-H4 staining. Diva Decloaking Buffer (pH 6.2, Biocare Medical) was used for other stainings. The slides were then blocked and incubated with mouse CD8 (CST, 98941), human CD8 (Abcam, ab17147), HLA-G (Abcam, ab7759), human SDC1 (Biolegend, 356502), CDH1 (GeneTex, GTX100443), and B7-H4 (Abcam, ab209242), mouse Foxp3 (CST, 12653) primary antibodies at 1:200 dilution overnight at 4°C. Secondary antibody (Rabbit on Rodent HRP-Polymer, Biocare Medical, RMR622) was stained for 30 min at room temperature. The slides were then developed with fresh DAB substrate (Vector, SK-4700) or Metal Enhanced DAB Substrate Kit (Thermo, 34065) under a microscope, washed, counterstained with hematoxylin, mounted with permanent mounting medium and coverslipped. Slides were scanned with Leica Aperio AT2 and images were analyzed with the software QuPath. For multi-color IHC staining, OPAL-3-plex detection kit (AKOYA, NEL810001KT), OPAL 620 reagent (AKOYA, FP1495001KT), anti-HLA-G (Abcam, ab52455), anti-human CD3 (Agilent, A0452), anti-human CD8 (Agilent, M7103), and anti-B7-H4 (Abcam, ab209242) were used for staining. Stained slides were scanned on the Mantra Automated Quantitative Pathology Imaging System and analyzed using Inform software (AKOYA). For immunofluorescent staining, mouse uterus tissues were embedded in the optimal cutting temperature compound (OCT) to produce cryosections at 10 μm. Slides were fixed with 4% paraformaldehyde (PFA) for 15 min at room temperature, blocked with 1% BSA for 1 h at 37°C, and stained with anti-B7-H4 overnight at 4°C. The slides were then stained with PE-conjugated anti-Rabbit IgG for 30 min at 37°C, counterstained with DAPI, mounted with ProLong Gold Antifade mountant (Invitrogen, P36930) and analyzed with a confocal microscope (Nikon, A1). Images were analyzed using ImageJ.

Western blotting

For tissue protein samples, tissues were lysed in 1x RIPA lysis buffer (Thermo Fisher, 89900) containing 1x protease and phosphatase inhibitor cocktail (Thermo Fisher, 78468) with a Dounce homogenizer. For *in vitro* cultured cell samples, cells were washed in PBS and lysed in RIPA lysis buffer containing protease and phosphatase inhibitor cocktail. Protein concentration was quantified using the BCA protein assay kit (Thermo Fisher, 23225). Protein samples were added with sample buffer (Bio-Rad, 1610747) and denatured at 95°C for 5 min. An equivalent amount of total protein was loaded and separated by SDS-PAGE and transferred to a nitrocellulose membrane (Bio-Rad, 1620146). Membranes were blocked with 5% nonfat dry milk for 1 h at room temperature, incubated with primary antibodies overnight at 4°C and then incubated with HRP-conjugated secondary antibodies (Vector Laboratories, PI-9400-1 or PA-9200-1.5) for 1 h at room temperature. Membranes were then developed using Clarity Western ECL Substrate (Bio-Rad,1705060) and captured using ChemiDoc Imaging System (Bio-Rad). Antibodies used were anti-B7-H4 (1:1000, Abcam, ab209242), anti-PD-L1 (1:1000, Thermo Fisher, PA5-20343), anti-PR (1:200, Santa Cruz, sc-810), anti-ERα (1:1000, CST, 8644), anti-HLA-G (1:1000, Abcam, ab7759), anti-BRD4 (1:1000, CST, 13440), and anti-Actin (1:1000, CST, 4967), anti-GAPDH (1:1000, CST, 97166).

Generation of knockout cells

Gene targeting by lentiCRISPR V2 vector (Addgene, 52961) was accomplished as previously described.[137] Briefly, lentiviruses were produced in HEK293T cells. Targeting cells (5 x 10^5) were infected with viruses expressing CRISPR sgRNA. Transduced cells were selected with (puromycin 3 μg/mL) and single clones were seeded into 96-well plates. Single clones were grown and expanded for validation of genetic knockout. For knocking-out of B7-H4 in mouse breast cancer cell 4H11, the following guide sequences targeting mouse B7-H4 were used: sg1-F CACCGTCAACGGCATCGTCATCCAG; sg1-R AAACCTGGATGACGATGCCGTTGAC; sg2-F CACCG-ATCGCACTCATCATTGGCTT; sg2-R AAACAAGCCAATGATGAGTGCGATC; 4H11 cells were transduced with lentiviruses expressing each CRISPR sgRNA or a lentiCRISPR V2 containing a nonspecific sgRNA (GFP) as control. Knock-out clones were validated by Western blotting. At least five individual clones were generated from one or two independent sgRNAs for further experiments. Mixed clones of the nonspecific sgRNA (GFP) were randomly chosen as control cells. For knocking-out of −58 kb enhancer region of B7-H4 in human breast cancer cell T-47D, the following guide sequences were used: sg1-F CACCGGTATTACGAA GGAGTTTTCT; sg1-R AAACAGAAAACTCCTTCGTAATACC; sg2-F CACCGAGGTTCACTTTGTTGTGATA; sg2-R AAACTATCACAA CAAAGTGAACCTC; sg3-F CACCGAGGGGGTCTTACGGAAATGC; sg3-R AAACGCATTTCCGTAAGACCCCCTC; sg4-F CACCGC CACAGCTGCTAAACCAAGC; sg4-R AAACGCTTGGTTTAGCAGCTGTGGC. T-47D cells were transduced with lentiviruses expressing four sgRNAs. Knock-out clones were validated by PCR using primers: CAAGTTGGCCTTCTCATAGAGGT (forward) and GCCCAAGAGATACAGGGCCA (reverse). The expected wild-type band should be 3628 bp, and the knock-out bands should be between 530 and 720 bp. Clones identified with a wild-type genotype were used for control cells for further experiments.

PCR for genotyping

For the genotyping of mouse fetuses, genomic DNA was extracted from fetal tissues using DNeasy Blood & Tissue Kit (Qiagen, 69506). PCR was performed to examine the genotype of the tissues. WT bands were detected using CCTACAGCCTTCAGTAT GCCAGAGA (P1) and GTTAGATAGGGTCTCACTGGGTAGC (P2), sized 900 bp. KO bands were detected using AGACTAGTGAG ACGTGCTACTTCCA (P3) and GTTAGATAGGGTCTCACTGGGTAGC (P2), sized 692 bp. PCR cycles were set as: 93°C 3 min; 35 cycles: 94°C 1 min, 58°C 1min, 72°C 1min; 72°C 10 min.

RT-qPCR

Total RNA was extracted using TRIzol Reagent (Invitrogen, 15596026) according to the manufacturer's instructions. cDNA synthesis was performed with 0.5–1 mg of total RNA using Revert Aid RT Reverse Transcription Kit (Invitrogen, K1691). Messenger RNA levels were measured with gene-specific primers using the SYBR Green PCR Master Mix (Invitrogen, 4309155) on a QuantStudio 3 Real-Time PCR System (Thermo Fisher Scientific). Fold changes in mRNA expression were calculated with the ΔΔCt method using β-actin as an endogenous control. The results are expressed as fold changes normalized to the controls. The following primers were used: human B7-H4, forward GCAGATCCTCTTCTGGAGCATAA, reverse CCGACAGCTCATCTTTGCCTT. Human β-actin forward: AGAGCTACGAGCTGCCTGAC, reverse AGCACTGTGTTGGCGTACAG.

ChIP-qPCR

ChIP assay was performed according to the SimpleChIP Enzymatic Chromatin IP Kit manufacturer instructions (CST, 9003). In brief, cells with or without progesterone treatment were fixed with formaldehyde and lysed, and chromatin was fragmented by partial digestion with Micrococcal Nuclease to obtain chromatin fragments of 1–5 nucleosomes. ChIP was performed using antibodies against PR (CST, 8757) and IgG control (CST, 2729), and ChIP-Grade Protein G Magnetic Beads. After reversal of protein-DNA cross-links, the DNA was purified using DNA purification spin columns, ChIP-enriched chromatin was used for real-time PCR. Relative expression levels were normalized to input. Two pairs of primers were used for PCR to detect the enhancer region: P1-forward TTGTTTTCGATTCCTTTTGTC, P1-reverse ATGGAAAGAATGGACAAGGC; P2-forward AGTATGGCAGGCTGGCTCCA, P2-reverse CCTGGAGTCAATCCCAGGTCT. Primers targeting the ESR1 enhancer region was used as positive control: forward GGAAAGCCG GCAGTTACA, reverse GGAGGCATGAAAGCCCTA. Non-targeting primers were used as negative control: forward CATGGACTGGC AGAGCATAA, reverse CCCAACATATTGAAGGTGTGC.

3C-qPCR

T-47D cells were treated with DMSO or 10 nM progesterone for 24 h. 3C-qPCR method was adapted from previous publications.[138,139] Briefly, 1 x 10^7 cells were cross-linked with 2% formaldehyde for 10 min and quenched with a final concentration of 0.125 mM ice-cold glycine for 5 min. Cells were lysed with 500 μL 1 x cold lysis buffer (10 mM Tris-HCl pH 8.0, 10 mM NaCl, 0.2% Igepal CA630) including 1 x protease inhibitor (Thermo Fisher, 78429) for at least 15 min on ice. Cell nuclei were pelleted, washed twice with 500 μL ice-cold 1x *Eco*RI buffer (NEB, R0101T), and then re-suspended in 500 μL 1x *Eco*RI buffer with 0.3% SDS and incubated for 1 h at 37°C, followed by adding 1% Triton X-100 and incubated for another 1 h to sequester the SDS. Each sample was digested overnight with 600 U restriction enzyme at 37°C. To stop the restriction digestion, 1.6% SDS (final concentration) was added, and samples were incubated at 65 °C for 20 min. Ligation was performed at 16°C for 4 h in 15 mL tubes containing 745 μL 10 x T4 ligase Buffer (Thermo Fisher, B69), 10% Triton X-100, 80 μL 10 mg/mL BSA, 6 mL water, 575 μL of cell lysate, 10 μL 1U/μL T4 ligase (Themro Fisher, EL0011). The crosslinks were reversed with Proteinase K (Thermo Fisher, 25530049) at 65°C overnight. 3C samples were then purified using phenol-chloroform extraction. A control template that contains all ligation products in

equal amounts was used to optimize PCRs and to establish the minimal amount of ligation product that can still be quantified reliably. Four bacterial artificial chromosome (BAC) clones (RP-11-88D6, RP11-73E16, RP11-237E5, RP11-194B2) were used to prepare the PCR control template. The following primers were used for 3c-qPCR:

P1, CCTGGGCTTGCTTAGGTCAC; P2, TCCACAGGCTGCAGCTAATTC; P3, TAGTGTGTTGAGGCCGGGAG; P4, CCCCAAGTACTGGAATTACAGG; P5, ACAACCTTCCCAAATAGAGGAGA; P6, CAGGCTCTTAGAATCTAGCCTGG; P7, CCTCCTGGAAGGGTCCATAG; P8, TGATGACCTTCGCACTGCTT; P9, ACCAACCCAAGCTATGGTATTGGCACA; P10, TGGCTTTGTGATCCCTGCTGG; P11, TGGCACTACTTTGGGTTGGA; P12, TCGATGACTCCTTGATTGGAGA; P13, ACAATAAAGCTTCTGGCAGA.

Luciferase activity assay

To validate the function of the putative enhancer of B7-H4 under the treatment of progesterone, the promoter of human *VTCN1* was cloned with primer pair B7P_Fwd/Rev and inserted into pGL3-basic at the site of XhoI and BglII. The enhancer of *VTCN1* was cloned with primer pair B7E_Fwd/Rev into pGL3-basic at the site of KpnI and MluI. An enhancer, together with promoter construct, was also generated.

B7P_Fwd: AGACGCGTGCTAGCCCGGGCTCGAGTGCTGCTGAAGGCCTGG;
B7P_Rev: CCAAGCTTACTTAGATCGCAGATCTGGCTGGGGAAGGTTCCCA;
B7E_Fwd: ATTTCTCTATCGATAGGTACCTAGTGGCATAATCTCGGC;
B7E_Rev: CACTCGAGCCCGGGCTAGCACGCGTCTATTATGGTTTCTAAATAAAGAGC.

The lentivirus expression plasmid with human PR (NM_000926.4) with C-terminal 3XFlag was ordered from VectorBuilder. The plasmid was sequenced, and the expression of PR was validated by Western blotting. To perform luciferase activity assay, HEK293T cells with stable expression of PR were transfected with pGL3-Basic, pGL3-promoter, and pGL3-promoter-enhancer for 24 h. Then the transfected cells were treated with DMSO or progesterone (500 nM) for an additional 48 h. Luciferase activity for firefly luciferase was measured using the Rapid Detection of Firefly Luciferase Activity (Promega, E1500). Relative firefly luciferase activity was normalized to the luciferase activity of the DMSO-treated group.

Data analysis

scRNA-seq datasets were obtained from Gene Expression Omnibus (GEO) or TISCH2 (Tumor Immune Single-cell Hub 2)[44] databases with indicated accession numbers. UMI counts, gene information, and barcodes were used for downstream analysis following the pipeline of Seurat (version 4).[140] Cell populations were annotated using markers defined in individual studies. The gene list for Major Histocompatibility Complex molecules, co-accessory molecules and other inhibitory molecules was obtained from the Molecular Signatures Database (MSigDB).[131] Violin plots were used to visualize gene expression level using the function of VlnPlot in Seurat. The normalized expression level of each gene was extracted from each dataset in the slots of "subject@assays$RNA". The averaged normalized expression level was calculated in each cell population in individual dataset. *Z*-scores for each gene were calculated by subtracting the average among cell types. Then, the averaged *Z*-scores with standard deviation for tumor cell from 8 datasets and trophoblast from 2 datasets were used for further visualization through scatterplot or heatmap using GraphPad Prism and Excel. Gene expression data of *VTCN1* (B7-H4) and *CD274* (PD-L1) at single-cell level were acquired from TISCH2 database. TCGA data for VTCN1 gene expression were obtained through HPA. Gene expression data for breast cancer samples from patients pre- and post-RU486 treatment were obtained from GSE212690. Gene expression data for *in vitro* differentiated trophoblast cells were from GSE216484 and GSE150616. ChIP-seq, ATAC-seq data were obtained from the indicated accession number and analyzed with Integrative Genomics Viewer (IGV). Hi-C data were analyzed with WashU Epigenome Browser.

QUANTIFICATION AND STATISTICAL ANALYSIS

Student's t tests were used to compare two independent groups. One-way ANOVA tests were used for multiple comparisons. two-way ANOVA tests were used for comparing tumor growth curves. Survival functions were estimated by the Kaplan-Meier methods and compared using the log rank test. All analyses were done using GraphPad Prism 8. $p < 0.05$ was considered significant. Sample size was determined at the basis of animal experimental trials and in consideration of previous publications on similar experiments to allow for confident statistical analysis. Unless noted, samples were independent biological replicates.

CellPress
OPEN ACCESS

Supplemental figures

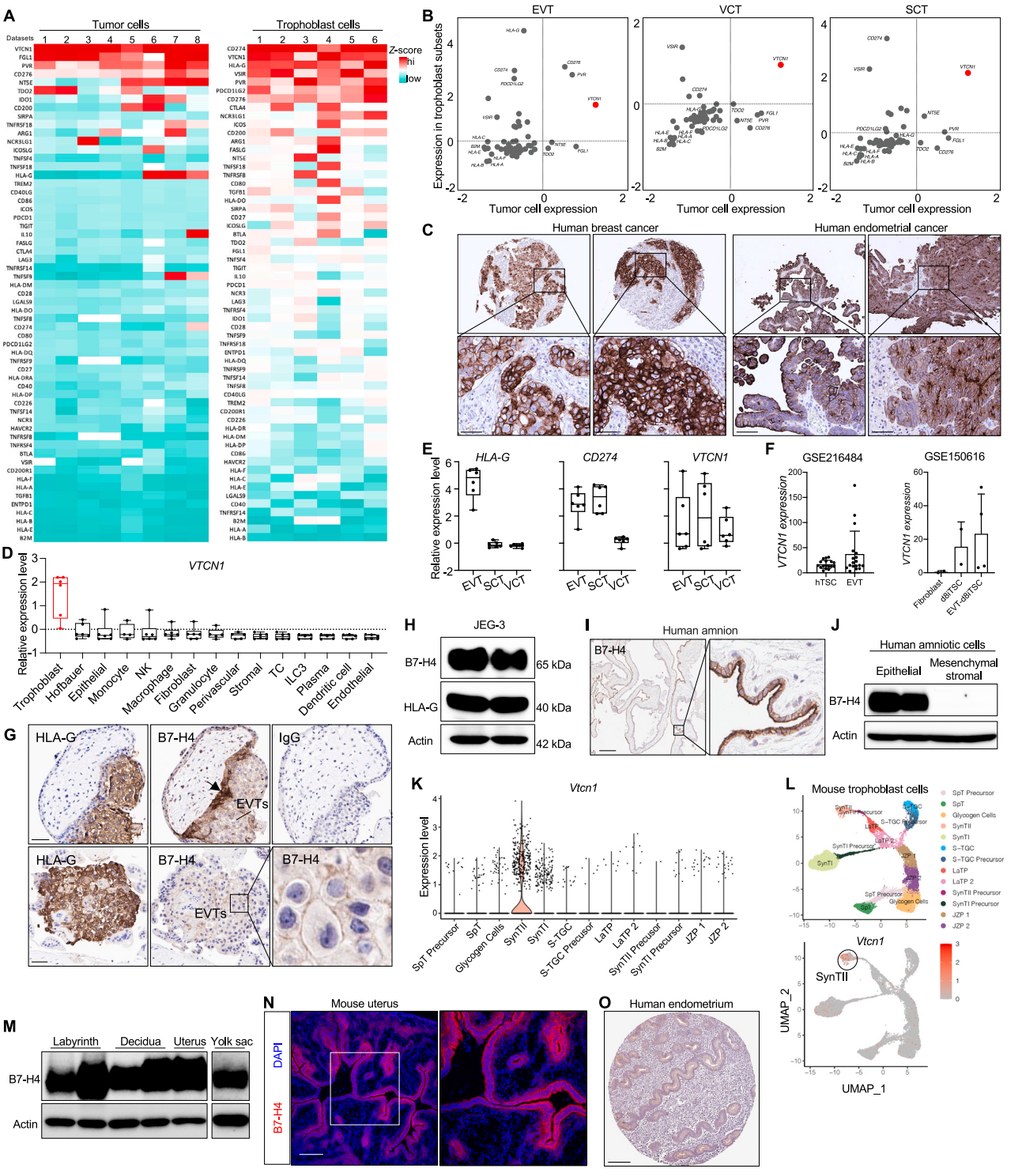

(legend on next page)

Figure S1. B7-H4 is an onco-fetal immune tolerance checkpoint, related to Figure 1

(A and B) Gene expression of B7 family members, TNF family members, major histocompatibility complex (MHC) molecules, and other typical inhibitory and co-stimulatory molecules in tumor and trophoblast cells (Datasets see STAR Methods). VCT, villous cytotrophoblast; EVT, extravillous trophoblast; SCT, syncytiotrophoblast.

(C) Representative IHC staining of B7-H4 in human breast and endometrial cancer samples. Scale bar, 50 μm.

(D) Expression *of VTCN1* in different types of cells at the maternal-fetal interface. (Datasets: see STAR Methods).

(E) Expression *of VTCN1*, *CD274*, and *HLA-G* in trophoblast subsets. (Datasets: see STAR Methods).

(F) RNA-sequencing data showing gene expression of *VTCN1* in *in vitro* differentiated EVTs.

(G) Representative IHC staining of HLA-G and B7-H4 in human first-trimester POCs. Scale bar, 50 μm.

(H) B7-H4 and HLA-G protein expression in JEG-3 cells.

(I and J) Representative IHC staining of B7-H4 in human amnion tissues (I) and B7-H4 expression in primary human amniotic epithelial and mesenchymal stromal cells (J). Scale bar, 250 μm.

(K and L) *Vtcn1* expression in mouse trophoblast cells. Violin plot (K) and UMAP (L) were presented.

(M) Western blot detection of B7-H4 in mouse labyrinth, decidua, uterus, and yolk sac.

(N) Representative IHC staining of B7-H4 in mouse uterus. Scale bar, 200 μm.

(O) Representative IHC staining of B7-H4 in human endometrium (data from Human Protein Atlas). Scale bar, 200 μm.

Data are presented as min to max (D, E), mean ± SD (F), violin plot (K). Each dot represents a dataset (D, E), a sample (F), or a cell (K).

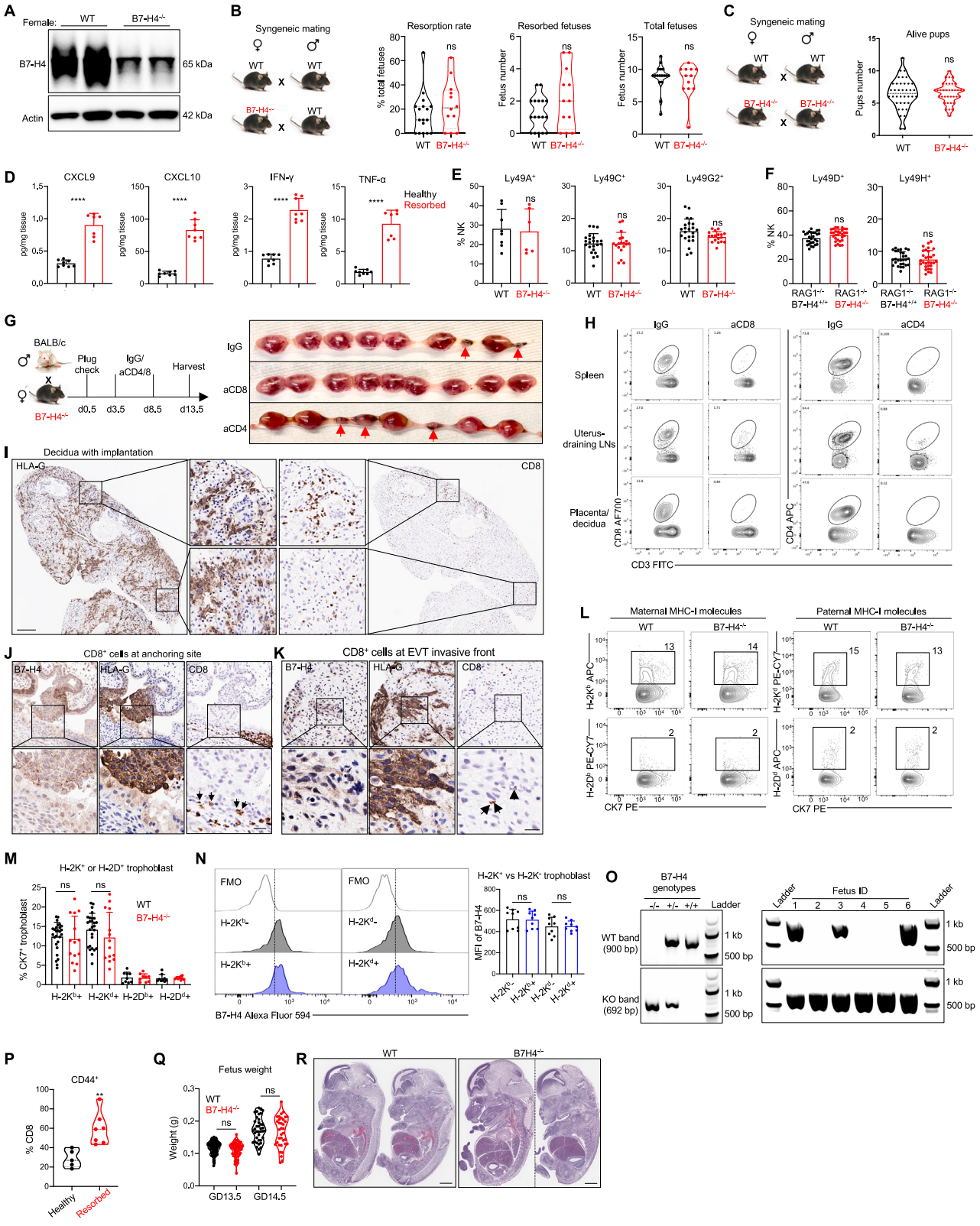

(legend on next page)

Figure S2. B7-H4 supports the maternal-fetal immune tolerance, related to Figure 2

(A) B7-H4 expression in placenta and decidua from allogeneic mating in Figure 2A.

(B) Syngeneic mating strategy for WT and B7-H4$^{-/-}$ on C57BL/6 background. The resorption rate, number of resorbed, and total fetuses were presented.

(C) The number of surviving pups of syngeneic breeding.

(D) Soluble CXCL9, CXCL10, IFN-γ, and TNF-α in homogenates of placental and decidual tissues from healthy or resorbed fetuses.

(E) Frequency of Ly49A^{+}, Ly49C^{+} and Ly49G2^{+} NK cells in placental and decidual tissues from pregnant WT and B7-H4$^{-/-}$ mice mated with male BALB/c mice.

(F) Frequency of Ly49D^{+} and Ly49H^{+} NK cells in placental and decidual tissues from pregnant RAG1$^{-/-}$B7-H4$^{+/+}$ and RAG1$^{-/-}$B7-H4$^{-/-}$ mice mated with male BALB/c mice.

(G and H) CD4 and CD8 depletion in female B7-H4$^{-/-}$ mice mated with male BALB/c mice (G). Depletion efficacy was examined (H).

(I–K) Representative IHC staining of HLA-G, CD8, or B7-H4 in decidua with implantation and anchoring villi of human first-trimester POCs. Scale bars, 200 μm (I) or 20 μm (J and K).

(L and M) H-2K and H-2D expression in CD45^{-}CK7^{+} trophoblast cells from WT and B7-H4$^{-/-}$ mice mated with male BALB/c mice.

(N) B7-H4 expression on H-2K^{+} trophoblast cells.

(O) Representative B7H4$^{-/-}$ genotyping of fetus and positive control with known B7H4$^{-/-}$, B7H4$^{+/-}$, and B7H4$^{+/+}$ samples.

(P) The frequency of CD44^{+}CD8^{+} T cells in the maternal-fetal interface of healthy and resorbed fetuses from Figure 2P. Healthy, n = 5; resorbed, n = 7.

(Q) Weight of non-resorbed WT and B7-H4$^{-/-}$ fetuses at gestational day 13.5 and 14.5 after embryo transfer (Figure 2P).

(R) Histology analysis of non-resorbed WT and B7-H4$^{-/-}$ fetuses at gestational day 13.5 after embryo transfer (Figure 2P). Scale bar, 1 mm. Data are presented as violin plots (B, C, P and Q), mean ± SD (D-F, M, N). ****p < 0.0001; ***p < 0.001; **p < 0.01; ns, not significant; by unpaired t test (B-Q).

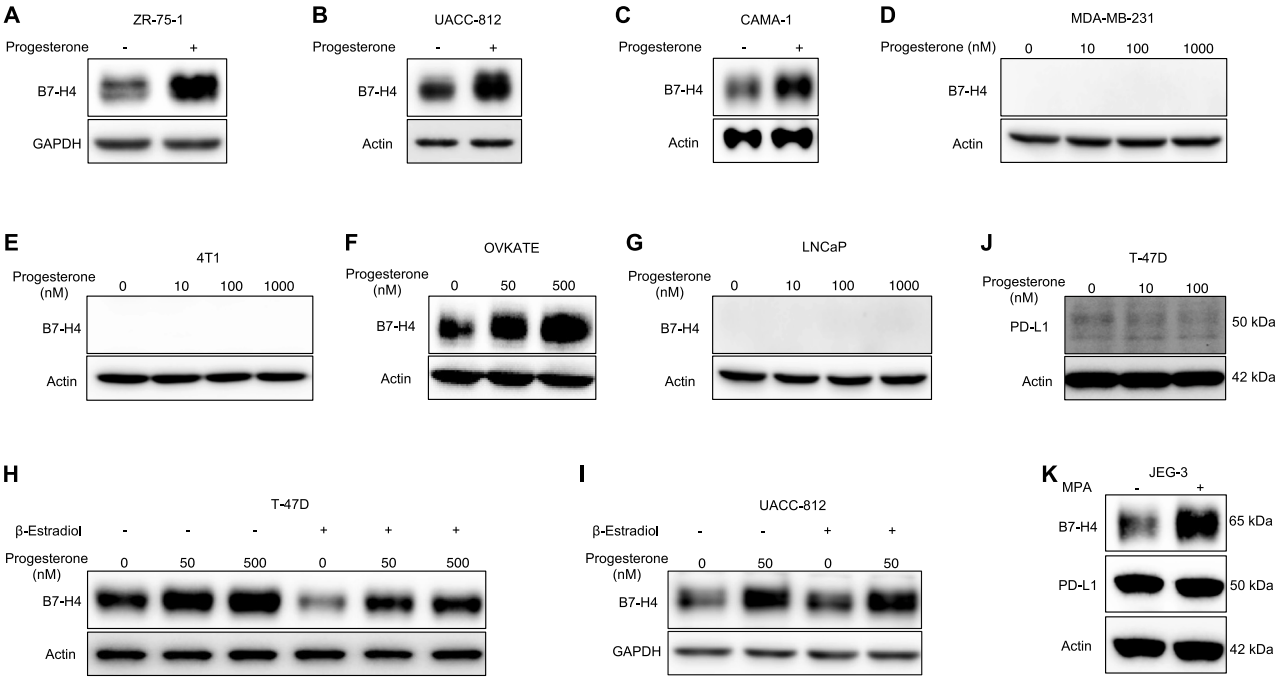

Figure S3. Progesterone promotes B7-H4 expression in cancer and placenta, related to Figure 3

(A–G) B7-H4 expression in ZR-75-1, UACC-812, CAMA-1, MDA-MB-231, 4T1, OVKATE, and LNCaP cells treated with progesterone. 50 nM progesterone was used in (A-C).

(H and I) B7-H4 expression in T-47D and UACC-812 cells treated with progesterone and β-Estradiol in RPMI medium without phenol red and supplemented with charcoal-stripped FBS. 100 nM β-Estradiol was used.

(J) PD-L1 expression in T-47D cells treated with progesterone at indicated concentration. Cells were treated for 48 h.

(K) B7-H4 and PD-L1 expression in JEG-3 cells treated with 50 nM MPA.Cells were treated for 48 h.

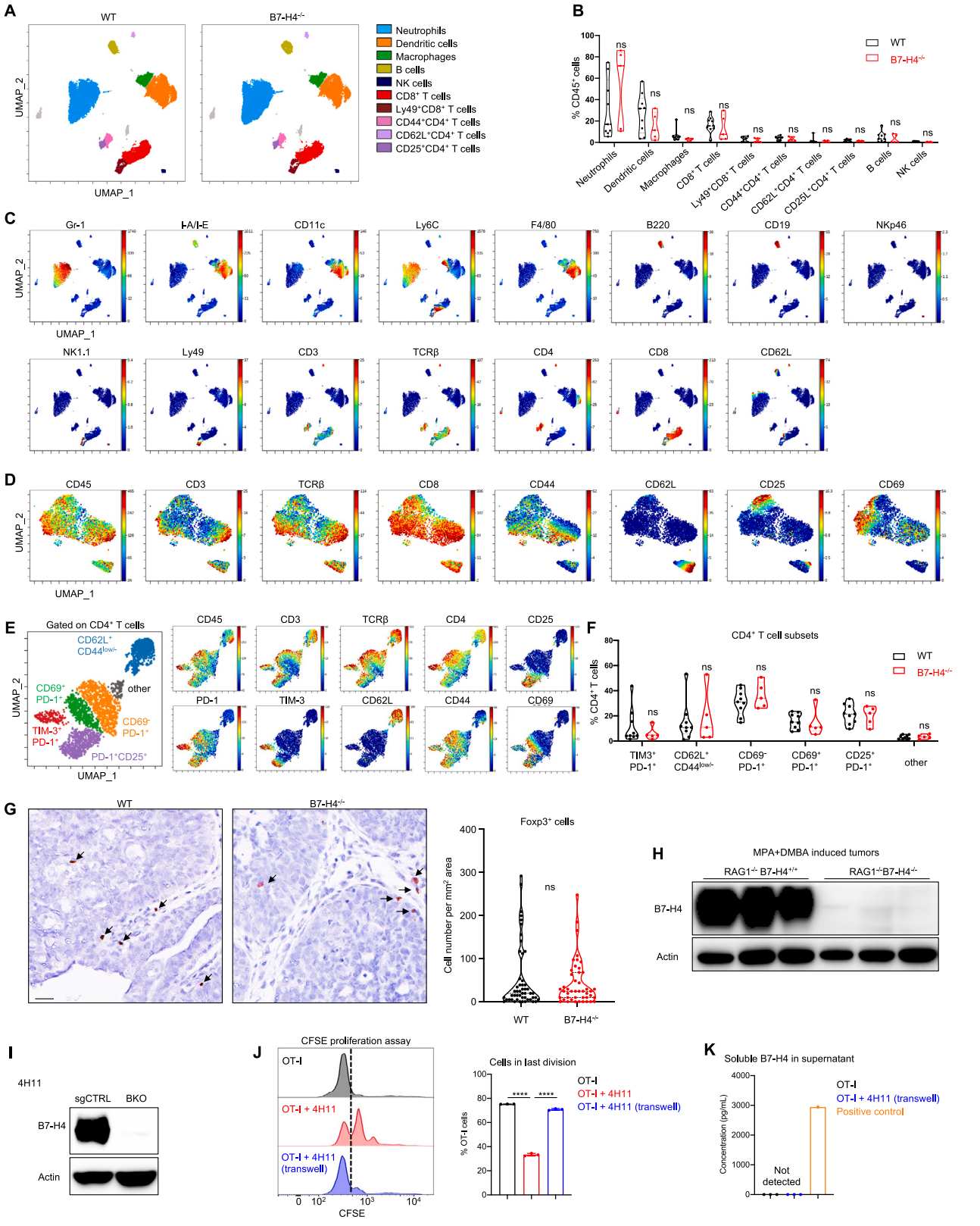

(legend on next page)

Figure S4. B7-H4 promotes breast cancer progression by inhibiting CD8$^+$ T cells, related to Figure 4

(A–F) CyTOF analysis of immune cells from the spontaneous breast cancer model. UMAP plots showing major immune populations in concatenated WT and B7-H4$^{-/-}$ samples (A), frequency of major immune population (B), expression of key markers in the concatenated sample (C), phenotypic markers in CD8$^+$ (D) and CD4$^+$ T cells (E), and the frequency of subpopulations in CD4$^+$ T cell (F).

(G) Representative image and statistics for IHC staining of Foxp3 in WT and B7-H4$^{-/-}$ tumors. Scale bar, 20 μm.

(H) B7-H4 expression in tumor tissues from RAG1$^{-/-}$B7-H4$^{+/+}$ and RAG$^{-/-}$B7-H4$^{-/-}$ mice induced with MPA plus DMBA.

(I) B7-H4 expression in B7-H4$^{+/+}$ (sgCTRL) or B7-H4$^{-/-}$ (BKO) 4H11 tumor cells.

(J) Representative histograms and statistics of OT-I cell proliferation.

(K) Soluble B7-H4 in the supernatant of OT-I co-culture assay. Data are presented as violin plots (B, F, G), mean ± SD (J, K). ****$p < 0.0001$; ns, not significant; by unpaired t test (B, F, G), one-way ANOVA (J).

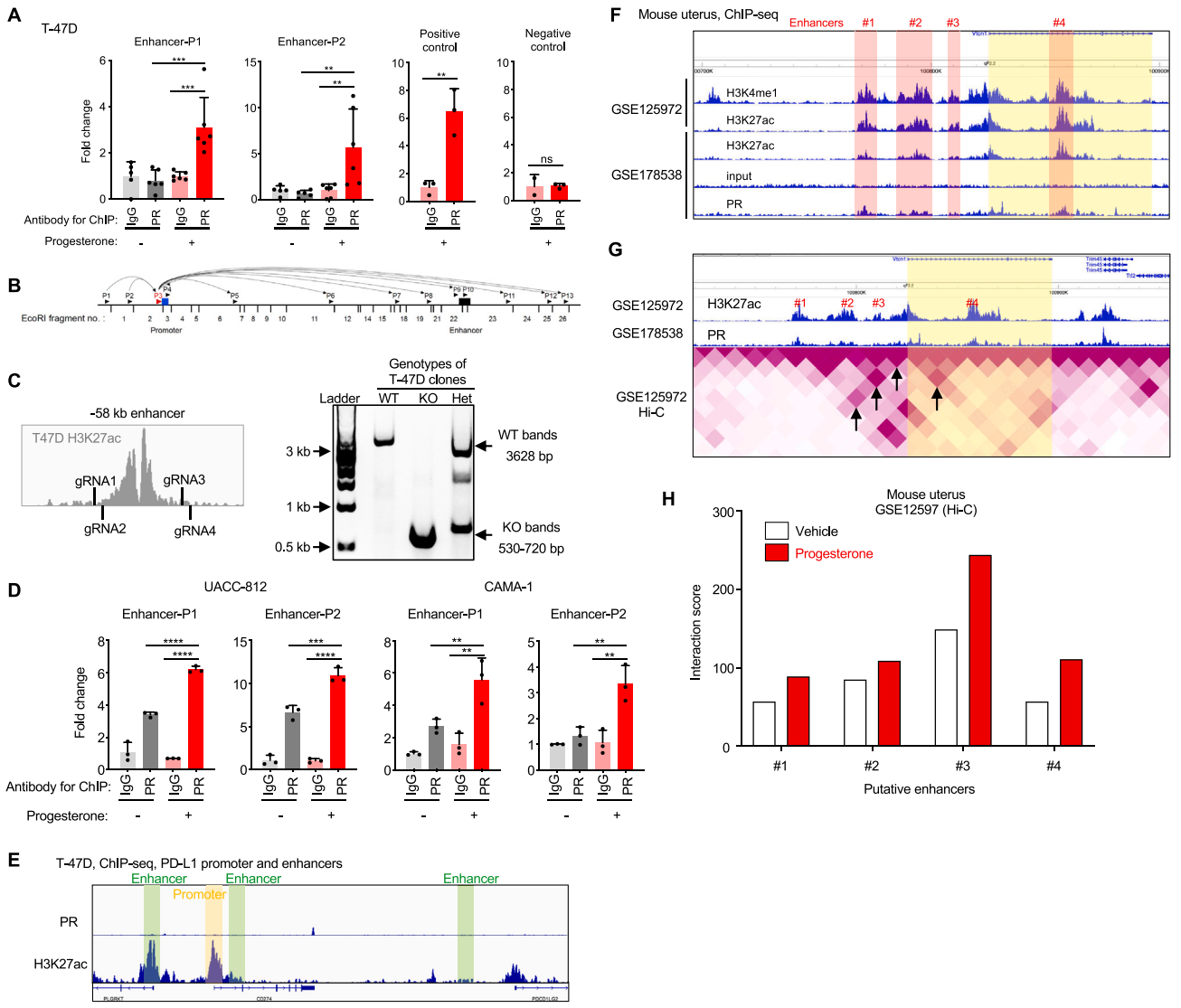

Figure S5. PR signaling promotes B7-H4 transcription via binding to the -58 kb enhancer, related to Figure 5

(A) T-47D cells were treated with 100 nM progesterone for 4 h. ChIP-qPCR was performed to examine PR binding to the putative B7-H4 enhancer region. Two pairs of primers were designed to detect the putative enhancer region of B7-H4. Primers targeting *ESR1* enhancer region were used as positive control. Random primers were used as negative control.

(B) Schematic picture describing 3C-qPCR method. The *Eco*RI restriction fragments are indicated. *Eco*RI fragments are numbered from fragment 1 to 26. Blue box indicates the promoter of B7-H4. Black box represents the putative −58 kb enhancer of B7-H4. Primers used for the 3C-PCR are indicated accordingly. Note P3 and P4 were in the promoter region, while P9 and P10 were in the putative enhancer region. P3 was used as the anchor primer for PCR analysis.

(C) Four gRNAs were used to knock out the putative enhancer region indicated by H3K27ac binding signal (left). Genomic DNA was extracted from different T-47D clones established after CRISPR-cas9 mediated genome editing. Genotyping of the putative enhancer region was performed. Representative genotypes are shown (right).

(D) ChIP-qPCR targeting enhancer region of B7-H4 in UACC-812 and CAMA-1 treated with or without 50 nM progesterone.

(E) Overlayed PR ChIP-seq and H3K27ac signal tracks in T-47D cells with reported promoter and enhancers of PD-L1 (*CD274*). The data range of PR ChIP-seq is the same as in Figure 5B.

(F) H3K4me1, H3K27ac, and PR ChIP-seq signal tracks in mouse uterus tissue. Four putative enhancers (#1, #2, #3, and #4) of B7-H4 were highlighted.

(G and H) Hi-C data from mouse uterus tissue showing the interaction (G) and score (H) of the 4 putative enhancers with the promoter region of B7-H4 (arrows).

Data are presented as mean ± SD (A and D). ****$p < 0.0001$; ***$p < 0.001$; **$p < 0.01$; ns, not significant; by one-way ANOVA (A and D).

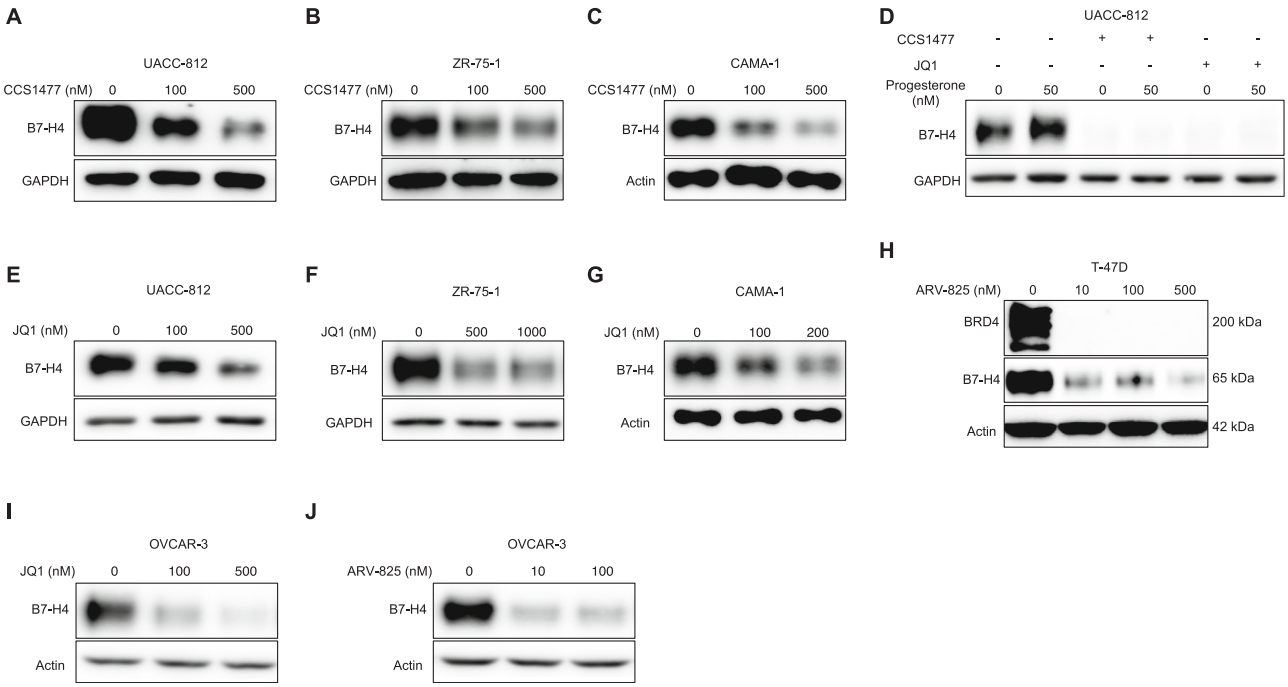

Figure S6. Progesterone promotes B7-H4 expression via the PR-P300-BRD4 axis, related to Figure 6

(A–C) B7-H4 expression in UACC-812, ZR-75-1 and CAMA-1 cells treated with CCS1477.

(D) B7-H4 expression in UACC-812 cells treated with progesterone together with CCS1477 (500 nM) or JQ1 (500 nM).

(E–G) B7-H4 expression in UACC-812, ZR-75-1 and CAMA-1 cells treated with JQ1.

(H) BRD4 and B7-H4 expression in T-47D cells treated with ARV-825.

(I and J) B7-H4 expression in OVCAR-3 cells treated with JQ1 and ARV-825.Cells were treated for 48 h.

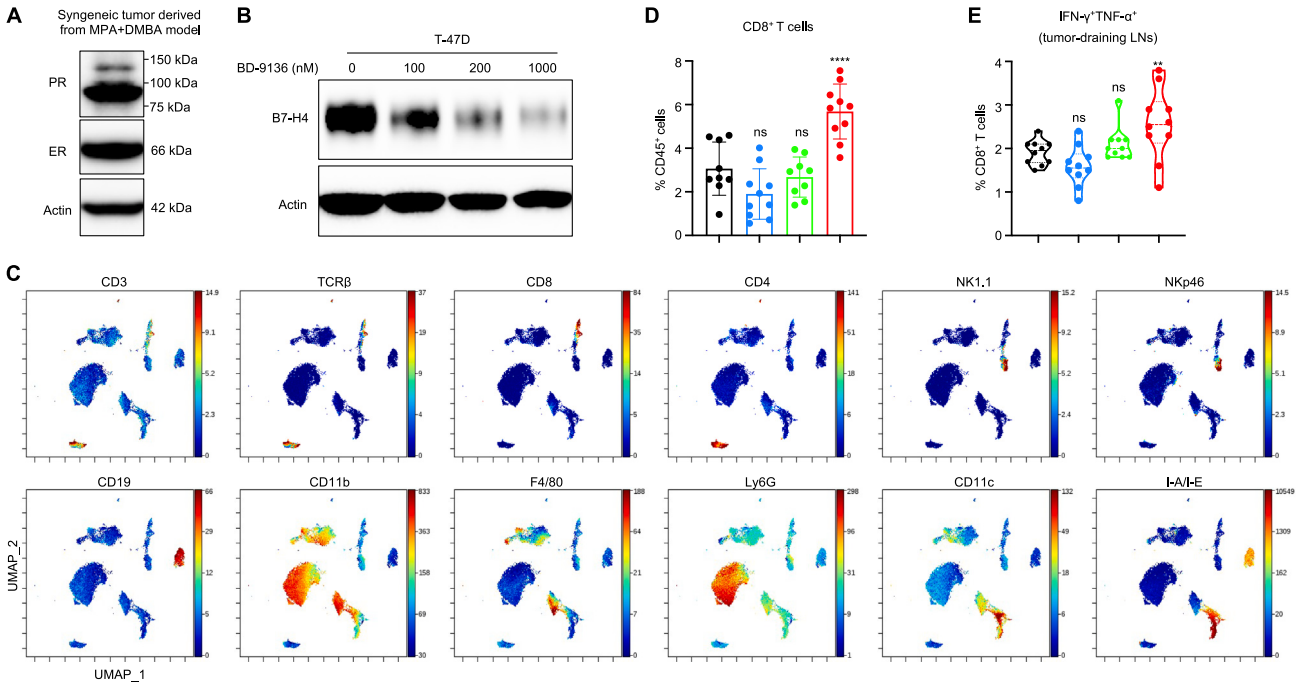

Figure S7. Targeting the regulatory axis of B7-H4 via RU486 and BRD4 degrader potentiates ICB efficacy, related to Figure 7

(A) PR and ER expression in syngeneic tumors from primary tumor cells isolated from spontaneous breast cancers induced by MPA and DMBA.

(B) B7-H4 expression in T-47D cells treated with BD-9136 for 48 h.

(C and D) CyTOF analysis of immune cells from syngeneic tumors in Figure 7F. The expression of key phenotypic markers for major immune populations (C), and percentages of $CD8^+$ T cells among $CD45^+$ cells are presented (D).

(E) Frequency of IFN-γ^+TNF-$\alpha^+$$CD8^+$ T cell in tumor-draining lymph nodes (LNs). Data are presented as mean ± SD (D), violin plots (E). ****$p < 0.0001$; **$p < 0.01$; ns, not significant; by one-way ANOVA (D and E).